STABILITY STUDY OF PHOSLACTOMYCIN B AND ANALYSIS OF DEGRADATION PRODUCTS

A thesis submitted in partial fulfillment of the
requirements for the degree of Master of Science at
Virginia Commonwealth University

By

Suparna Das Choudhuri
B.Pharm., Rajiv Gandhi University of Health Sciences, 2001

Director: Kevin A Reynolds, Ph.D.
Professor, Department of Medicinal Chemistry

Virginia Commonwealth University
Richmond, Virginia
May, 2005

Acknowledgements

I would like to thank my advisors Dr. Kevin Reynolds and Dr. William Soine, who were vital to the success of this research project. Their moral support and intellectual guidance has been invaluable and much appreciated by me.

I would like to thank Dr Michael Hindle for helping me with the Mass spectroscopy and Dr. Neel Scarsdale with NMR. I would like to thank the entire department of Medicinal Chemistry, VCU for their helpful suggestions during the project.

It is with great appreciation that I acknowledge the support and encouragement of my fellow lab members Galina Florova, Mohini Ghatge, Nadaraj Palaniappan, Sang Joon Mo, Sloan Ayers, Konstantin Akopiants, Mamoun Al-Hamadsheh, Chauxuan Li and Vidya Dhote. I also thank my friend Nagesh for his relentless motivation and support.

I thank my parents Sarajit and Rina Das Choudhuri and my brother Sumanta for everything I am and will be. Having their continuous support, even from thousands miles away, made it easier to go extra miles before retiring for each day. I dedicate this dissertation to them.

Table of Contents

List of Tables

Table **Page**

List of Figures

List of Schemes

Schemes **Page**

List of Abbreviations

PLM-B	Phoslactomycin B
ESI	Electrospray Ionization
LC-MS	Liquid Chromatography- Mass Spectroscopy
HPLC	High Pressure Liquid Chromatography
NMR	Nuclear Magnetic Resonance
^{1}H NMR	Proton Nuclear Magnetic Resonance
COSY	Correlation Spectroscopy
MPF	Maturation Promoting Factor
SY	Starch Yeast Extract
cdc25	Cell Division Control Protein 25
HSQC	Heteronuclear Single Quantum Correlation

ABSTRACT

STABILITY STUDY OF PHOSLACTOMYCIN B AND ANALYSIS OF DEGRADATION PRODUCTS.

By Suparna Das Choudhuri, M.S.

A thesis submitted in the partial fulfillment of the requirements for the degree of Masters of Science from Virginia Commonwealth University.

Virginia Commonwealth University, 2005

Chairperson of the Graduate Committee- Dr. Kevin A. Reynolds, PhD

Department of Medicinal Chemistry.

Phoslactomycin B (PLM-B), a potent and selective inhibitor of serine threonine phosphatase is of interest for its antitumor, antifungal and antiviral activity. The objective of this study was to evaluate the stability of phoslactomycin B at various pH and temperature conditions. Phoslactomycin B was produced from the mutant strain NP1 of *Streptomyces* sp.HK-803 and was purified by semi-preparative HPLC . A study of PLM-B degradation was carried out in the pH range of 2-10 at 30ºC and 50°C using HPLC. The PLM-B decomposition was observed to exhibit a U-shaped pH profile and demonstrated both acid and base-catalyzed decomposition. The decomposition could be described by the equation $k_{OBS} = k_H \times 10^{-pH} +$

k_{OH} x 10^{pH-14} (k_H = 45±7 M^{-1} h^{-1}; k_{OH} = 448± 73 M^{-1} h^{-1}). PLM-B was found to be most stable at pH 6.63. The degradation products in both acidic and basic pH have been collected and analyzed. Under basic condition, mass spectroscopic analysis revealed addition of water and NMR was consistent with the major products being formed due to lactone ring opening and/or a Micheal type addition reaction. Under acidic condition MS revealed loss of water for all three compounds. NMR analysis of one product (product **8**) was consistant with C_9-C_{11} phosphorinane derivative of PLM-B. The remaining compounds were shown to be mixture of various dehydration products.

The degradation products despite containing small structural changes to PLM-B lost all detectable levels of antifungal activity.

INTRODUCTION

Streptomyces produce a series of structurally novel antifungal and antitumor agents named phoslactomycins (PLMs) [1], phospholine, phosphazomycin A, leustroducsins and fostriecin. These agents are structurally related and contain an unusual phosphate ester, an α,β- unsaturated δ-lactone and either a conjugated diene or triene chain. PLMs (Figure 1) were isolated from several *Streptomyces* strains including *Streptomyces*. sp HK 803 [2]. The principal structural differences distinguishing PLMs from fostriecin [3] are replacement of the C-8 methyl substituent by ethylamine and the terminal allylic triene alcohol by a cyclohexane diene. All the above compounds including fostriecin (**2**) are produced in multiple forms (see Figure 1). For phoslactomycins, PLM-B [1] contains a fully reduced cyclohexyl ring, [4] whereas other PLMs and leustroducsins contain a hydroxyl substituent at (C-18) that is esterified with a wide array of carboxylic acids of length 4 to 9 carbons.

Antifungal activity of PLMs

The PLMs and phosphazomycins were isolated based on their antifungal activity. All the analogs were found to exhibit comparable antifungal activity [5]. PLM-E was shown to be active against various fungi, particularly phytopathogenic fungi (*Botrytis cinerea, Alternaria kikuchiana, Alternaria mali, Mycosphaerella melonis, Chaetomium globosum, Verticillium albo-atrum* and *Pseudcercisporella herpotrichiodes*). PLMs A, B, C, D, E, and F on comparison were also found to have almost the same antifungal activity [6]. The difference in the chemical structures between each compound is the substituent bound to a cyclohexane ring. This substituent would appear not to be important for antifungal activity.

Fostriecin though closely related to PLMs lacked antifungal activity [3]. Therefore, comparing their structures, the antifungal activity of PLMs was predicted to be due to the presence of aminoethyl and cyclohexyldienyl moieties.

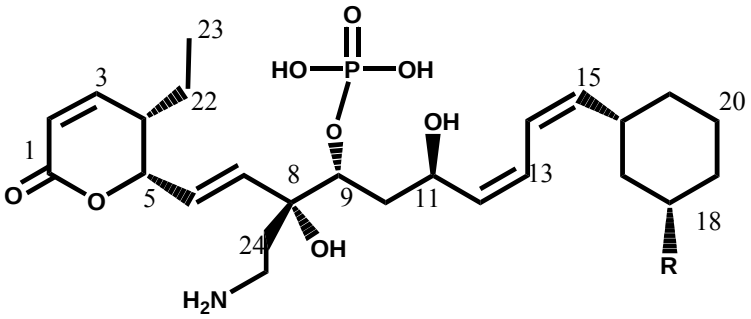

(1)

Phoslactomycins (PLMs)
PLM A R= $OCOCH(CH_3)_2$
PLM B R= H
PLM C R= $OCOCH_2CH(CH_3)_2$
PLM D R= $OCOCH_2CH_2CH_2(CH_3)_2$
PLM E R= $OCOC_6H_{11}$
PLM F R= $OCO(CH_2)_2CH(CH_3$

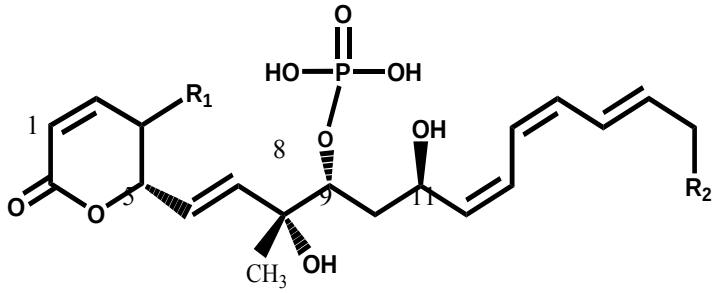

(2)

Fostriecin R_1= H, R_2= OH
PD 113,270 R_1= H, R_2= H
PD 113,270 R_1= OH, R_2= OH

Figure 1. Structures of phoslactomycin B (**1**) and fostriecin (**2**).

PLMs were subsequently reisolated (as phospholines and leustroducsins) along with other related structures based on their cytotoxicity [5].

Inhibition of Topoisomerase II

Fostriecin and the PLMs (phospholines) have been shown to have topoisomerase II inhibitory activity [7]. Topoisomerase II (topo II) [8] functions to unwind double stranded DNA during two distinct phases of cell cycle. In S phase, topo II relaxes supercoiled DNA generated for transcription and DNA synthesis but this function can be replaced by topoisomerase I (topo I). In M phase, topo II is required for unwinding of sister chromatids and subsequent chromatid segregation [9]. Classical inhibitors of topo II [10-12] induce irreversible DNA strand cleavage, and prevent binding of enzyme to DNA or stabilize the topo II-DNA complex.

It has been proposed that fostriecin's cytotoxic properties [5] can be attributed to a direct inhibition of the topo II enzyme prior to or without an interaction with DNA. Fostriecin was found to inhibit the catalytic activity of purified topo II from Ehrlich ascites carcinoma at 100μM concentration [13]. The low potency of fostriecin as a topo II inhibitor, could be attributed to poor binding with the primary target. More recent studies however, suggest a different mechanism for fostriecin's activity, implicating the Ser/Thr protein phosphatase (PP) family as the key cellular target. Potent inhibition of PPs (IC_{50} 3.2 nM) along with other studies has suggested that this is more likely the mechanism for antitumor activity for fostriecin [14] and PLM are due to PPs.

Inhibition of Serine Threonine Phosphatases

This family of PPs is a highly homologous (35-65%) class of bimetalloenzymes of which several subtypes have been identified [15-17].

The most well studied are PP1, PP2A, PP2B, PP2C, PP4, PP5, PP6, and PP7 [18-20]. Because of the high degree of homology that exists in the family, differentiating which enzyme is responsible for regulation of a particular biochemical pathway has proved challenging. The use of natural product inhibitors that target individual members of the family has become an indispensable tool in determining specific function.

A number of PP2A-selective inhibitors are known including okadaic acid, cantharidin and calyculin. Okadaic acid was found to inhibit PP2A and PP4 phophatases with same the IC_{50} 0.2nM [21]. The inhibition of protein phosphatases including PP1 (IC_{50} 131 nM) and PP2A (IC_{50} 3.2 nM) [22-23] with high specificity is proposed to be the principle mechanism for antitumor activity of fostriecin. PLMs like fostriecin are also potent and selective inhibitors of phosphatase PP2A, which, as discussed in detail below, is implicated in regulating the progression of cell cycle [24-27]. There are two proposals on the possible role of fostriecin-mediated PP2A [28] inhibition in regulating the tumor cell's entry into mitosis. One suggests that it induces premature mitosis, whereas the second suggests that it prevents mitosis from beginning.

Premature Mitosis Hypothesis

A basic outline of the cell cycle is represented in Fig. 2. Cells proceed through a resting G_1 phase, followed by S phase during which the synthesis of DNA and histones occurs. The first two stages are followed by a 'quality control' phase, G_2, in which the transcriptional errors are corrected [29]. Entry into M phase, during which cell division occurs, is regulated by the Maturation Promoting Factor (MPF) complex. This consists of Ser/Thr kinase p34cdc2 and cyclin B [30, 31] (Figure 3). When activated the complex is thought to stimulate normal chromosome condensation [32].

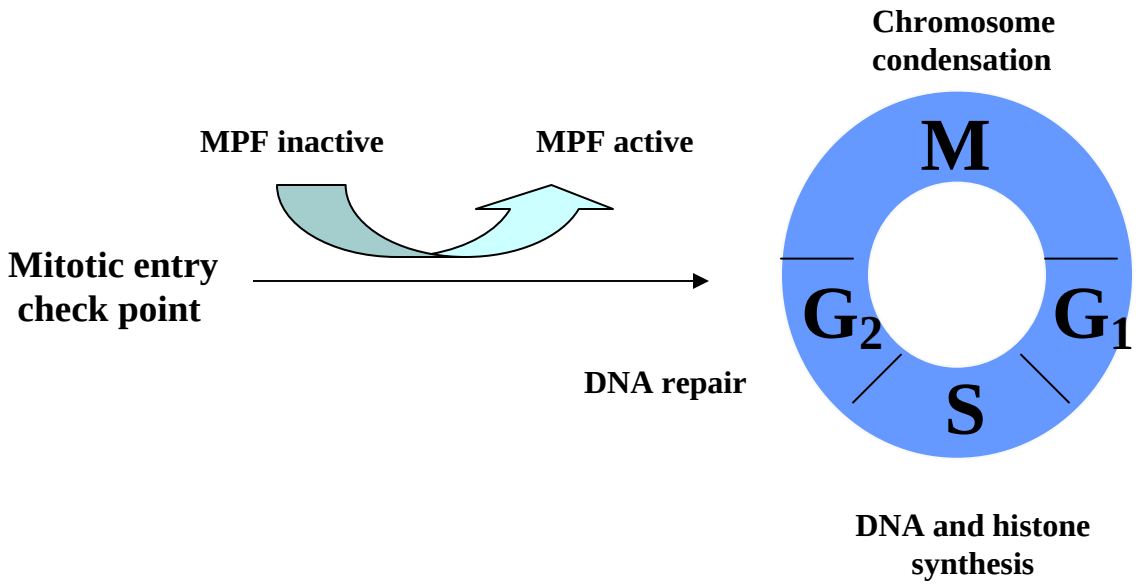

Figure 2. Schematic of the cell cycle.

Many antitumor agents interfere with the normal cell cycle control mechanism or mitotic entry checkpoint that occurs at the interface between the G_2 and M phase. Usually the agents do so by initiating G_2 arrest, a normal control mechanism for preventing a cell from undergoing division with imperfect DNA [29]. An early study of fostriecin's effects on the cell cycle showed that at 375μM concentration it induced baby hamster ovary (BHK) cells to enter the mitosis prematurely rather than suffer G_2 arrest, as evidenced by chromosome condensation, separation of spindle poles, and formation of asters. Premature mitosis with damaged, incomplete or incorrect DNA sequence results in cell death [33, 34].

G_2 Arrest Hypothesis

The mechanism by which G_2 arrest occurs is likely through disruption of normal changes that take place in the cytoskeleton preceeding mitosis. Normally, the microtubules which form the mitotic spindle radiate from phosphorylated centrosomes. Fostriecin [35], okadaic acid, and cantharidin-treated cells displayed numerous spindle poles extending from multiple centrosomes, consistent with G_2 arrest.

Pathway Connecting PP2A and Topo II.

It is possible that by inhibiting PP2A, compounds such as fostriecin may indirectly affect the activation of topo II in addition to direct inhibition of topo II [36-40]. PP2A is a negative regulator of MPF both directly, via dephosphorylation of a threonine 161 (T161) residue of active MPF, and indirectly, through dephosphorylation and deactivation of the phosphatase cdc25 and dephosphorylation and activation of the inhibitory kinase Wee1 (Figure 3). PP2A's main function is to phosphorylate tyrosine 15 (Y15) and threonine 14 (T14) residues on MPF, keeping MPF in a hyperphosphorylated, inactive state [41-45]. An active MPF caused by PP2A inhibition by fostriecin could lead to premature mitosis. There may also be a link between the activated MPF and increased topoisomerase II activity through MPF mediated activation of the intermediary casein kinase 2 (CK2), which is the major kinase known to phosphorylate topo II [46, 47]. The other major enzyme that phosphorylates topo II is protein kinase C, which is known to regulate MPF [48-51].

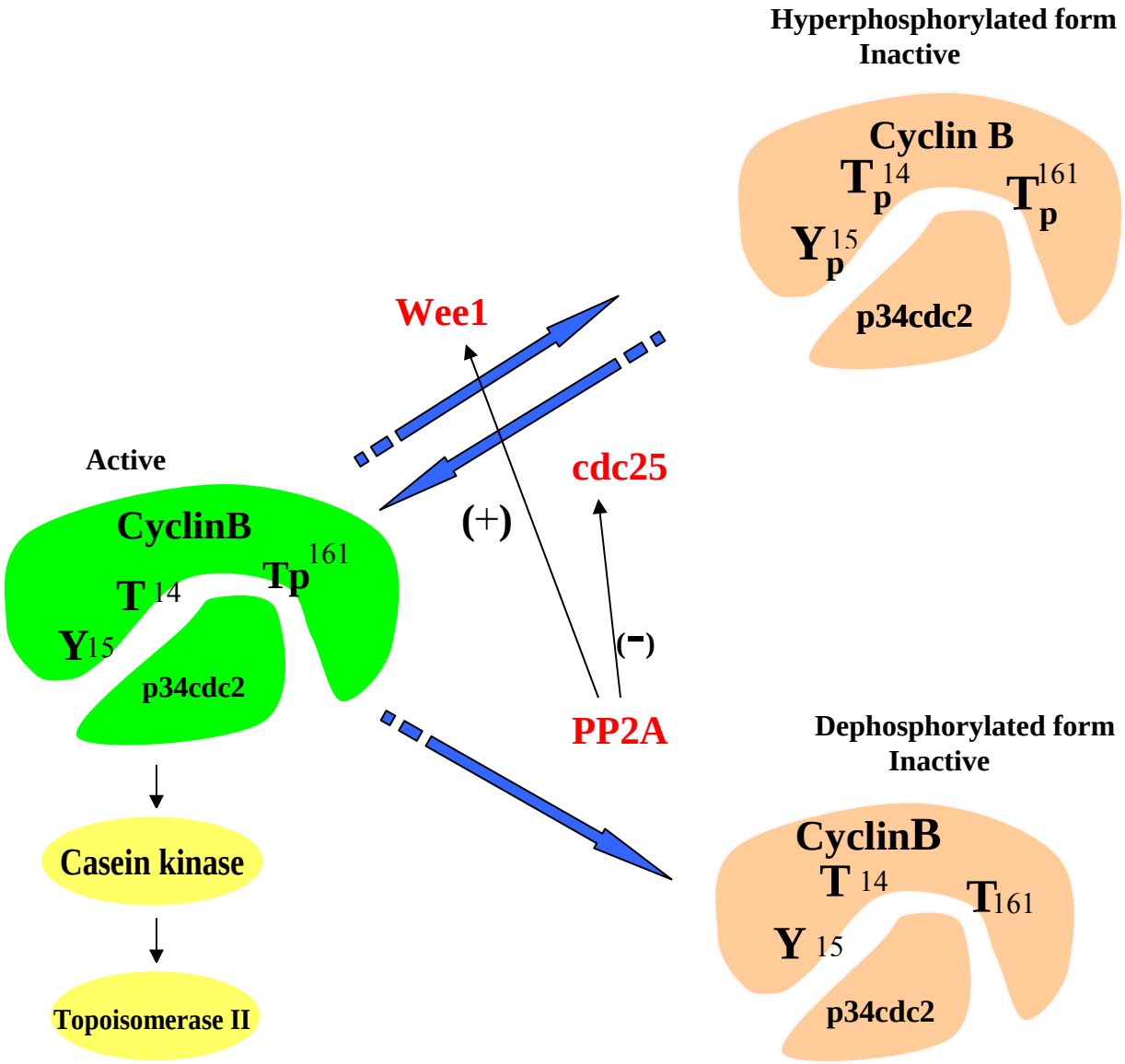

Figure 3. Activation of MPF and a biochemical pathway linking topoisomerase II and MPF. (+) indicates activation of Wee1 by PP2A-catalysed dephosphorylation and (-) deactivation of cdc25 by PP2A dephosphorylation.

Actin Disorganization by PP2A Inhibitors

Protein Phosphorylation is also a key regulatory mechanism of the organization and dynamics of the actin cytoskeleton during cell motility, differentiation, and cytokinesis. The effects of PLMs on the organization of the cytoskeleton in the murine fibroblast NIH/3T3 cells [52] were investigated. Exogenously added PLM A, B, C, and E induced actin depolymerization. Actin polymerization/depolymerization, known to be regulated by phosphorylation was confirmed by *in vitro* protein phosphatase assay using Ser/Thr phosphatase PP1 (IC_{50} 1250μM) and PP2A (IC_{50} 3.7-5.8μM), tyrosine phosphatase PTP-S2, and dual specificity phosphatase VHR. PLMs were found to selectively inhibit PP2A activity and bring about actin depolymerisation.

PLMs are not as potent an inhibitor as fostriecin (IC_{50} 3.2 nM), but are still selective for PP2A. The significant structural difference between PLMs and fostriecin is the presence of an amino group in the PLM structure. The amino group may decrease the inhibitory activity toward PP2A through intramolecular hydrogen bond formation with the phosphate ester [52].

Clinical Development of Fostriecin and PLMs

Phase I clinical trials of fostriecin were reportedly halted due to unpredictable purity of the clinical supply of the natural products and storage instability [53]. Subsequently, six different total syntheses of fostriecin were reported and provide an alternative source for pure material. Total synthesis poses [54, 55] a challenge and is not always successful, but clearly has very practical value for developing complex natural products for research and therapeutics. Analog generation by chemical modification or total synthesis can also be accomplished but remains problematic because of the rich variety of functional groups

that are characteristic of natural products, and often requires multiple protection and deprotection steps, making the process difficult, laborious and costly.

Genetic Engineering of Fostriecin and PLM Biosynthesis

Complementary to chemical synthesis, the manipulation and exchanging of genes governing secondary metabolic pathways (combinatorial biosynthesis) gives a promising alternative for the preparation of complex natural products and their analogs biosynthetically [2]. It is now possible to introduce specific structural alterations into a natural product in the presence of abundant functional groups by rational manipulation of the gene cluster governing its biosynthesis [56]. The reported limitation of chemical purity of fostriecin and related compound could be addressed through rational engineering of the corresponding biosynthetic pathway.

To date there has been no reports on analysis of fostriecin biosynthesis, however significant success has been reported in understanding and manipulating PLM biosynthesis. PLMs were proposed to be of polyketide origin, the biosynthesis of which should be catalyzed by a modular polyketides synthase (PKS) that uses cyclohexanecarboxylic acid (CHC) as a starter unit. This hypothesis was supported by the specific incorporation of isotope labeled CHC into all PLMs in *Streptomyces* sp. HK-803. PLM-B (Figure 1) would most likely be the first product synthesized from the PLM PKS biosynthetic machinery, and modification of PLM-B at C-18 by a hydroxylase ($PlmS_2$) and then esterification could eventually yield all the other PLMs. The PLM biosynthetic gene cluster (Figure 4) from *Streptomyces* sp. HK-803 was identified and cloned using the *chcA* gene, which is necessary for endogenous CHC biosynthesis as a probe. Sequencing and bioinformatics analysis, of the entire PLM gene cluster not only

confirmed the PLM PKS assembly line for PLM biosynthesis, but also identified the putative hydroxylase, PlmS2, that was responsible for most PLM-B hydroxylation at C-18. It was shown that inactivation of *plmS2* in *Streptomyces* sp.HK-803 led to a mutant strain (NP1) incapable of C-18 hydroxylation, hence producing PLM-B exclusively.

Having obtained such a strain, it was necessary to determine if the drug instability [57 - 64] reported for fostriecin occurred with PLM-B. This thesis details an analysis of PLM-B degradation under a range of pH and temperature conditions. The decomposition products were isolated and characterized by mass spectroscopy and NMR analysis. Overall, PLM-B was observed to be unstable at either strongly acidic or basic conditions, but exhibited reasonable stability on solution at pH 6.63 ($t_{1/2}$ = 72 days, 50°C).

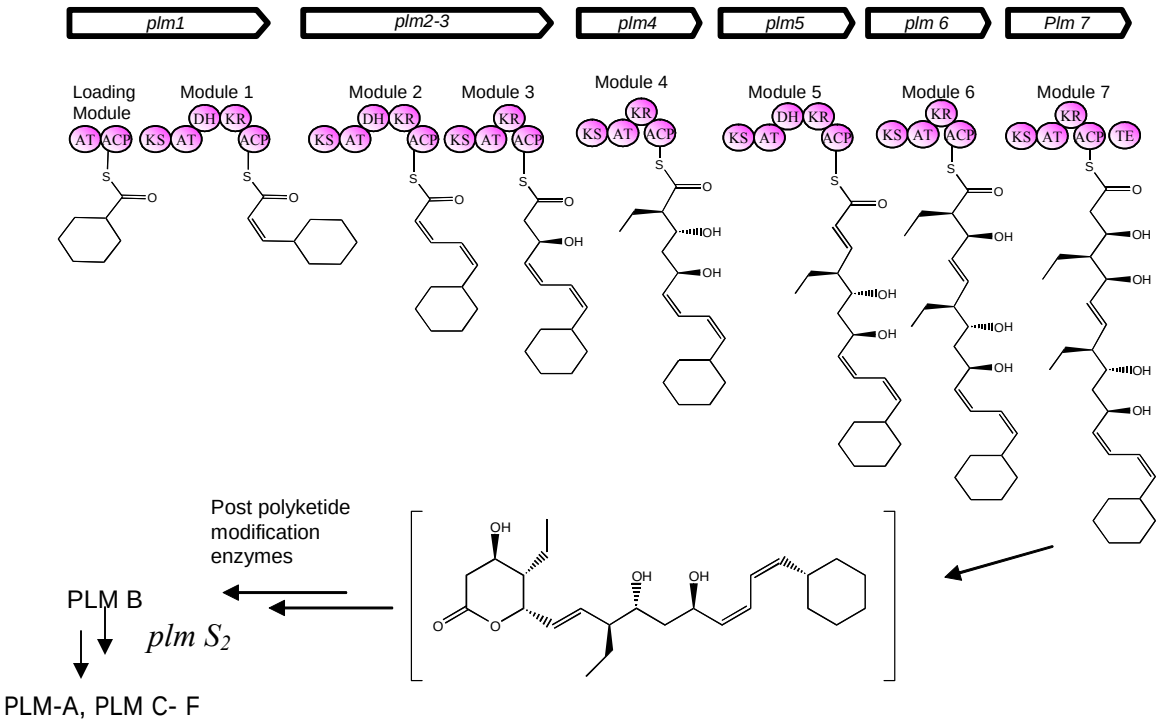

Figure 4. Proposed role for the six polypetides of the PLM PKS in PLM B biosynthesis**.**

EXPERIMENTAL PROCEDURES

Materials and Bacterial Strain.

Materials- Soluble starch, NaCl, K_2HPO_4, glucose, 100 % methanol, acetonitrile (HPLC grade), and formic acid were purchased from Fisher Scientific. Yeast extract, N, Z-amine type A and beef extract were obtained from Difco. Soybean flour, L-phenylalanine and XAD-4 were purchased from Sigma- Aldrich.

Strain and Culture Conditions

The mutant species NP1 of *Streptomyces* HK 803 yielding only PLM-B was obtained in our laboratory previously by a gene deletion technique [2]. The PLM-B producer NP1 strain was grown at 28º C in SY agar medium (1.0 % soluble starch, 0.1 % yeast extract, 0.1 % N,Z-amine, type A at pH 7.0). A loop full of inoculum (from SY agar plate) was inoculated into a baffled 500 ml flask containing 75ml of the production medium (2.0 % glucose, 0.1% beef extract, 1.0 % soybean flour, 0.2 % NaCl, 0.005 % K_2HPO_4 and 0.2% L-phenylalanine at pH 7.0) and was incubated in the dark for 96 h on a rotary shaker (New Brunswick Model G-25D, 200 rpm) at 28°C [50, 51].

Equipment

HPLC was performed on a system equipped with Waters 600 pump connected to Waters 2487 Dual Absorbance Detector. The semi-preparative and analytical column used was a Phenomenex C18, 5 µm (10.0 x 250 mm) or a Waters Symmetry C18 5µm. (4.6x 250 mm), respectively. The mobile phase was solvent A; acetonitrile/ 0.05% formic acid (20:80); solvent B, acetonitrile/0.05% formic acid (80:20). The gradient conditions were 0%B-60%B from 0-60 minutes. The flow rate for the semi-preparative HPLC column

was 3ml/min and the analytical HPLC column was 1ml/min, UV detection was at 235nm. Mass spectroscopic analysis was carried out using a Waters 2990 Separation Module, Waters 2996 Photodiode Array Detector, and Micromass ZMD 4000 mass spectrometer. The electrospray probe was operated at 3.5kV with a cone voltage of 50 V. The source and desolvation temperatures were 150°C and 400°C. Spectra were processed using Masslynx^{TM} 3.4V (Micromass, Manchester, UK). NMR spectra were typically acquired on a Varian Inova 400MHz spectrometer with a Sun Microsystems Ultra 1 processor and VNMR version 5.1c software. All constant temperature incubations were done using an incubator (±0.5°C, Precision Scientific, Chicago, IL.)

Preparation of Spore Suspensions

Spore suspensions [62] were prepared in 20% glycerol to maintain the NP1 strain. The bacteria were allowed to grow and sporulate on SY agar for 14 days (Figure 5). About 5mL of sterile water was added to each plate. Using an inoculating loop the spores [65] were scraped off the top of the plates and into suspension. The spore suspension was transferred using a biosterile pipette to a sterile tube, combined with 1 mL of what and stored at -20°C.

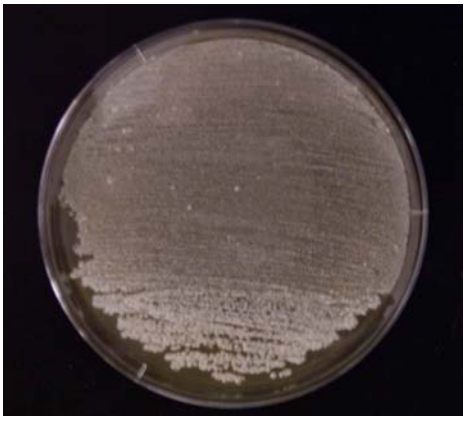

Figure 5. Spores of the strain NP1 grown on SY agar medium appear grey in colour.

Isolation and Purification of PLM-B

After completion of fermentation, a typical 24 x 75mL fermentation broth was centrifuged. The precipitant were treated with 70% acetone then centrifuged, filtered and the acetone was evaporated. This filtrate was combined with the fermentation broth and loaded on a 500mL XAD-4 (Sigma- Aldrich) column. The column was washed with deionized water (five column volumes) and eluted with 100 % methanol. The methanol eluate containing the active component was concentrated to dryness to give a brown residue. The residue was dissolved in methanol, filtered (0.2μL PTFE filter, Millipore Corp, MA), and purified by reverse-phase semi-preparative HPLC using the semi-preparative column and the conditions previously described [66, 67]. The eluate that was collected from the HPLC was first concentrated under reduced pressure to remove acetonitrile and the remaining aqueous solution was lyophilized to obtain PLM-B.

Preparation of Buffers

Chemicals used for the preparation of buffers were of analytical grade (Fisher Scientific). The following buffers [68, 69] were used KCl-HCl (pH 2.0), glycine-HCl (pH 3.0), sodium citrate–citric acid (pH 4.0), potassium phosphate (pH 5.0), potassium phosphate (pH 6.0), potassium phosphate (pH 7.0), Tris-HCl (pH 8.0), boric acid (pH 9.0), carbonate bicarbonate (pH 10.0) and sodium phosphate-NaOH (pH 11.0). The ionic strength of the buffers was maintained at 0.1M.

Decomposition of PLM-B

The decomposition reactions [70] were initiated by addition of 100µL of 19.4 – 23.3 µmol PLM-B (dissolved in methanol) in 900µL of buffer previously equilibrated to either 30ºC or 50ºC. All incubations contained 10% methanol to maximize solubility of PLM-B and were carried out in Teflon- lined screw-cap vials. Aliquots (100µL) were withdrawn at suitable time intervals and analyzed [71] until the concentration of PLM-B was negligible (for pH of 2.0, 3.0, 9.0 and 10.0) or, the concentration had decreased by more than 75%. Analysis of the decomposition was carried out by HPLC using the same the conditions used to analyze for PLM-B purity.

Kinetic Analysis of PLM-B decomposition

The analysis of the disappeared PLM-B was carried out using Microsoft Excel v2000 and the software program Sigmaplot v8.0. The pH-rate constant profile was obtained using Excel. The rate constants for acid (k_H) and base degradation (k_{OH}) were obtained from the rate equation $k_{OBS} = k_H \times 10^{-pH} + k_{OH} \times 10^{pH-14}$ by regression analysis using Sigmaplot.

Isolation and Characterization of PLM-B Degradation Products

Isolation of the degradation products was achieved using the same condition and the semi-preparative column under the same conditions previously described. The eluate corresponding to each decomposition product was collected and then evaporated to dryness under reduced pressure at 30°C. The purity of the isolated decomposition products were then confirmed by HPLC [72]. NMR, mass spectroscopy and UV analyses were obtained for each of the pure major degraded products as well as PLM-B.

PLM-B: (Phosphoric acid mono-{1-[1-(2-amino-ethyl)-3-(3-ethyl-6-oxo-3,6-dihydro-2H-pyran-2-yl)-1-allyl]-7-cyclohexyl-3-hydroxy-hepta-4,6-dienyl}ester). MS *m/z* 514 $[M+H]^+$, *m/z* 512 $[M-H]^-$; UV λ_{max} 235nm (in methanol), $\varepsilon = 0.3180 \times 10^{-4} L\ mole^{-1} cm^{-1}$; ^1H NMR: 7.10 (1H, dd, *J*= 4.4, 9.2 Hz, 3-H), 6.30-6.20 (2H, m, 13-H, 14-H), 6.09-5.93 (3H, m, 2-H, 6-H, 7-H), 5.43 (1H, dd, *J*= 8.0, 8.0 Hz, 12-H), 5.33 (1H, dd, *J*= 8.0, 8.0 Hz, 15-H), 5.11 (1H, dd, *J*= 4.4, 4.4 Hz, 5-H), 4.95 (1H, m, 11-H), 4.28 (1H, dd, *J*=9.2, 9.2 Hz, 9-H), 3.13-2.99 (2H, m, 25-H), 3.63 (1H, m, 4-H), 3.48 (1H, m, 16-H), 2.55 (1H, m, 4 –H), 2.01- 0.95 (7H, m, 17-H, 18-H, 19-H, 20-H, 21-H, 22-H, 23-H)

^{13}C NMR: 136.20 (C-7), 133.47 (C-12), 139.41 (C-15), 123.68 (C-13), 121.88 (C-14), 120.08 (C-2), 126.71 (C-6), 115.32 (C-3), 81.34 (C-5), 77.60 (C-9), 63.69 (C-11), 39.54 (C-4), 36.70 (C-16), 36.44 (C-25), 39.60 (C-10), 33.31 (C-21)

Degradation product **3**: (8-(2-Amino-ethyl)-15-cyclohexyl-4-ethyl-5,8,11-trihydroxy-9-phosphonooxy-pentadeca-2,6.12.14-tetraenoic acid). MS *m/z* 532 $[M+H]^+$, *m/z* 530 $[M-H]^-$; UV 235nm; ^1H NMR: 6.29-6.20 (2H, m, 13-H, 14-H), 6.03 (1H, d, *J*= 11.6 Hz, 2-H), 5.91-5.85 (1H, dd, *J*= 7.2, 15.6 Hz, 6-H), 5.62 (1H, d, *J*= 15.6 Hz, 7-H), 5.51 (1H, dd, *J*=

10.2, 10.2 Hz, 3-H), 5.42 (1H, dd, *J*= 8.4, 8.4 Hz, 12-H), 5.32 (1H, dd, *J*= 8.0, 8.0 Hz, 15-H), 4.25 (1H, dd, *J*= 8.0, 8.0 Hz, 9-H), 4.14 (1H, dd, *J*= 5.6, 5.6 Hz, 5-H), 3.3 (1H, m, 4 –H), 2.48-2.45 (1H, m, 16-H), 2.16-2.13 (1H, m, H-24b), 1.93-1.86 (1H, m, H-24a), 2.01-0.95 (7H, m, 17-H, 18-H, 19-H, 20-H, 21-H, 22-H, 23-H)

Degradation product **4**: (8-(2-Amino-ethyl)-15-cyclohexyl-4-ethyl-3,5,8,11-tetrahydroxy-9-phosphonooxy-pentadeca-6,12,14-trienoic acid methyl ester). MS *m/z* 564 $[M+H]^+$, *m/z* 562 $[M-H]^-$; UV 235nm, ^{1}H NMR: 6.29-6.19 (2H, m, 13-H, 14-H), 6.02- 5.96 (1H, dd, *J*= 8.0, 15.6 Hz, 6-H), 5.63 (1H, d, *J*= 16.0 Hz, 7-H), 5.41 (1H, dd, *J*= 4.8, 4.8 Hz, 12-H), 5.28 (1H, dd, *J*= 9.6, 9.6 Hz, 15-H), 4.29 (1H, dd, *J*= 12.8, 12.8 Hz, 9-H), 3.81 (1H, dd, *J*= 0.4, 4.0 Hz, 5-H), 3.13 (1H, m, 3-H), 2.59- 2.37 (2H, m, 4 –H, 16-H), 2.28- 0.95 (8H, m, 2-H, 17-H, 18-H, 19-H, 20-H, 21-H, 22-H, 23-H).

Degradation product **8**: (6-{5-Amino-3-[6-(4-cyclohexyl-buta-1,3 –dienyl)-2-hydroxy-2-oxo-2λ^5 –[1,3,2] dioxaphosphinan-4-yl]-3-hydroxy-pent-1-enyl}-5-ethyl-5,6-dihydri-pyran-2-one). MS *m/z* 496 $[M+H]^+$, *m/z* 494 $[M-H]^-$; UV 235- 237nm, ^{1}H NMR: 7.10 (1H, dd, *J*= 4.8, 10.0 Hz, 3-H), 6.22-6.15 (1H, dd, *J*= 12.0, 15.2 Hz, 13-H), 6.07-5.96 (4H, m, 2-H, 6-H, 7-H, 14-H), 5.69- 5.65 (2H, m, 12-H, 15-H), 5.12-5.09 (1H, dd, *J*= 4.8, 6.8 Hz, 5-H), 4.61 (1H, dd, *J*= 9.2, 15.6 Hz, 9-H), 4.54 - 4.48 (1H, m, 11-H), 2.99 (2H, t, 25-H), 2.62- 2.58 (1H, m, 4-H), 2.01- 0.95 (7H, m, 17-H, 18-H, 19-H, 20-H, 21-H, 22-H, 23-H).

^{13}C NMR: 151.68 (C-3), 141.84 (C-15), 136.43 (C-7), 132.86 (C-13), 130.97 (C-12), 127.22 (C-6), 126.67 (C-14), 120.08 (C-2), 81.68 (C-5), 79.30 (C-9), 77.0 (C-11), 48.34

(CD_3OD), 35.93 (C-25), 39.65 (C-4), 41.20 (C-16), 37.57 (C-10), 35.43 (C-24), 10.35 (C-23), 21.85 (C-22), 26.13 - 33.07 (C-17, C-18, C-19, C-20, C-21).

Antifungal assay

Antifungal activity was determined using agar diffusion tests [73, 74] against *Rhodotorula glutinitis* (ATCC 2527). The strain was rehydrated with a few drops of Butterfields buffer (International Bioproducts) and 100µL of this suspension was transferred to a standard potato dextrose agar (PDA) plate (Culture Media and Supplies, Oswego, IL). The plate was incubated at 25°C for 3 days. The pink colonies were harvested on the tip of a micro loop and smeared onto PDA slants in 50 mL centrifuge tubes and incubated under the same conditions. These were stocks for the entire assay and stored at room temperature for several weeks. In each slant about 10mL of Butterfields buffer was added and vortexed. The resulting suspension was transferred in a sterile 50mL tube and diluted to 50mL. About 100µL of this cell suspension was overlaid on a PDA plate. Sterile assay discs (~7mm diameter, from Whatman No.1 filter paper) were loaded with pure PLM-B as well as both the acidic (pH 2.0) and basic (pH 10.0) degradations products and placed on the inoculated plates. Two different concentrations (0.05mg/mL and 0.08mg/mL) of PLM-B and the degradation products were used. The plates were incubated at 25°C for 3 days, and inhibition zones [75, 76] surrounding the discs was measured.

RESULTS AND DISCUSSION

PLM-B was obtained from fermentations of *Streptomyces* sp. HK803, mutant NP1 and purified by reverse-phase HPLC [2]. Using the semi preparative HPLC system PLM-B eluted out at approximately 40.0 minutes and the fraction from 40.5 to 41.4 minutes was collected. The eluate was concentrated under reduced pressure to remove acetonitrile and then lyophilized to obtain PLM-B. The purity of the PLM-B was determined using the analytical column and PLM-B's retention time was approximately 37 minutes under these conditions. Typical chromatograms of crude and purified PLM-B are shown in figures 6 and 7.

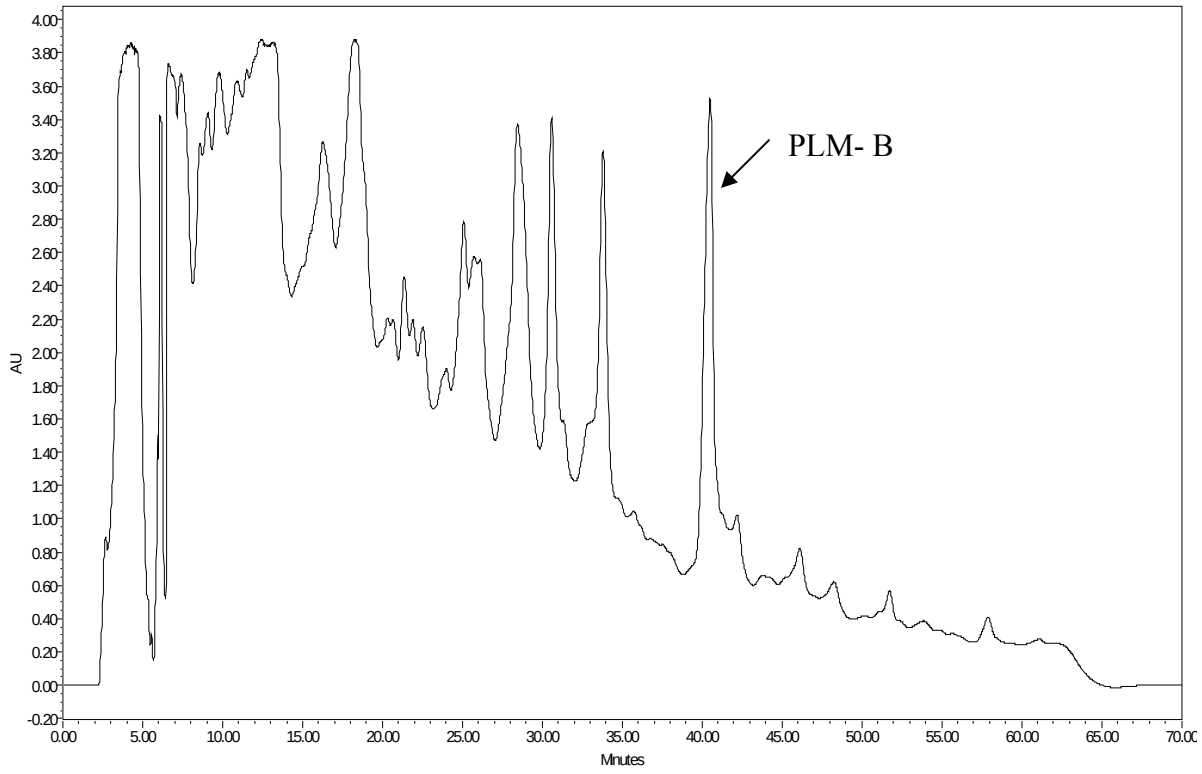

Figure 6. HPLC chromatogram of crude PLM-B using a semi preparative C-18 column

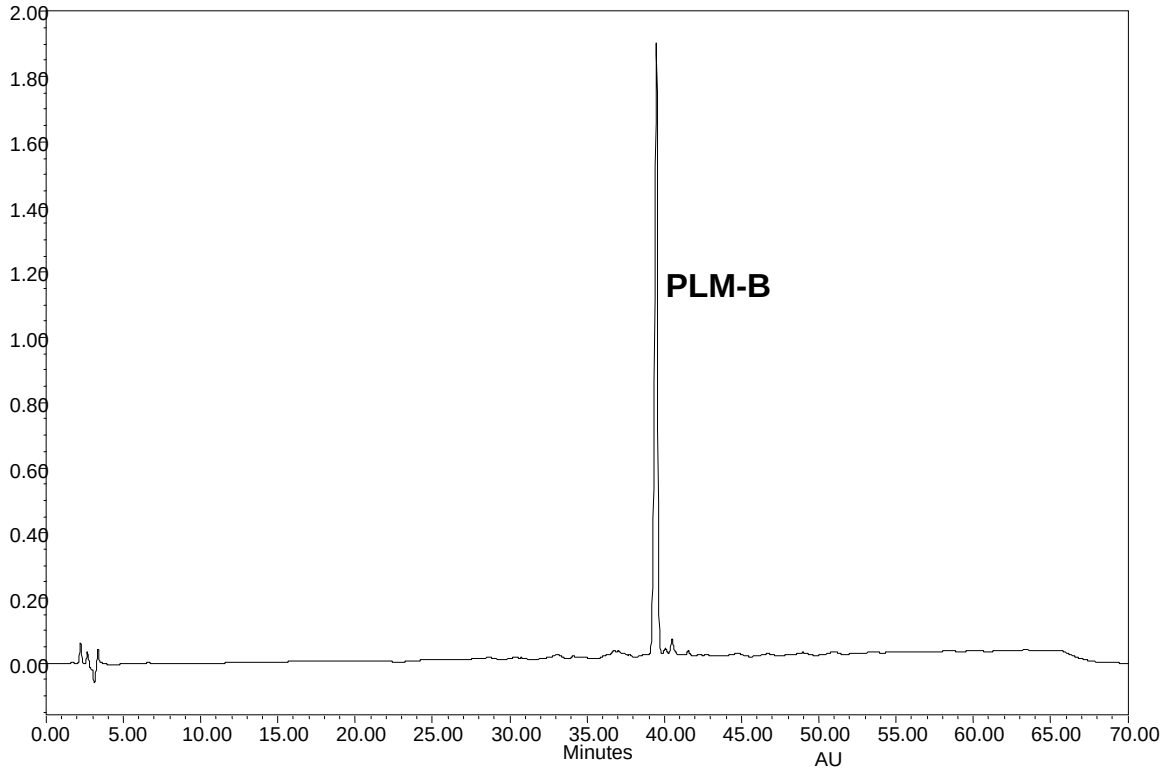

Figure 7. HPLC chromatogram of purified PLM-B using a C-18 analytical column.

UV Quantification of PLM-B Production

To be able to quantify the yield of PLM-B from the fermentation, a UV spectrum was obtained for 2mg/L of PLM-B. This analysis demonstrated that PLM-B in methanol exhibited a λ_{max} at 235 nm ($\varepsilon = 0.3180 \times 10^{-4}$L mole^{-1}cm^{-1}) [Figure 8]. A standard plot of concentration versus area is shown in Figure 9 was obtained by analyzing specific dilutions of 3.89×10^{-2}mM of PLM-B. Using this plot we determined the yield of PLM-B from a single fermentation was approximately 10mg/L from which 2mg/L were obtained after purification.

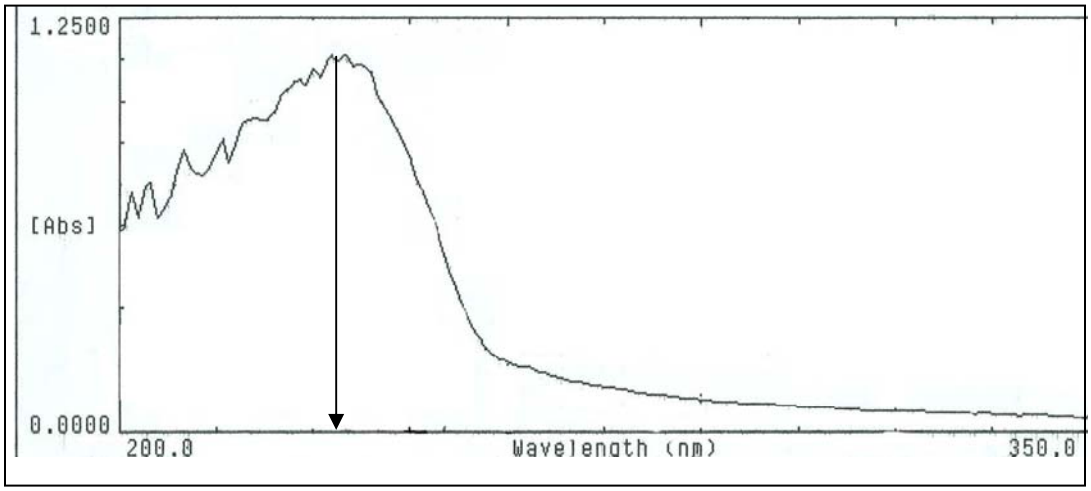

Figure 8. UV spectrum of PLM-B with maximal absorbance at 235 nm.

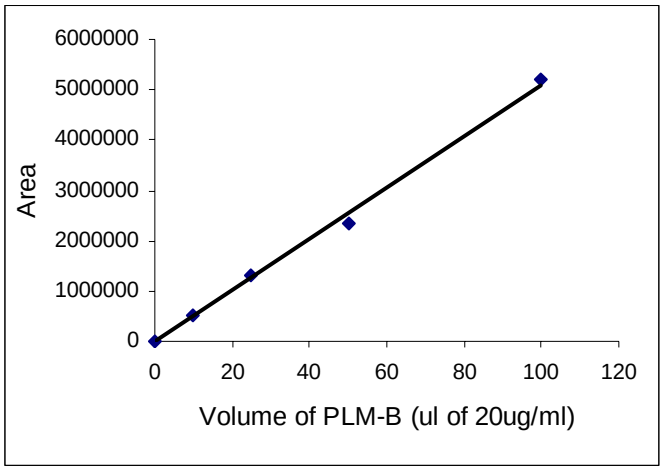

Figure 9. Standard curve for the quantification of PLM-B by HPLC (Slope = 50931).

Kinetic Analysis of PLM-B Degradation

The aqueous stability of PLM-B was determined at 50°C and 30°C by measuring the disappearance of the PLM-B peak in the HPLC analysis. The decomposition of PLM-B at

30°C was slowest in the pH range of 5-8. However, because the decomposition was so slow at 30°C significant evaporation of H_2O/ methanol from the reaction vials occurred during the incubations. To obtain reasonable estimates of the rate of decomposition it was important to monitor the disappearance of PLM-B for at least 2-3 half-lives. Therefore, the additional stability study was carried out at 50°C.

The 50°C time profile for the disappearance of PLM-B at varying pH is shown in Figures 10-18 and tabulated in Tables 1- 9. The rate of reaction for the decomposition of PLM-B was determined by regression analysis at all pH and temperatures. The rate of disappearance of PLM-B, half-life and correlation coefficient at 50°C and 30°C are indicated in Table 10.

(A)

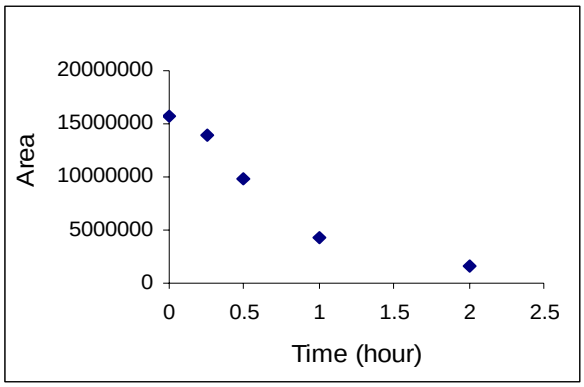

(B)

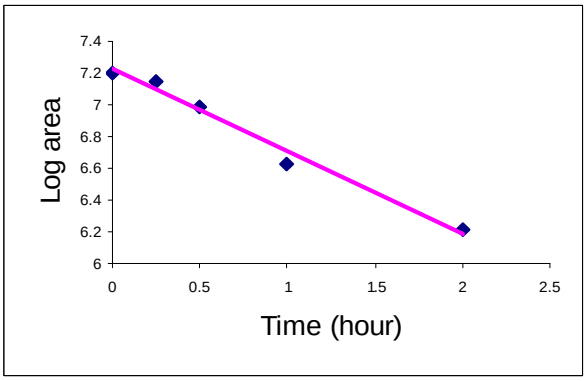

Figure 10. (A) Time profile and (B) Semilogarithmic plot for decomposition of PLM-B (6.1µg/mL) at pH 2.0 in KCl – HCl buffer (0.1M) (50°C).

Table 1. Decomposition of PLM-B at pH 2.0 as a function of time as determined by peak areas in an HPLC analysis

Time(h)	Area	log area
0	1.6E+07	7.198
0.25	1.4E+07	7.142
0.5	9743756	6.988
1	4294778	6.632
2	1617220	6.208

(A)

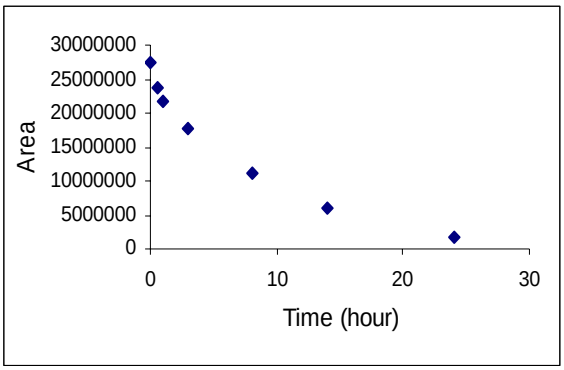

(B)

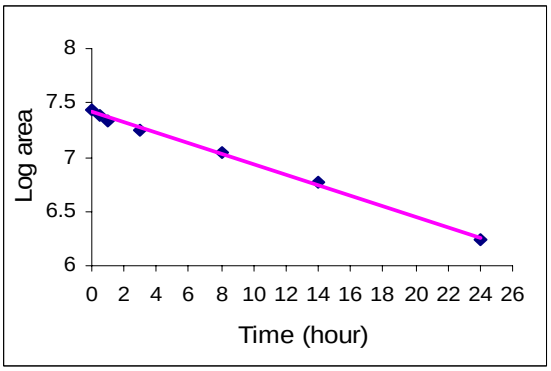

Figure 11. (A) Time profile and (B) Semilogarithmic plot for decomposition of PLM-B (10.5µg/mL) at pH 3.0 in glycine -HCl buffer (0.1M) (50°C).

Table 2. Decomposition of PLM-B at pH 3.0 as a function of time as determined by peak areas in an HPLC analysis.

Time(h)	Area	log area
0	27336508	7.436
0.5	23826827	7.377
1	21813431	7.338
3	17823328	7.250
8	11035928	7.042
14	5976224	6.776
24	1723489	6.236

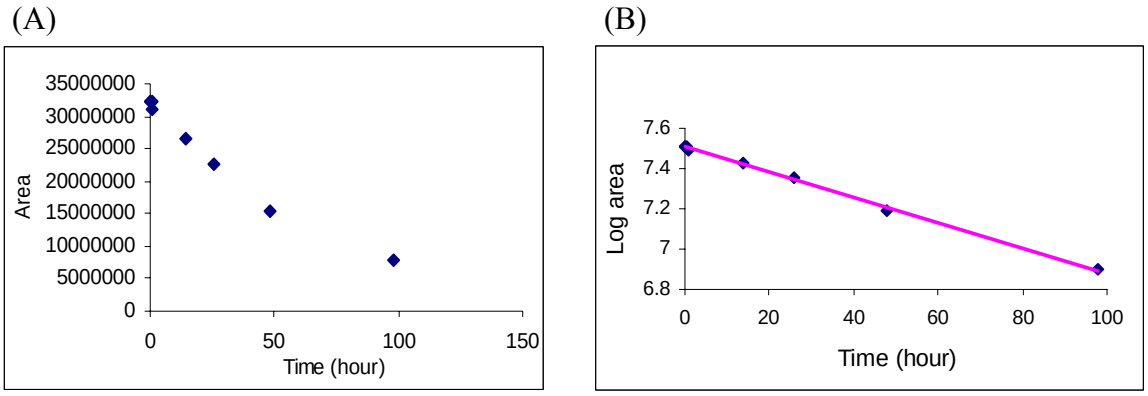

Figure 12. (A) Time profile and (B) Semilogarithmic plot for decomposition of PLM-B (12.4µg/mL) at pH 4.0 in sodium citrate-citric acid buffer (0.1M) (50°C).

Table 3. Decomposition of PLM-B at pH 4.0 as a function of time as determined by peak areas in an HPLC analysis.

Time(h)	Area	log area
0	32254601	7.508
0.5	32354925	7.509
1	31156061	7.493
14	26669154	7.426
26	22562713	7.353
48	15427673	7.188
98	7944500	6.900

(A)

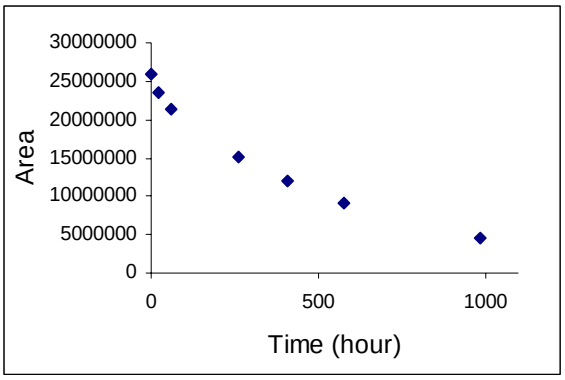

(B)

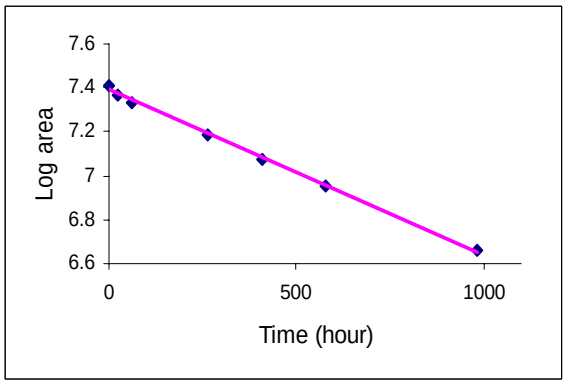

Figure 13. (A) Time profile and (B) Semilogarithmic plot for decomposition of PLM-B (10.0µg/mL) at pH 5.0 in potassium phosphate buffer (0.1M) (50°C).

Table 4. Decomposition of PLM-B at pH 5.0 as a function of time as determined by peak areas in an HPLC analysis.

Time(h)	Area	log area
0	25943996	7.414
24	23525480	7.371
60	21461332	7.331
262	15238608	7.182
408	11928142	7.076
576	9059703	6.957
984	4565000	6.659

(A) (B)

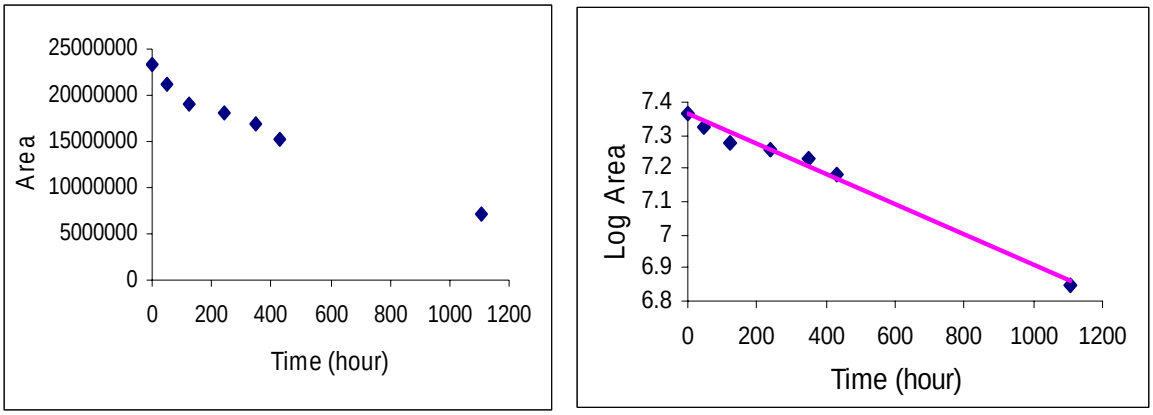

Figure 14. (A) Time profile and (B) Semilogarithmic plot for decomposition of PLM-B (9.0µg/mL) at pH 6.0 in potassium phosphate buffer (0.1M) (50°C).

Table 5. Decomposition of PLM-B at pH 6.0 as a function of time as determined by peak areas in an HPLC analysis.

Time(h)	Area	log area
0	23381840	7.368
48	21071752	7.323
123	19023948	7.279
240	18188839	7.259
348	17017286	7.230
432	15300506	7.184
1104	7033899	6.847

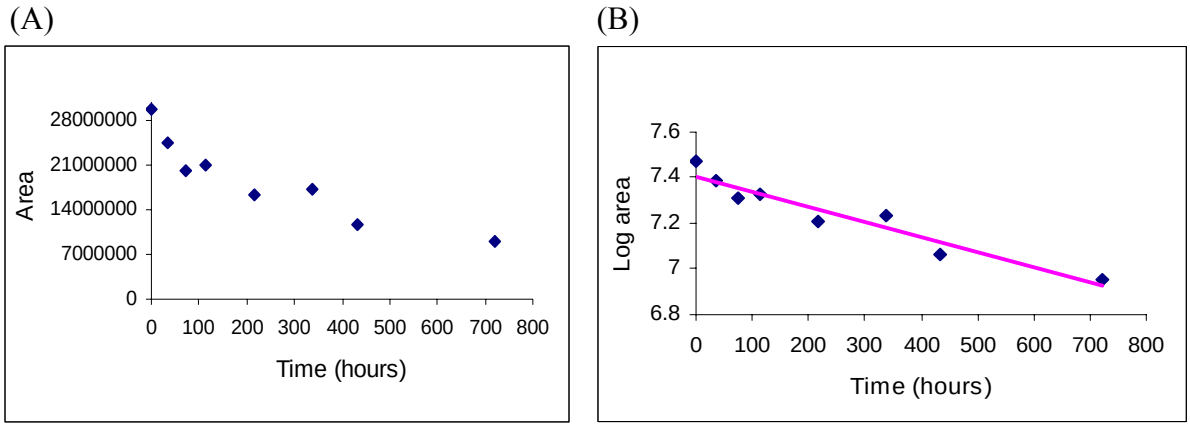

Figure 15. (A) Time profile and (B) Semilogarithmic plot for decomposition of PLM-B (11.5µg/mL) at pH 7.0 in potassium phosphate buffer (0.1M) (50°C).

Table 6. Decomposition of PLM-B at pH 7.0 as a function of time as determined by peak areas in an HPLC analysis.

Time	Area	log area
0	29915921	7.475
36	24579822	7.390
73	20281547	7.307
112	21166012	7.325
216	16282111	7.211
336	17269229	7.237
432	11569656	7.063
720	8927490	6.950

(A)

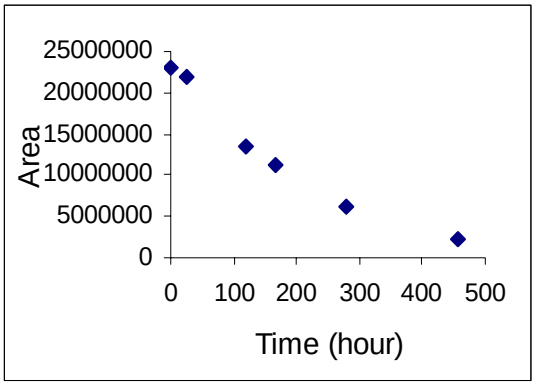

(B)

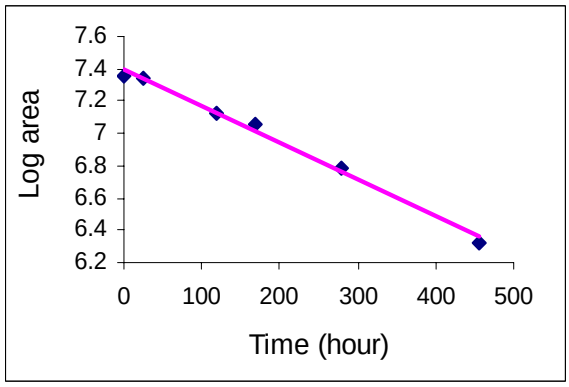

Figure 16. (A) Time profile and (B) Semilogarithmic plot for decomposition of PLM-B (8.8µg/mL) at pH 8.0 in KH_2PO_4- NaOH buffer (0.1M) (50°C).

Table 7. Decomposition of PLM-B at pH 8.0 as a function of time as determined by peak areas in an HPLC analysis.

Time (hr)	Area	Log Area
0	22907232	7.359
24	21808588	7.338
120	13408061	7.127
168	11242790	7.050
280	6074919	6.783
456	2118518	6.326

(A) (B)

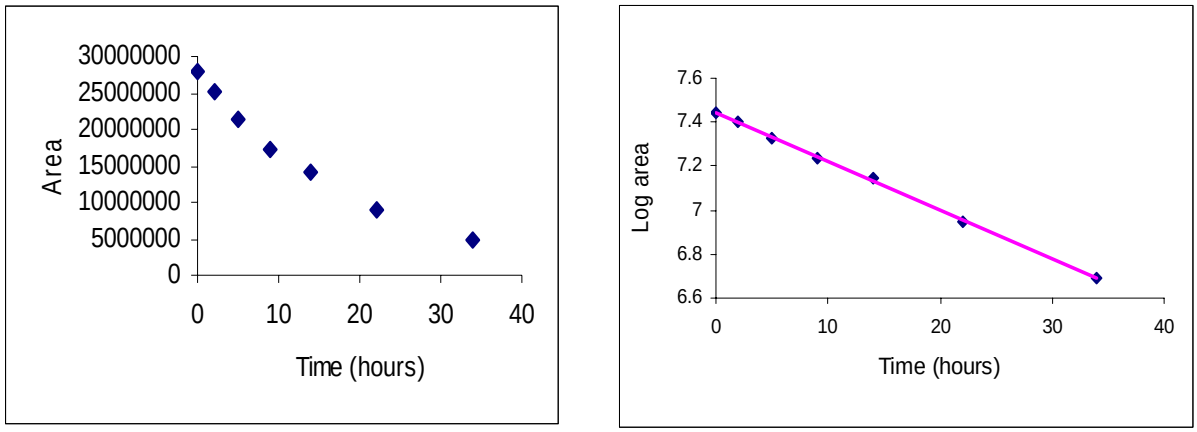

Figure 17. (A) Time profile and (B) Semilogarithmic plot for decomposition of PLM-B (10.7µg/mL) at pH 9.0 in KCl- H_3BO_3- NaOH buffer (0.1M) (50°C).

Table 8. Decomposition of PLM-B at pH 9.0 as a function of time as determined by peak areas in an HPLC analysis.

Time	Area	log area
0	27835566	7.444
2	25289887	7.402
5	21438891	7.331
9	17186454	7.235
14	14089871	7.148
22	8867375	6.947
34	4933724	6.693

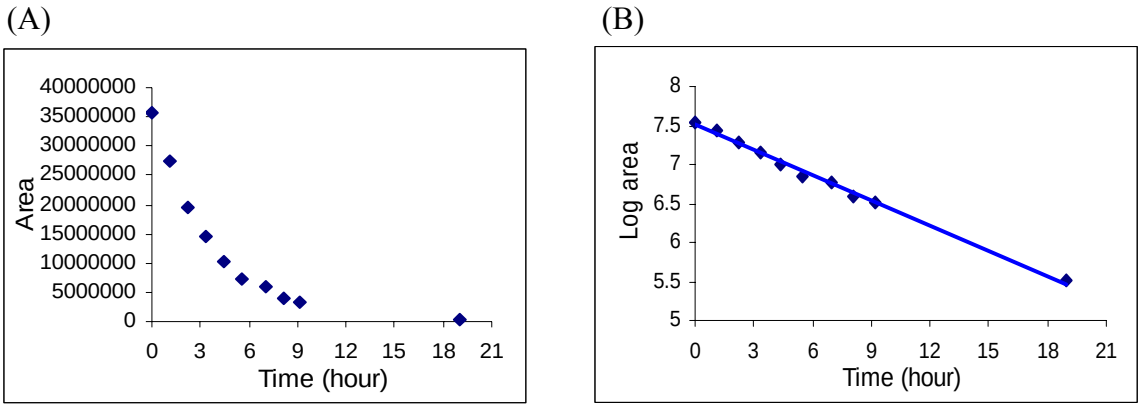

Figure 18. (A) Time profile and (B) Semilogarithmic plot for decomposition of PLM-B(13.7µg/mL) at pH 10 at 50°C in carbonate -bicarbonate buffer (0.1M).

Table 9. Decomposition of PLM-B at pH 10.0 as a function of time as determined by peak areas in an HPLC analysis.

Time	Area	log area
0	35548791	7.550
1.1	27302093	7.436
2.2	19533280	7.290
3.3	14522978	7.162
4.4	10250039	7.010
5.5	7216871	6.858
7	5853039	6.767
8.1	3850829	6.585
9.2	3164701	6.500
19	318655	5.503

(A)

pH	k_{OBS} (h^{-1})	$t_{1/2}$ (hr)	r^2
2.0	8.01×10^{-2}	8.65	0.99
5.0	8.0×10^{-4}	8662 *	0.37
7.4	1.0×10^{-4}	6930 *	0.56
8.0	2.0×10^{-4}	3465 *	0.03
9.0	1.4×10^{-3}	495	0.87
10.0	2.02×10^{-2}	34	0.98

(B)

pH	k_{OBS} (hr^{-1})	$t_{1/2}$ (hr)	r^2
2.0	5.19×10^{-1}	1.33	0.98
3.0	4.49×10^{-2}	15.4	0.99
4.0	6.30×10^{-3}	110	0.95
5.0	7.00×10^{-4}	990	0.92
6.0	4.00×10^{-4}	1730	0.98
7.0	7.00×10^{-4}	990	0.91
8.0	2.30×10^{-3}	301	0.99
9.0	2.22×10^{-2}	31.2	0.94
10.0	4.30×10^{-2}	9.40	0.99

Table 10. Pseudo first-order degradation rate constants, half lives and calculated correlation coefficient (r^2) for acid and basic degradation of PLM-B at (A) 30°C and (B) 50°C. * represents estimated values only.

pH Effects on PLM-B Degradation

The rate of disappearance of PLM-B in aqueous buffers was dependent on the solution pH. Using the k_{OBS} from Tables 10 A and B, the rate constant-pH profiles for the degradation of PLM-B at 30°C and 50°C was obtained (Figure 19). The pH-rate constant profile was U-shaped, showing a marked dependence of the degradation rate on pH.

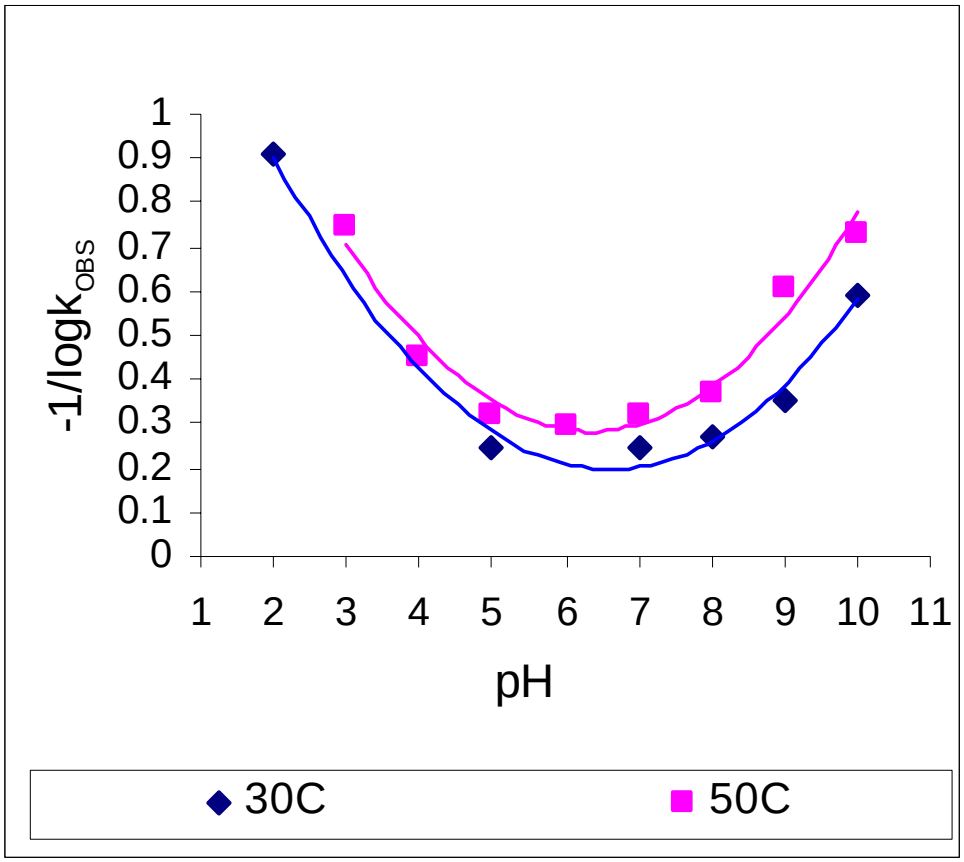

Figure 19. Plot showing the rate constant-pH profile for the degradation of PLM-B at temperature 50ºC and 30ºC.

From the rate constant-pH profile, it can be concluded that the rate of degradation was faster at high and low pH (k_{OBS} = 0.5193 hr^{-1} at pH 2.0 and k_{OBS} = 0.0430hr^{-1} at pH 10.0), whereas in the pH range 5-7, PLM-B exhibited relatively slow degradation. The pH of maximum stability is pH 6.0 with k_{OBS} = 0.0004 hr^{-1} (50ºC) ($t_{1/2}$ = 72 days); approximately three orders of magnitude slower than at either pH 2.0 or 10.0.

For the U shaped graphs, k_{OBS} at a given pH can be defined as $k_{OBS} = k_H \times 10^{-pH} + k_{OH} \times 10^{pH-14}$ where k_H and k_{OH} are the rate constants (see Scheme 1 for the derivation).

Let $I \xrightarrow{H_3O^+} I'$ (where I = PLM B, I'= acid degraded product)

$I \xrightarrow{OH^-} I''$ (I'' = base degraded product)

$$-d[I]/dt = k_H [I] [H_3O^+] + k_{OH} [I] [OH^-]$$

$$= (k_H [H_3O^+] + k_{OH} [OH^-]) [I]$$

Integrating both sides,

$$\int_{[I]_0}^{[I]} -d[I]/[I] = \int_0^t (k_H [H_3O^+] + k_{OH} [OH^-])$$

$$\ln [I]/[I]_0 = -(k_H [H_3O^+] + k_{OH} [OH^-]) t$$

$$[I] = [I]_0 \, e^{-(k_H [H_3O^+] + k_{OH} [OH^-]) t}$$

Therefore,

$$k_{OBS} = k_H \, M^{-1} h^{-1} \times [H_3O^+] M + k_{OH} M^{-1} h^{-1} \times [OH^-] M$$

$$k_{OBS} = k_H \times 10^{-pH} + k_{OH} \times 10^{pH-14}$$

Scheme 1. Derivation of the rate equation for acid and base catalysed reaction.

Using the above mathematical expression two independent rate constants, k_H and k_{OH} can be determined by Sigma plots. In the sigma plot k_{OBS} is plotted against pH and thus k_H and k_{OH} are obtained (by fitting). k_{EST} at each pH can then be also obtained by sigma plot using these k_H and k_{OH} values and gives an excellent correlation with k_{OBS} (Table 11 and 12). The observed and estimated rate constant- pH profiles for the degradation of PLM-B at 30°C and 50°C are shown in Figures 20 and 21.

PLM-B was found to be 10-15 times more stable in acid than in base at 30°C and 50°C. Comparing k_H and k_{OH} values, PLM B was found to be more stable at 30°C than at 50°C.

Using the Arrhenius equation [54] the activation energy in the basic pH (11884 Kcal/mole) was found to be much lower than in acidic pH (16322 Kcal/mole) consistent with a faster reaction under basic pH conditions.

The pH at the minimum of the U shaped graph is found by differentiating the expression $k_{OBS} = k_H \times 10^{-pH} + k_{OH} \times 10^{pH-14}$ and setting the derivative equal to zero; the result is $pH_{min} = ½\ pk_w - ½ \log k_{OH}/ k_H$. This equation can be used to calculate the pH of maximum stability [54]. The pH of maximum stability for PLM-B at 50°C and 30°C were found to be 6.6 and 7.3, respectively, consistent with the observation of slowest degradation at pH 6 and 7.

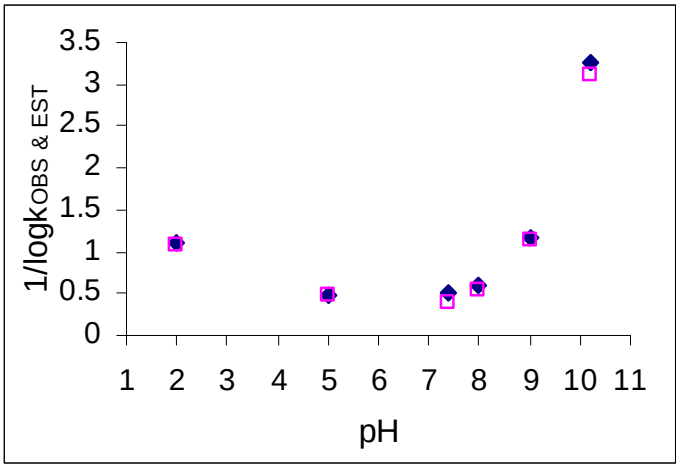

Figure 20. Plot showing the observed (♦) and estimated (□) rate constant-pH profile for the degradation of PLM-B at temperature 30°C.

Table 11. Observed rate constants at varying pH and estimated k_{OBS} (30°C).

pH	k_{OBS}	100x k_{OBS}	k_{EST}
2.0	0.0801	8.01	8.446
5.0	0.00008	0.008	0.008
7.4	0.0001	0.01	0.003
8.0	0.0002	0.02	0.013
9.0	0.0014	0.14	0.132
10.2	0.0202	2.02	2.096

At 30°C, $k_{OBS} = k_H \times 10^{-pH} + k_{OH} \times 10^{pH-14}$

Regression analysis $k_H = 8.4 \pm 0.1\ M^{-1}\ h^{-1}$; $k_{OH} = 132 \pm 3\ M^{-1}\ h^{-1}$

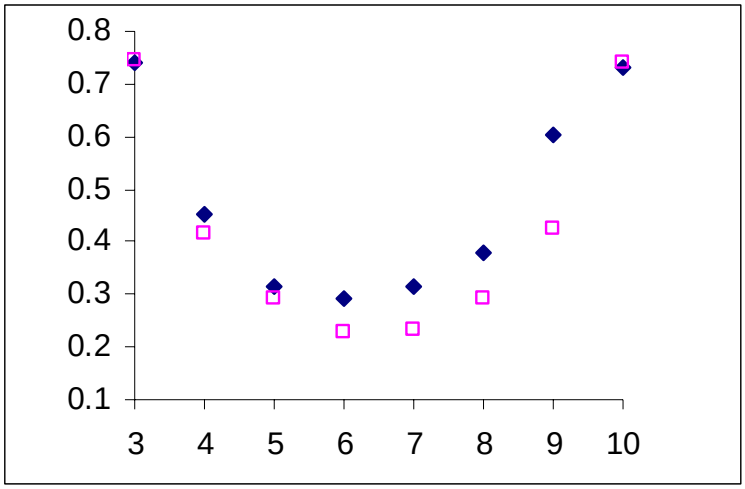

Figure 21. Plot showing the observed (♦) and estimated (□) rate constant-pH profile for the degradation of PLM-B at temperature 50°C.

Table 12. Observed rate constants at varying pH and estimated $k_{OBS.}$(50°C)

pH	k_{OBS}	k_{EST}
3.0	0.0449	0.045
4.0	0.0063	0.004
5.0	0.0007	0.0004
6.0	0.0004	0.00004
7.0	0.0007	0.000049
8.0	0.002	0.0004
9.0	0.022	0.0044
10.0	0.043	0.0447

At 50°C, $k_{OBS} = k_H \times 10^{-pH} + k_{OH} \times 10^{pH-14}$

Regression analysis $k_H = 45 \pm 7\ M^{-1}\ h^{-1}$; $k_{OH} = 448 \pm 73\ M^{-1}\ h^{-1}$.

HPLC Analysis of PLM-B Degradation Products

As described above, PLM-B (Figure 1) was found to degrade in solution at both acidic and basic pH. Three different degradation products **3**, **4**, and **5** were formed from pH range of 7 to 10 (Figure 22). From pH 2.0 to 5.0, three different degradation products **6**, **7** and **8** were evident in the HPLC chromatograms (Figure 23). At pH of 6.0 all six degradation products were observed when PLM-B was decomposed at 30°C (Figure 24).

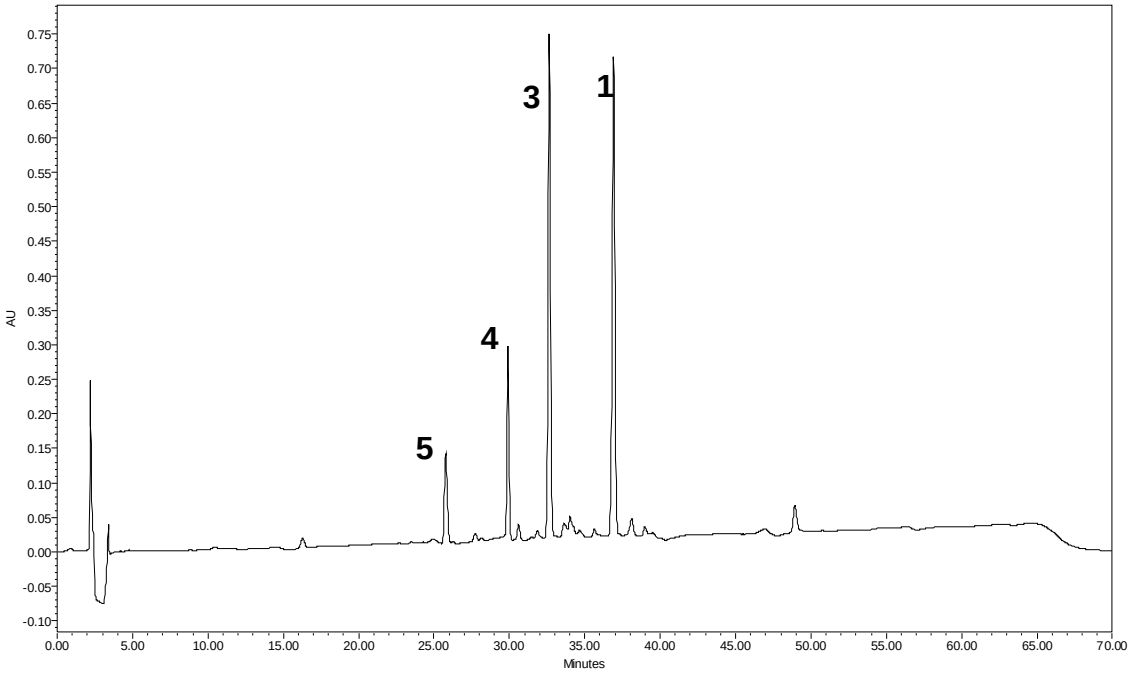

Figure 22. Typical HPLC chromatogram of degradation of **1** at pH 10.0. Degradation products are denoted by **3**, **4** and **5**.

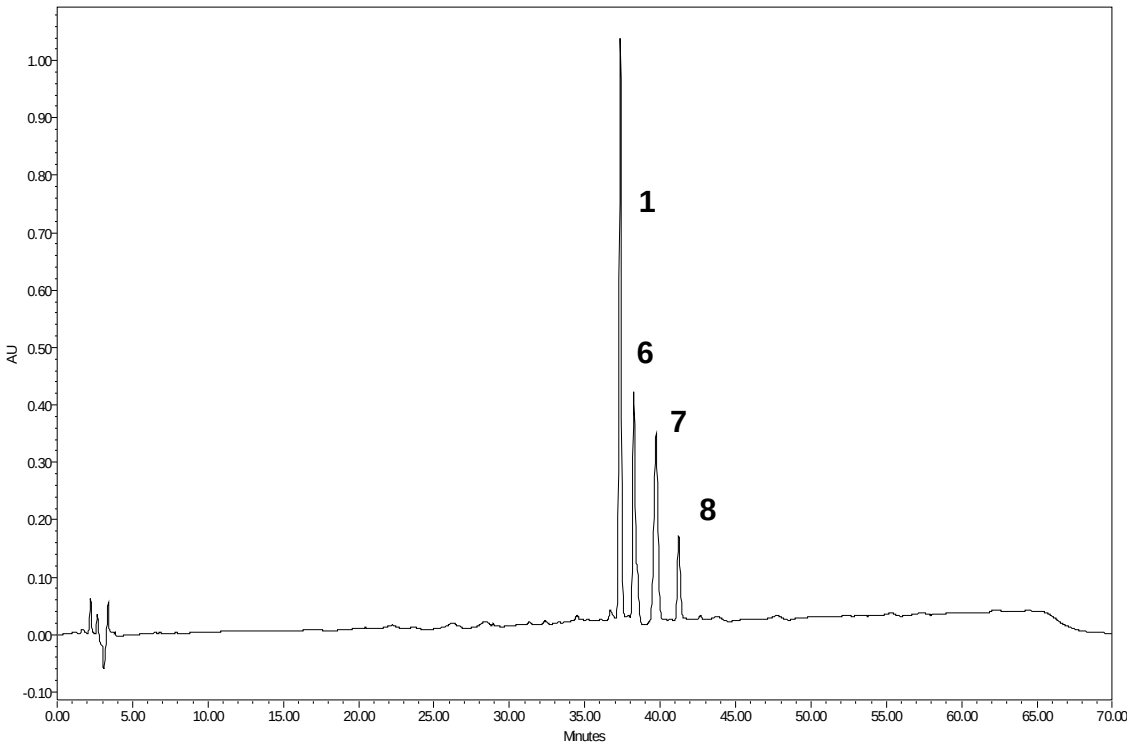

Figure 23. Typical HPLC chromatogram of degradation of **1** at the pH 2.0. Degradation products are denoted by **6**, **7** and **8**.

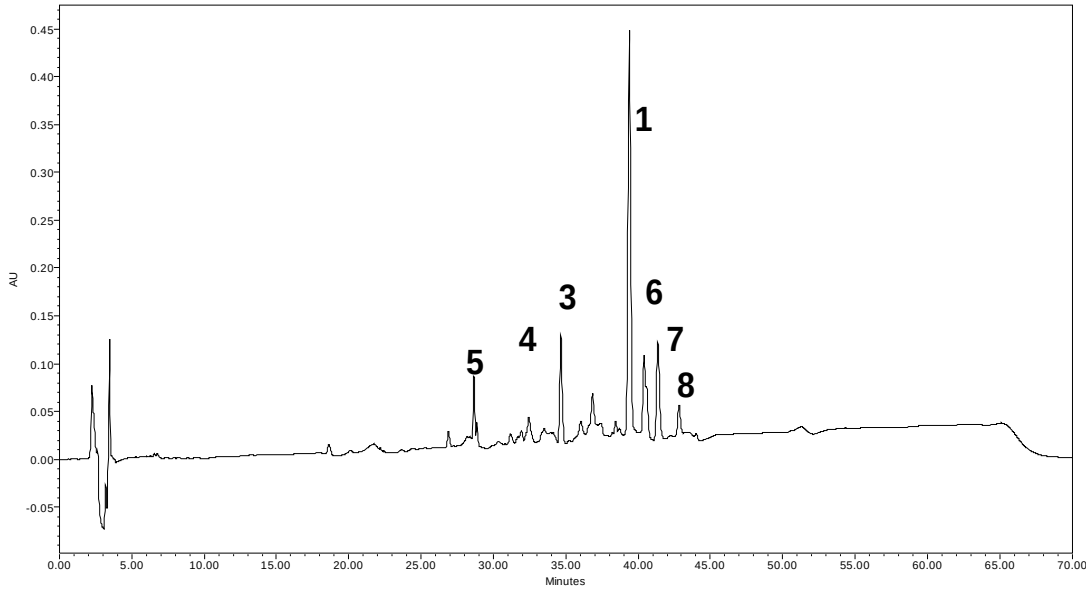

Figure 24. Typical chromatogram for PLM-B degradation at pH 6.0.

Relative Rates of formation of the PLM-B Basic Degradation Products **3**, **4** and **5**

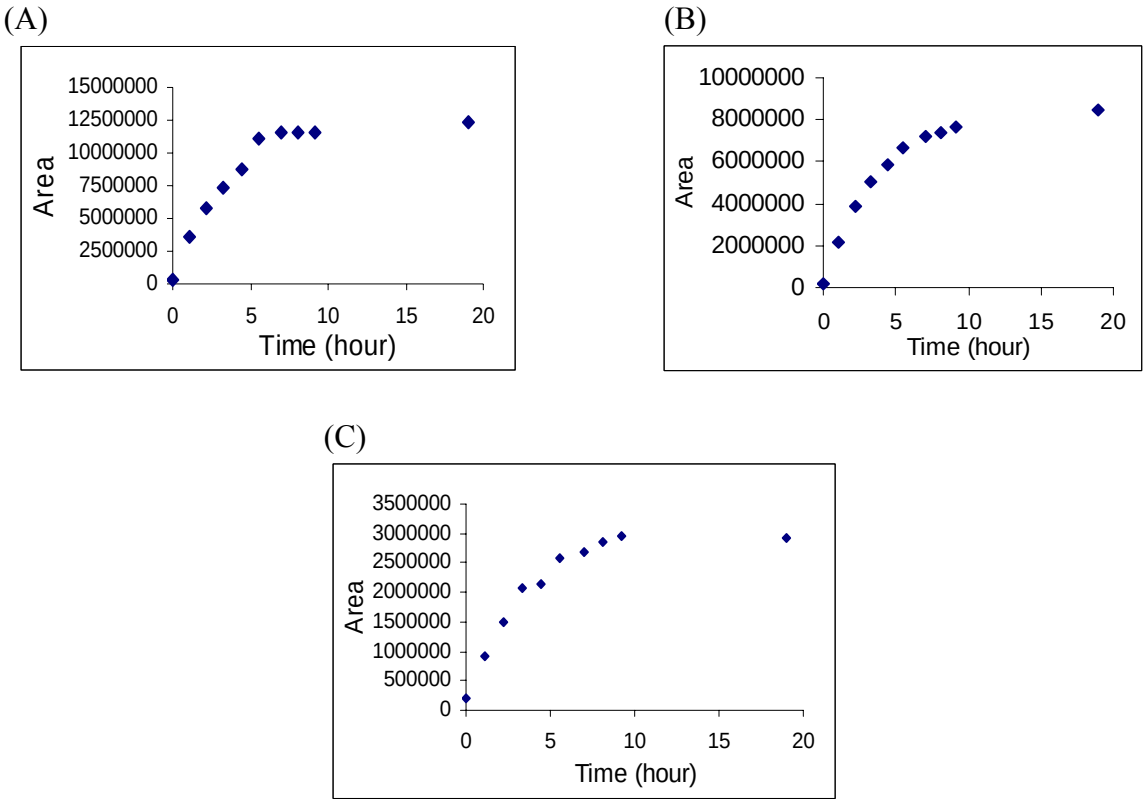

Figure 25. Representative time profile for the formation of the degradation products **3**, **4**, **5** at pH 10.0 (50°C).

Table 13. Formation of degradation products **3**, **4**, **5** at pH 10.0 as a function of time as determined by peak areas in an HPLC analysis.

Time (hour)	Area **3**	Area **4**	Area **5**
0	245409	203207	217946
1.1	3637384	2137548	911677
2.2	5720191	3838197	1483588
3.3	7289664	5024671	2063680
4.4	8714546	5833528	2145246
5.5	11078282	6682420	2579228
7.0	11621491	7179174	2692052
8.1	11592047	7393747	2853236
9.2	11597011	7620810	2956342
19	12338607	8495203	2934660

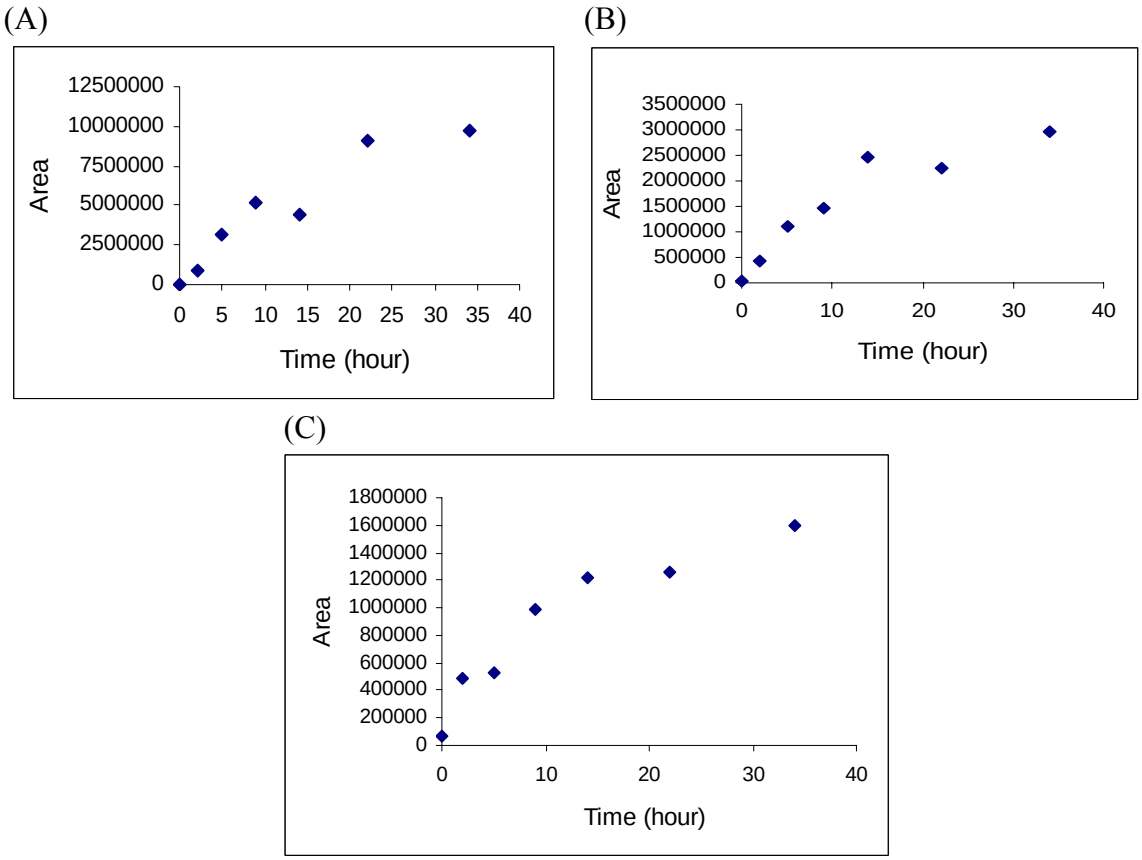

Figure 26. Representative time profile for the formation of the degradation products **3**, **4**, **5** at pH 9.0 (50°C).

Table 14. Formation of degradation products **3**, **4**, **5** at pH 9.0 as a function of time as determined by peak areas in an HPLC analysis.

Time (hour)	Area **3**	Area **4**	Area **5**
0	460056	40132	70344
2	853018	427597	488583
5	3144900	1091255	527646
9	5114702	1446964	981222
14	4413680	2464096	1215633
22	9092412	2262476	1257880
34	9757873	2976990	1601257

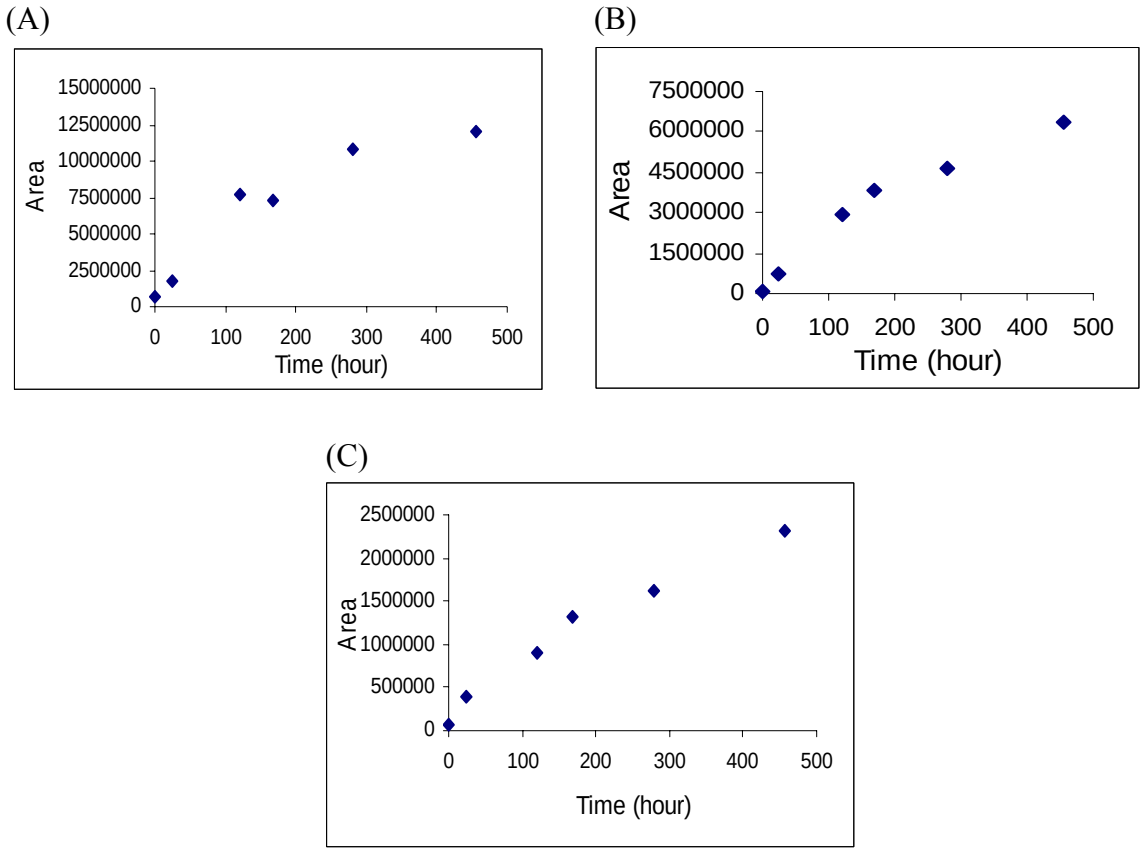

Figure 27. Representative time profile for the formation of the degradation products **3**, **4**, **5** at pH 8.0 (50°C).

Table 15. Formation of degradation products **3**, **4**, **5** at pH 8.0 as a function of time as determined by peak areas in an HPLC analysis.

Time (hour)	Area **3**	Area **4**	Area **5**
0	711945	46597	61960
24	1789408	770237	392581
120	7707858	2911709	902857
168	7245286	3797329	1316011
280	10788893	4629876	1614466
456	12045056	6327361	2321257

Representative plots of formation of degradation products **3**, **4** and **5** at pH of 8-10 are shown in Figures 25-27. The rate of formation of all three products increases with the increase in pH. All of these plots appear non linear. In Figure 28A a histogram of the peak area associated with the degradation products formed after 24 hours at pH 8.0, 9.0 and 10.0. The relative formation of degradation products was **3** > **4** > **5** at all basic pH conditions. The extinction coefficient of product **3** is predicted to be about 50% more compared to product **4** and **5**, due to the presence of the α, β unsaturated acid (see discussion later on structures). Thus the actual amount of **3** relative to **4** and **5** is likely to be even greater.

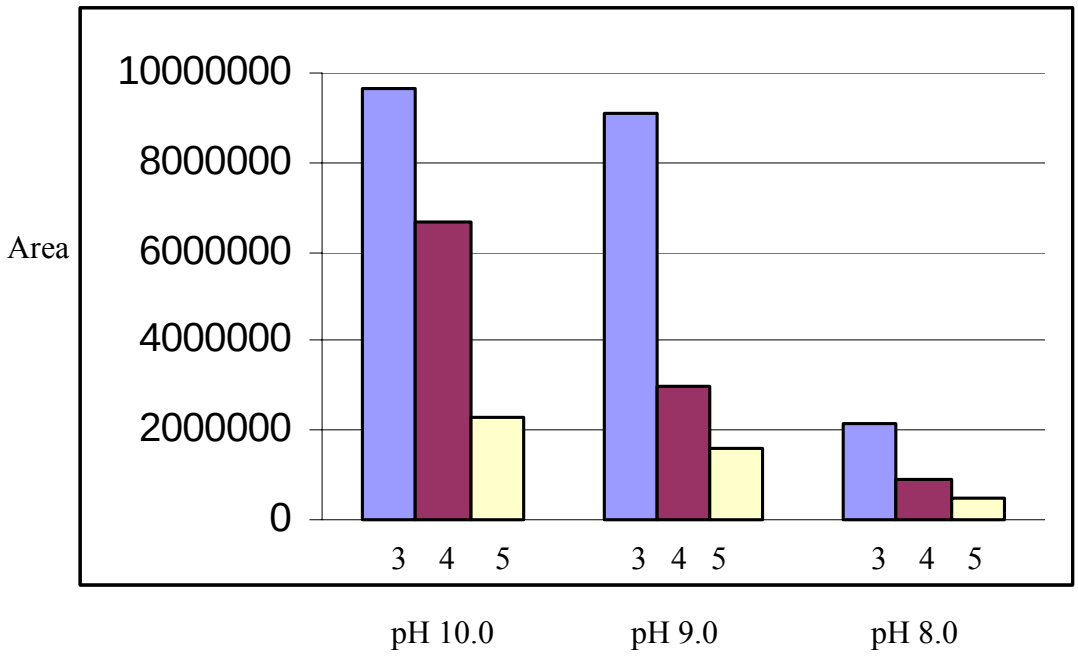

Figure 28A. Histogram representing the degradation products **3**, **4** and **5** formed at pH 10.0, 9.0 and 8.0 after 24 hours.

Relative Rates of Acid Degradation Products **6**, **7** and **8**.

Similarly, the rate of formation of the acidic degradation products **6**, **7** and **8** was found to increase with the decrease in pH (Figures 29-31). At the end of the degradation the amount of products based on HPLC area was consistent **7** > **6** > **8**. But the ratio was **6** > **7** > **8** initially as product **6** was formed faster in the initial stages of acid catalyzed degradation reaction. This is shown in the histogram (Figure 29) representing the degradation products **6**, **7** and **8** formed at pH 3.0, 4.0 and 5.0 where the ratio is **7** > **6** > **8** at pH 3.0 due to faster rate of degradation of PLM-B in contrast to the ratio **6** > **7** > **8** at pH 4.0 and 5.0 after 24 hours. All the plots appear non linear.

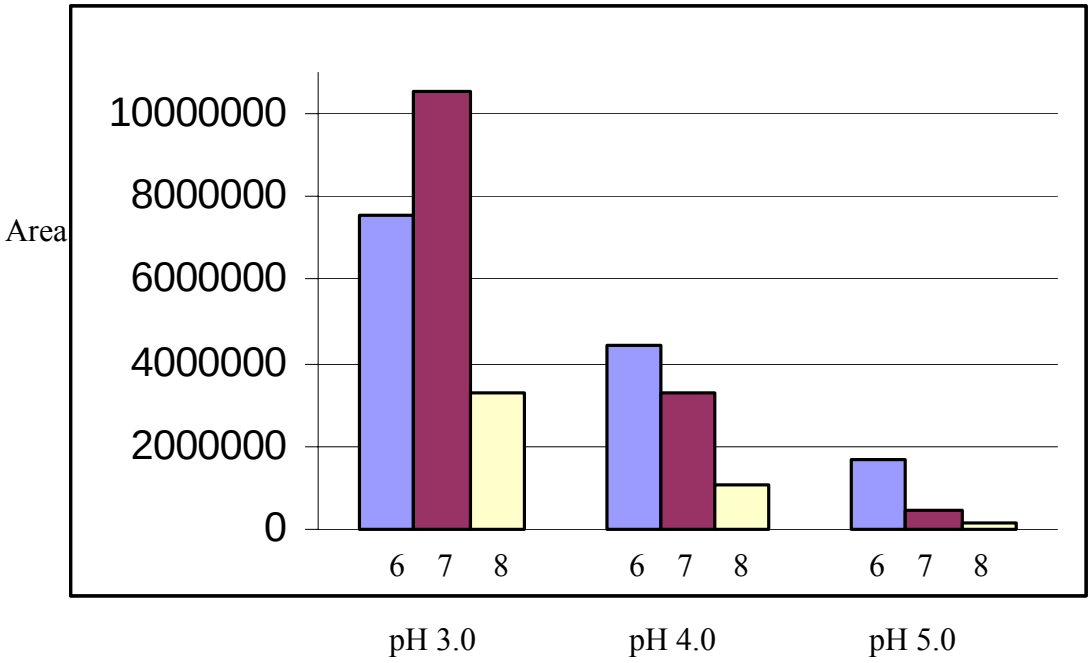

Figure 28B. Histogram representing the degradation products **6**, **7** and **8** formed at pH 3.0, 4.0 and 5.0 after 24 hours.

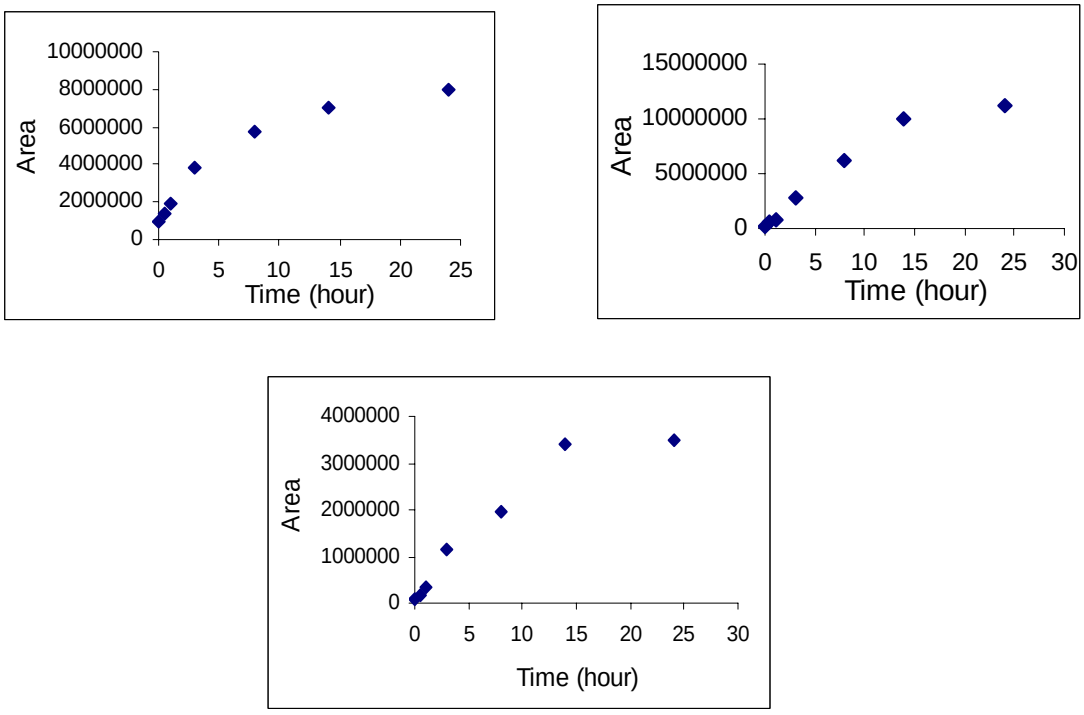

Figure 29. Representative time profile for the formation of the degradation products **6**, **7**, **8** at pH 3.0 (50°C).

Table 16. Formation of degradation products **6**, **7**, **8** at pH 3.0 as a function of time as determined by peak areas in an HPLC analysis.

Time (hour)	Area **6**	Area **7**	Area **8**
0	1002269	268288	75020
0.5	1422795	518348	161511
1	1880138	757981	325790
3	3857504	2724209	1156901
8	5700102	6223690	1957629
14	7072786	9933376	3399766
24	8026297	11196139	3501414

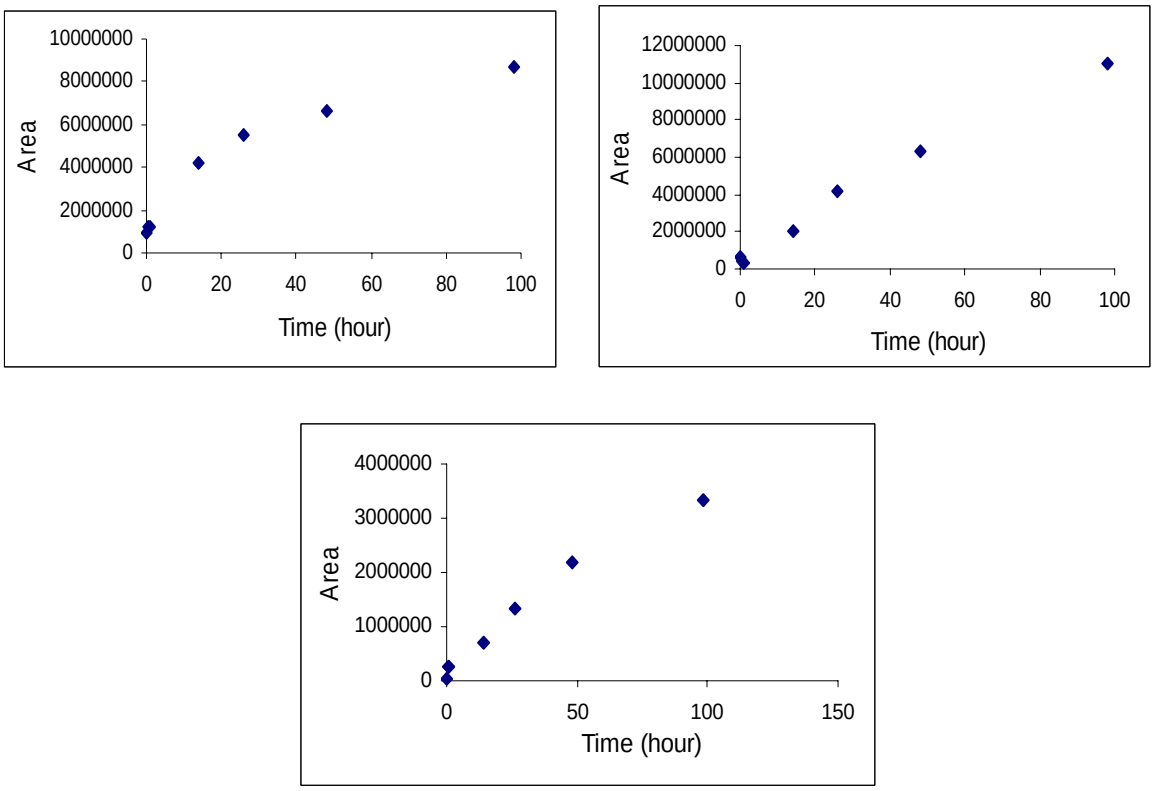

Figure 30. Representative time profile for the formation of the degradation products **6**, **7**, **8** at pH 4.0 (50°C).

Table 17. Formation of degradation products **6**, **7**, **8** at pH 4.0 as a function of time as determined by peak areas in an HPLC analysis.

Time (hour)	Area **6**	Area **7**	Area **8**
0	961094	621372	43634
0.5	1210724	429348	261247
1	1242234	359857	241792
14	4178524	2038658	708783
26	5542972	4134390	1324712
48	6666250	6273698	2202882
98	8733030	11020266	3338381

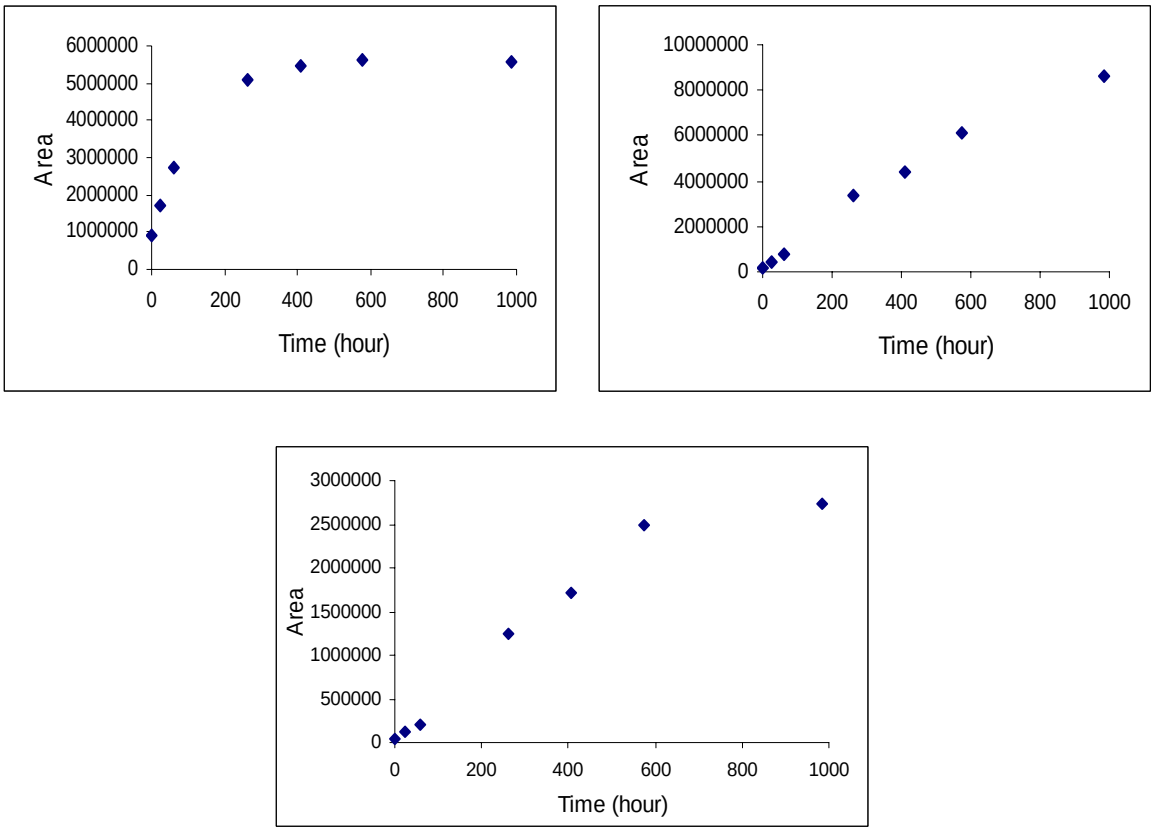

Figure 31. Representative time profile for the formation of the degradation products **6**, **7**, **8** at pH 5.0 (50°C).

Table 18. Formation of degradation products **6**, **7**, **8** at pH 5.0 as a function of time as determined by peak areas in an HPLC analysis.

Time (hour)	Area **6**	Area **7**	Area **8**
0	909236	209063	32143
24	1701861	455968	121962
60	2710789	777831	207868
262	5114166	3364650	1251212
408	5457861	4376189	1715894
576	5609567	6085410	2496409
984	5592505	8613119	2732892

Chemical Analysis of PLM-B

For confirmation of the structure of PLM-B, MS, ^{1}H NMR, ^{1}H-^{1}H COSY and HSQC (Figures 33-35) analysis were carried out. Initially, the LC/MS spectra of PLM-B was obtained in both positive and negative ESI mode (*m/z* 514 $[M+H]^{+}$, *m/z* 512 $[M-H]^{-}$) to evaluate detection conditions for phoslactomycins (Figure 32).

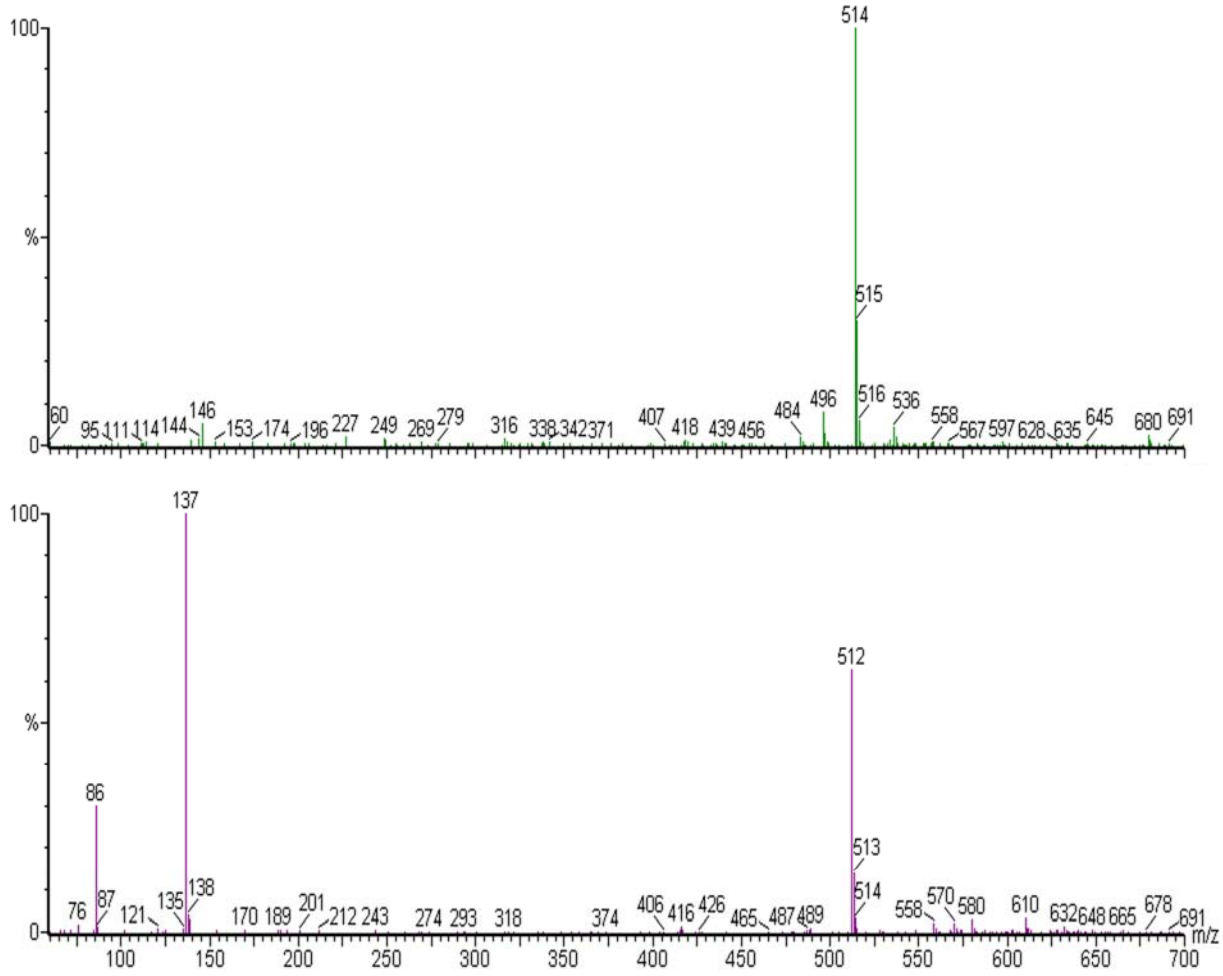

Figure 32. Mass spectroscopic analysis of PLM-B in both positive and negative ESI mode confirming the molecular mass of 513.

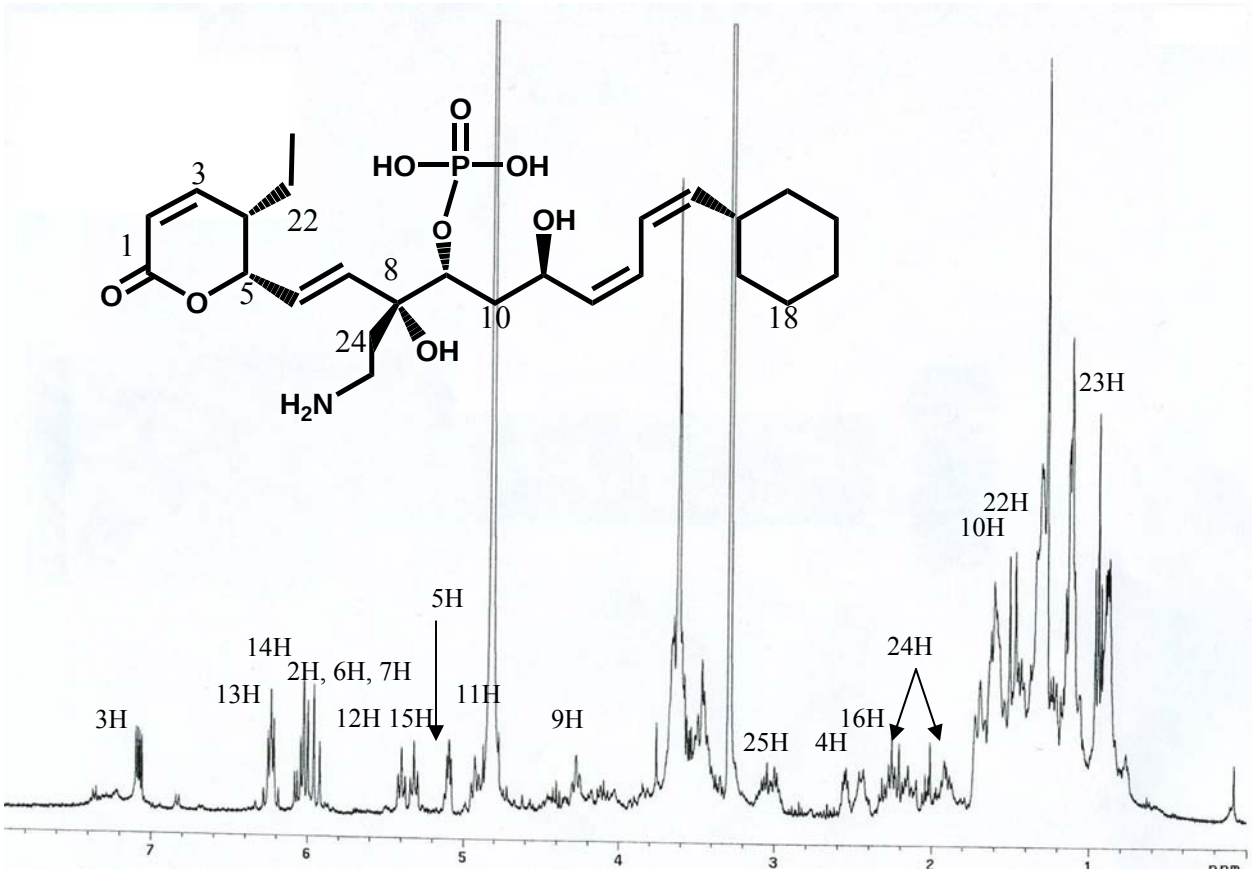

Figure 33. ^{1}H NMR of PLM-B (**1**).

The ^{1}H NMR of PLM-B is shown in Figure 33 and was used to aid in the identification of the decomposition products (Table 19). The proton and ^{13}C NMR have previously been reported [63] for PLM-B and were consistent with the assignment done in this study using the ^{1}H -^{1}H COSY (Figure 34) and HSQC analyses (Figure 35 A and B).

Table 19. ^{1}H NMR spectral data for PLM-B.

δ (ppm)	Assignment
7.09	3-H
6.2~6.32	13,14 -H
6.04	6-H
6.09	2-H
5.97	7-H
5.41	12-H
5.33	15-H
5.11	5-H
4.95	11-H
4.28	9-H
3.04	25-H
2.55, 2.48	4-H, 16-H
0.99~2.01	10-H, 22-H, 24-H, 17-H, 18-H,19-H, 20H, 21-H

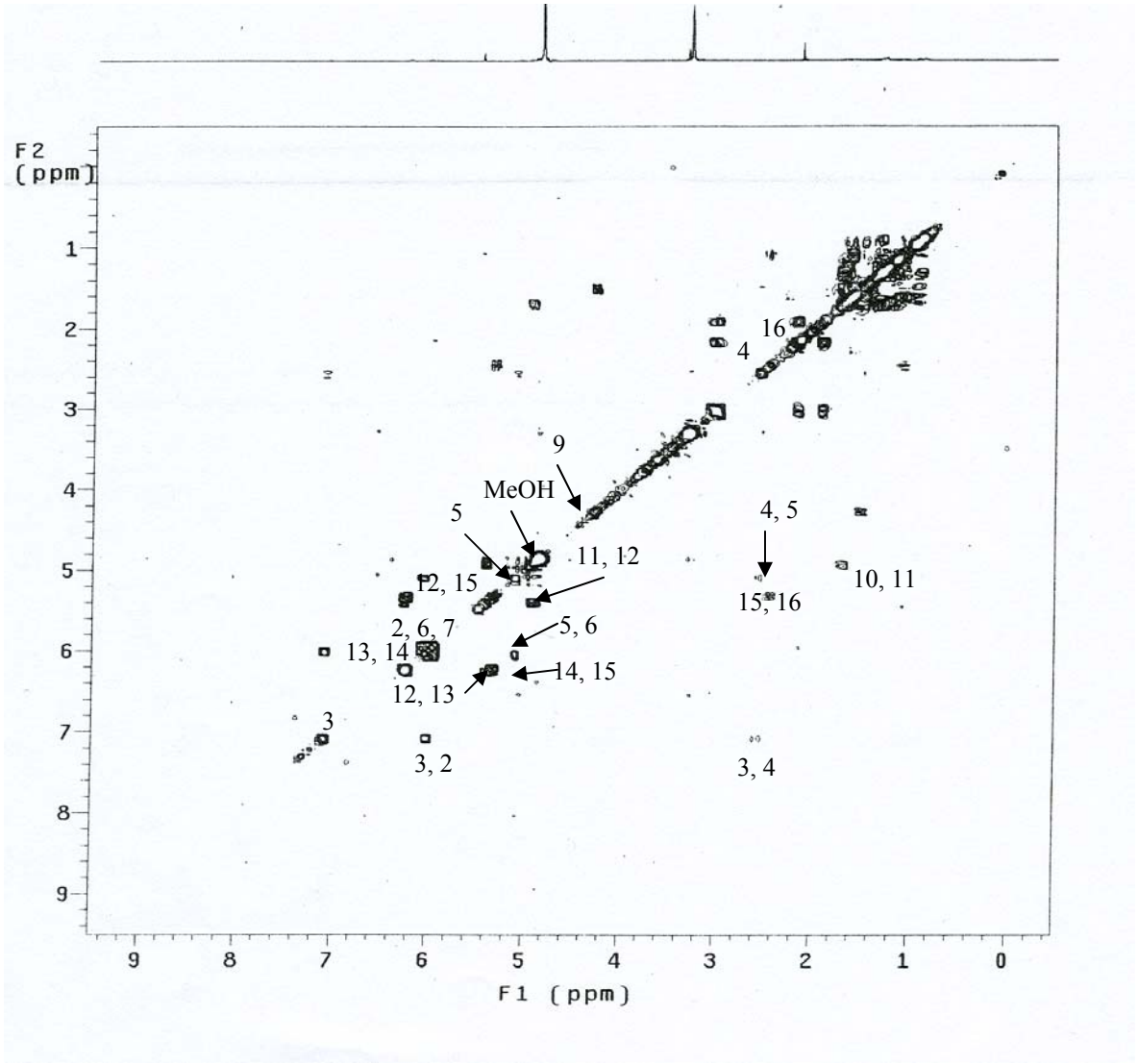

Figure 34. ^{1}H -^{1}H COSY of PLM-B (**1**). See Figure 33 for PLM-B structure and numbering.

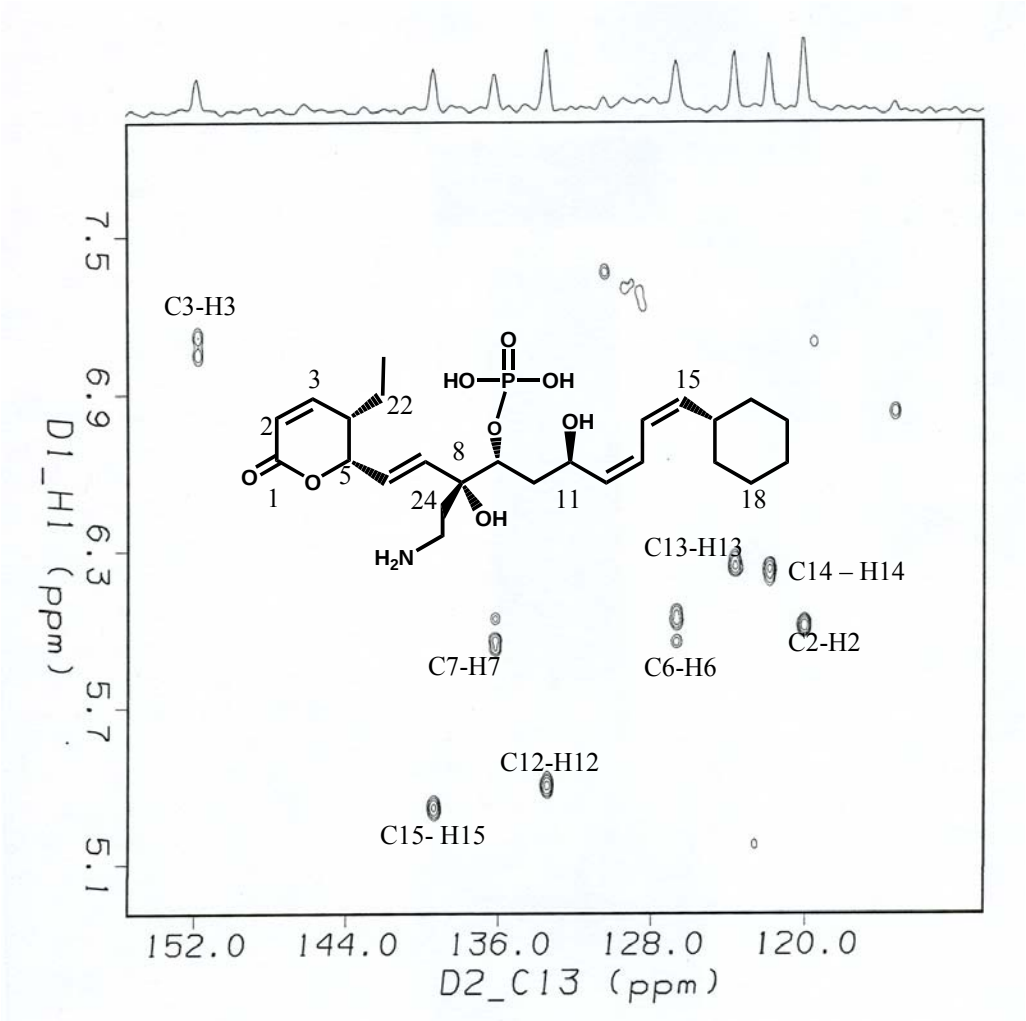

Figure 35A. HSQC analysis of PLM-B (**1**) showing the correlation between the proton and heteronuclei (downfield region).

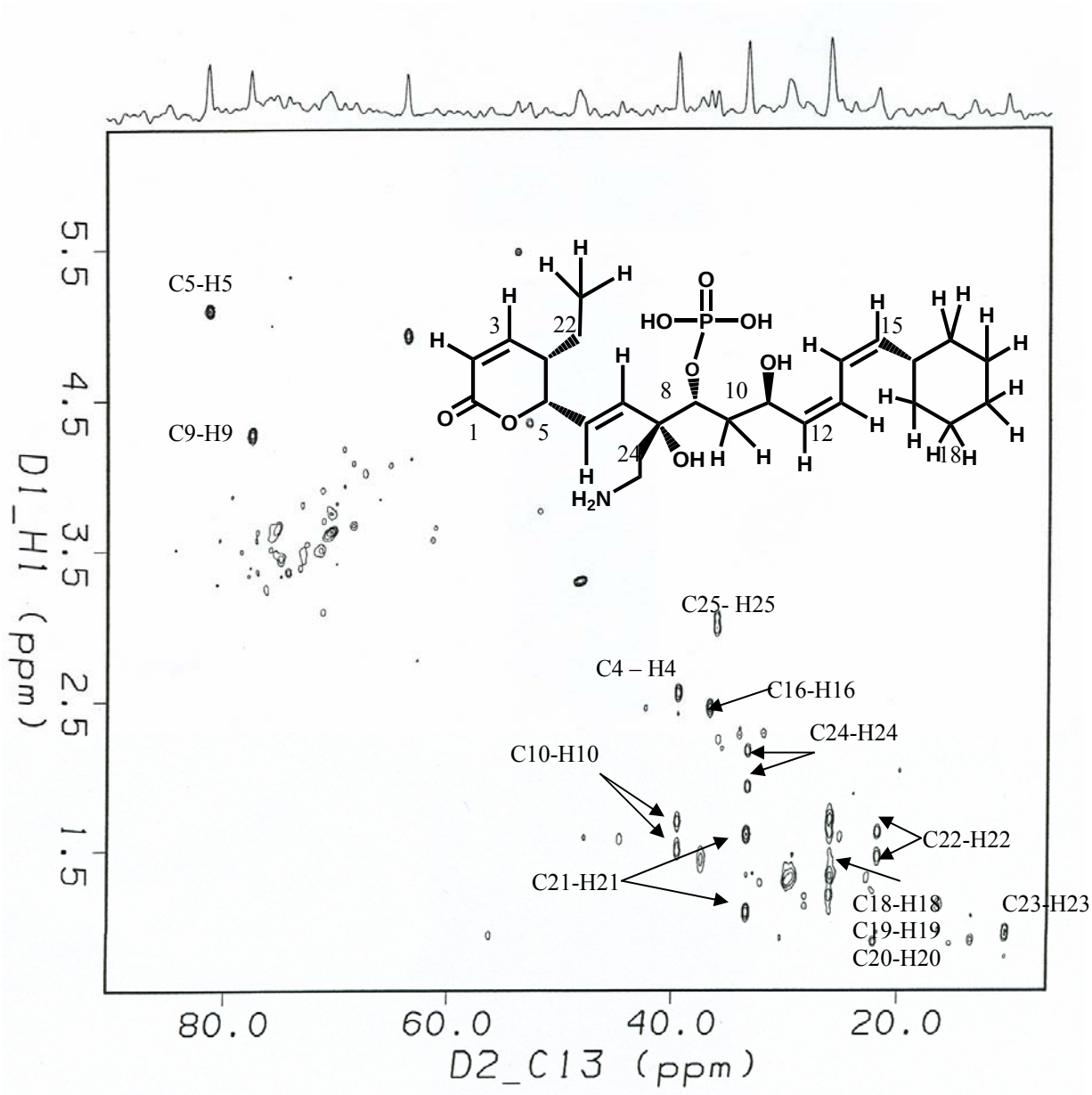

Figure 35B. HSQC analysis of PLM-B (**1**) showing the correlation between the proton and heteronuclei (upfield region).

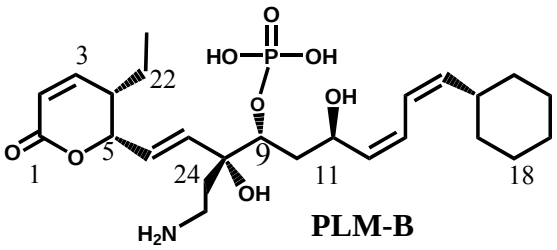

PLM-B

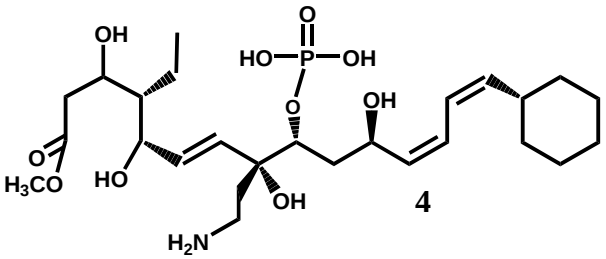

4

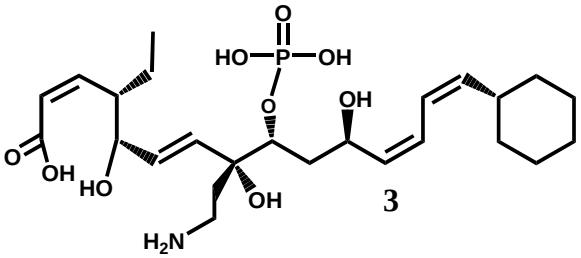

3

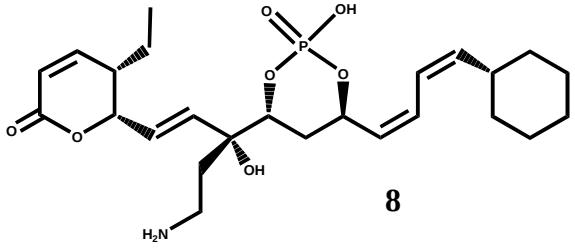

8

Assignment	δ (ppm) PLM-B	δ (ppm) **3**	δ (ppm) **4**	δ (ppm) **8**
2-H	6.09	6.03	1.72 (H_a) 2.28 (H_b)	6.07
3-H	7.09	5.51	3.13	7.10
4-H	2.55	3.03	2.59	2.61
5-H	5.11	4.14	3.81	5.12
6-H	6.04	5.91	6.02	5.69~ 5.60
7-H	5.97	5.62	5.63	
9-H	4.28	4.25	4.29	4.61
11-H	4.95	5.10	5.10	4.54~4.48
12-H	5.41	5.42	5.41	5.69~5.60
15-H	5.33	5.32	5.28	
13-H, 14-H	6.32~6.20	6.29~6.20	6.29~6.19	6.22~5.98
16-H	2.48	2.48	2.37	1.97
25-H	3.04	3.06	3.08	2.99

Table 20. Comparative significant ^{1}H-NMR chemical shifts changes for PLM-B and degraded products **3**, **4** and **8**.

Chemical Analysis of PLM-B Degradation Product **3**

LC/MS spectra of the basic degradation product **3** gave a parent $[M+H]^+$ at *m/z* 532 and a parent $[M-H]^-$) at *m/z* 530. This product indicates an increase in mass of 18 Da, consistent with addition of one H_2O molecule (Figure 36).

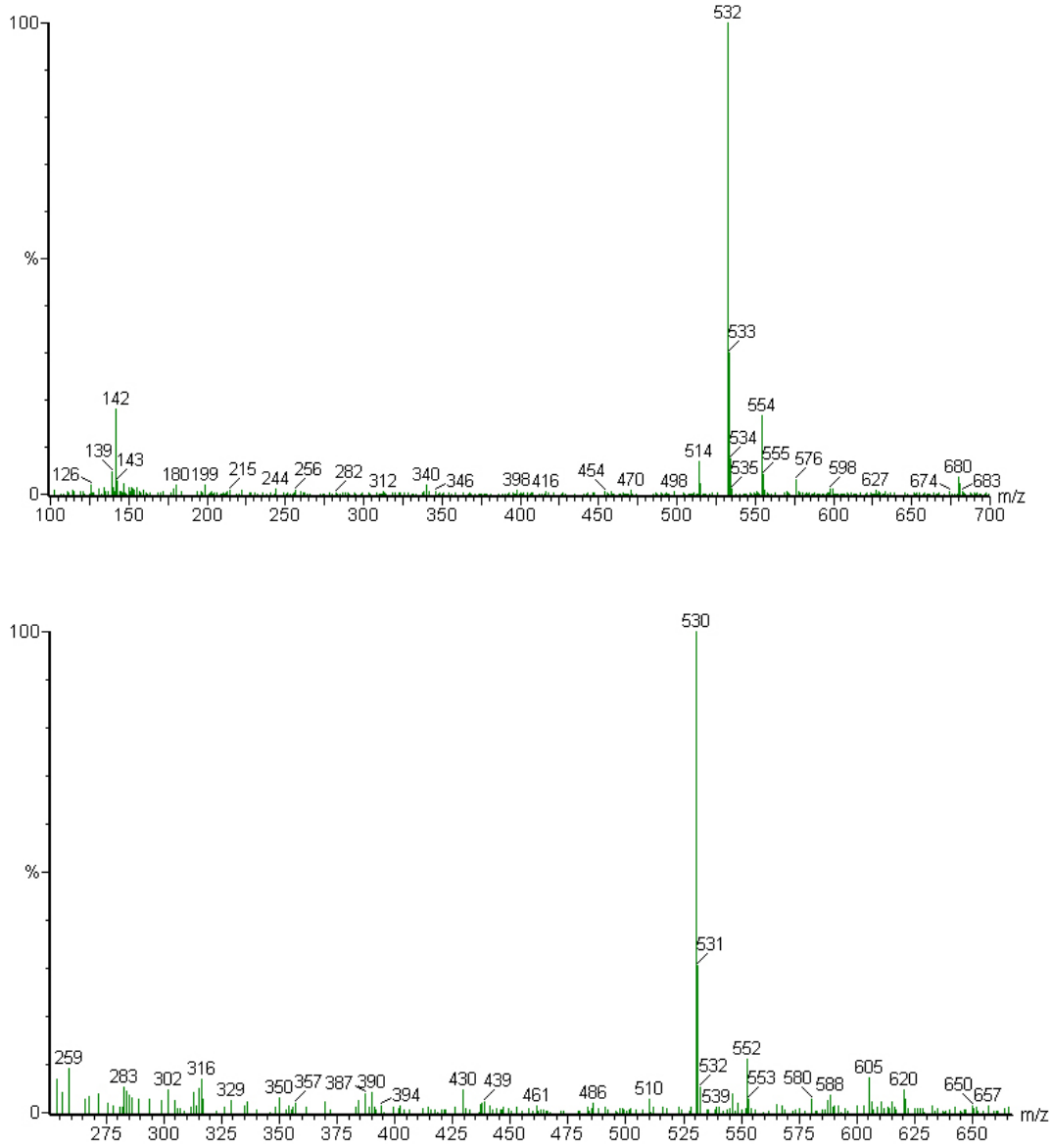

Figure 36. Mass spectroscopic analysis of product **3** in both positive and negative ESI mode.

The major degraded product **3** which showed evidence of lactone opening was a result of base catalyzed reaction. The ^{1}H-NMR of **3** was very similar to PLM-B except for the absorbance associated with the lactone ring. The proton absorbance could be assigned by using the ^{1}H-NMR and ^{1}H -^{1}H COSY (Figure 38) with the most significant chemical shift listed in Table 20. The assignment of the vinyl protons at H-2 and H-3 indicate that the double bond alpha to the carbonyl has been retained in **3**.

The proton signals corresponding to H-6 and H-7 in PLM-B appear very close to one another, separated by less than 0.2 ppm (see Table 20). In the product **3** (and other base degraded products), these absorbances are separated by approximately 0.4 ppm with the H-7 signal shifting slightly upfield. This shift is explained by the change in environment around the C-6/C-7 double bond due to opening of the lactone ring. A ring opened product would have a different shape after opening of the lactone and so changes in chemical shifts of nearby protons would be expected. In product **3** (and the other base degradation products), the diene system of C-12/C-13/C-14/C-15 was intact. The MS and NMR are consistent with the structure shown in Figure 37 in which the hydrolysis of the lactone ring has occurred. Purified product **3** on incubation at pH 10.0 (50°C) for 72 hours consistent with this structure is that it was stable at pH 10.0. This indicates that it is not an intermediate on a pathway to formation of products **4** and **5**.

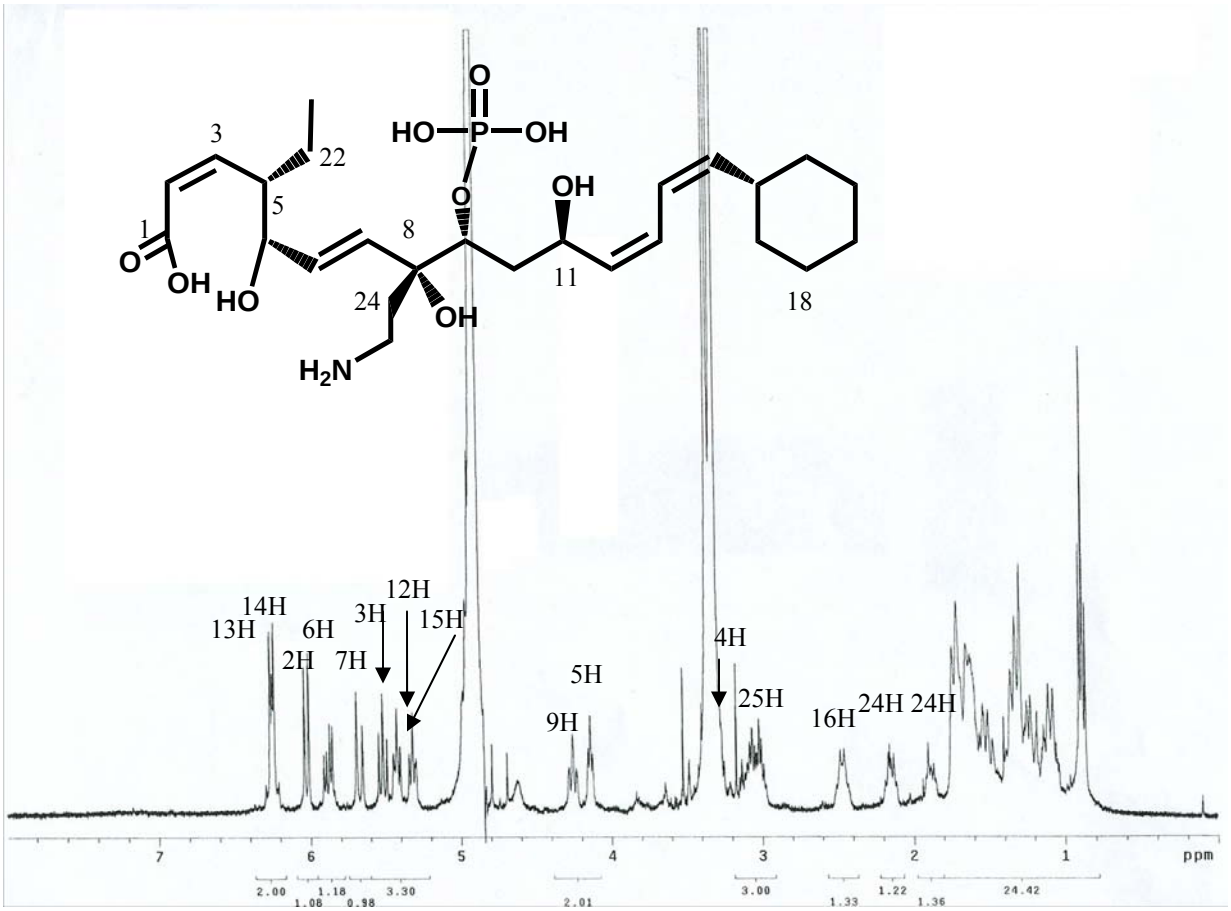

Figure 37. ^{1}H NMR of degradation product **3**.

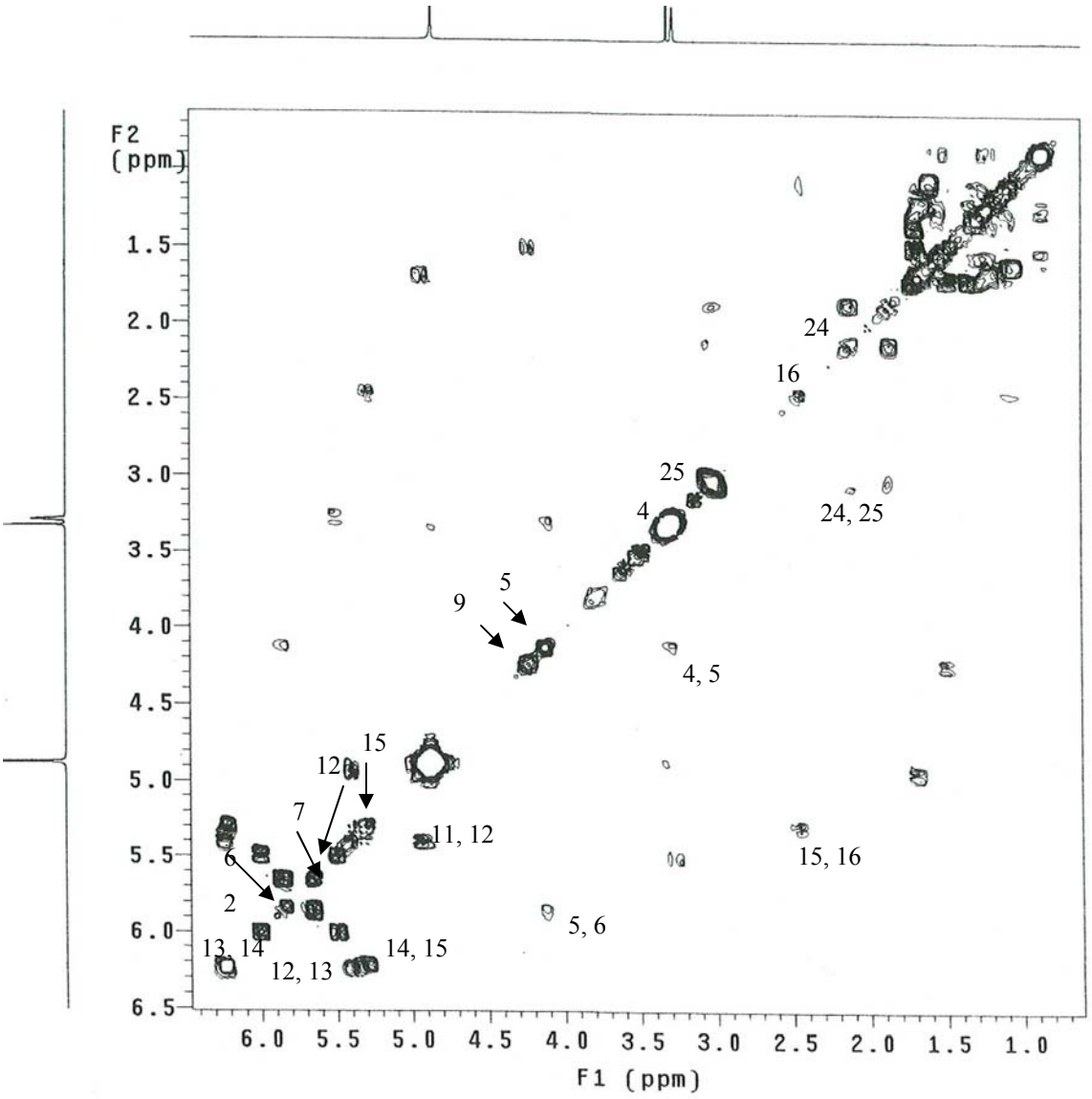

Figure 38. ^{1}H -^{1}H COSY of degradation product **3**.

Chemical Analysis of PLM-B Degradation Product **4**

The LC/MS of product **4** showed an increase in mass by 50 Da (*m/z* 564 $[M+H]^+$, *m/z* 562 $[M-H]^-$) compared to PLM-B, consistent with addition of a water molecule and methanol (Figure 39).

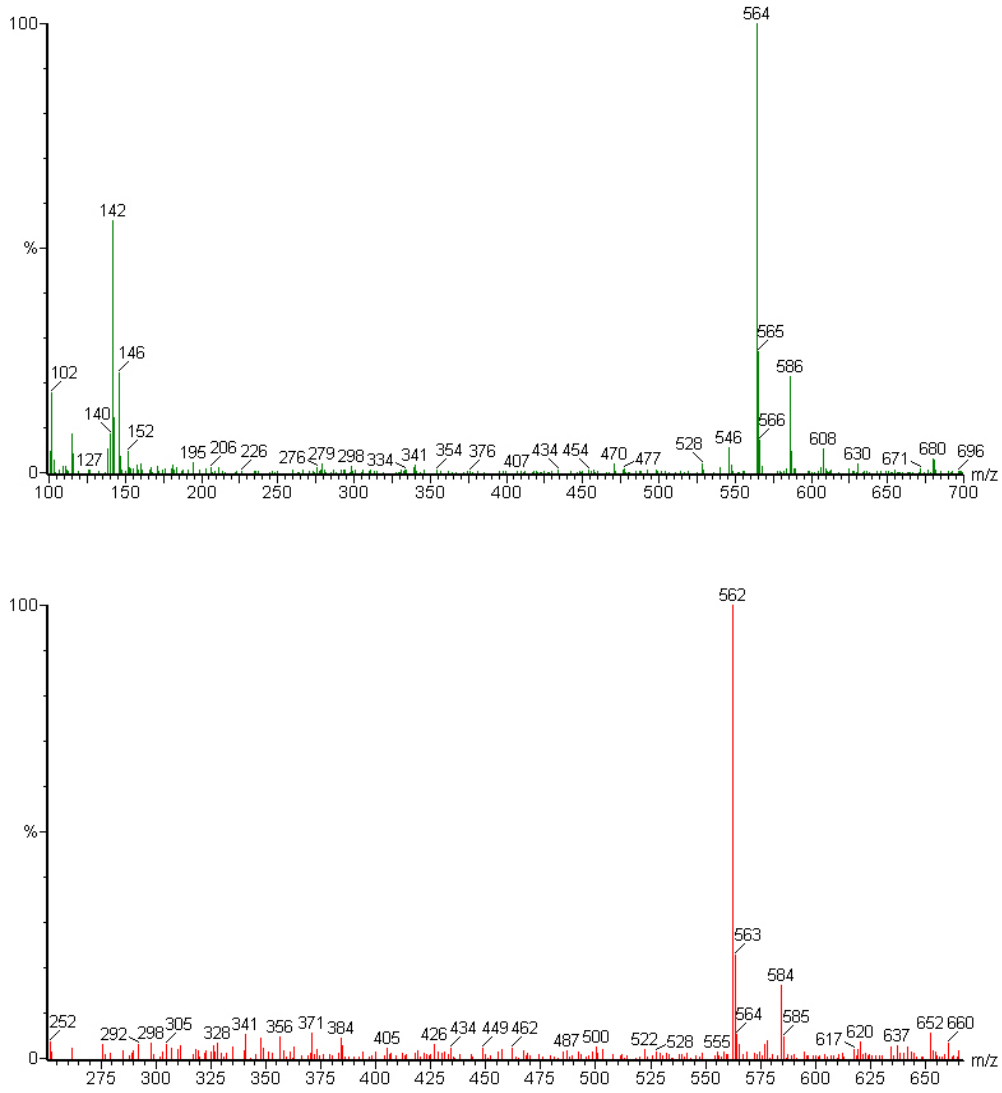

Figure 39. Mass spectroscopic analysis of product **4** in both positive and negative ESI mode.

The ^{1}H-NMR and ^{1}H-^{1}H COSY of Product **4** are given below (Figure 40, 41). The diene system of C-12/C-13/C-14/C-15 appears intact similar to all basic degradants. However, the doublet of doublets (integrating for one proton) at 7.09 ppm due to H-3 has disappeared, indicating loss of the C-2/C-3 double bond (see Table 20). Consistent with this hypothesis is the loss of another proton resonance at ~6.0 ppm, which is the chemical shift of H-2 for PLM-B. Similar to Product **3**, this product also showed evidence of lactone opening by the upfield shift of the H-5 signal and the change in environment around the C-6/C-7 double bond, with the H-7 signal shifting slightly upfield. As product **4** shows an increase in mass of 50 Da by LC/MS, the product is likely formed by hydration of the C_2-C_3 double bond and methanolysis of the lactone ring. Alternatively, this compound may be formed by hydrolysis of the lactone ring and addition of methanol across the C_2-C_3 double bond. No resonance for the proposed methoxy group of **4** was observed and it is likely that the solvent (CD_3OH) signal (3.24 ~ 3.38) masks this signal.

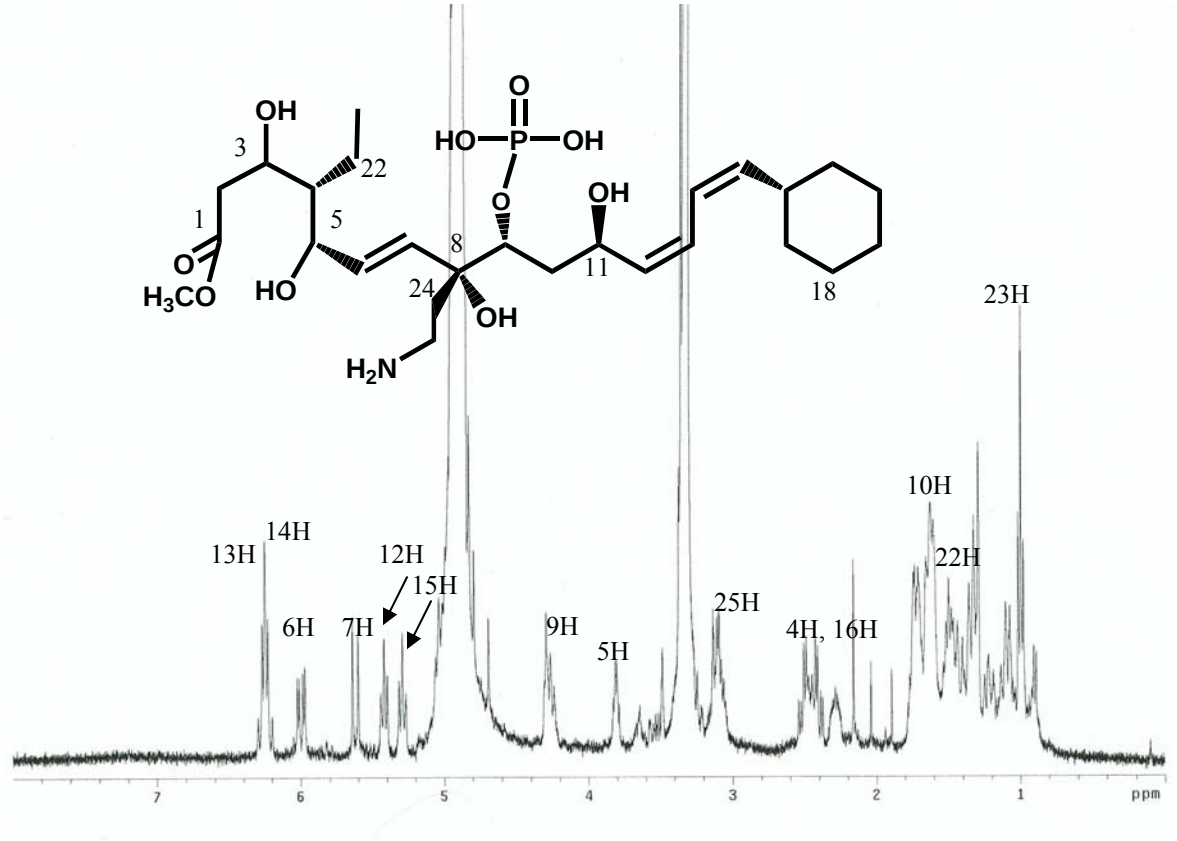

Figure 40. ^{1}H NMR of degradation product **4**.

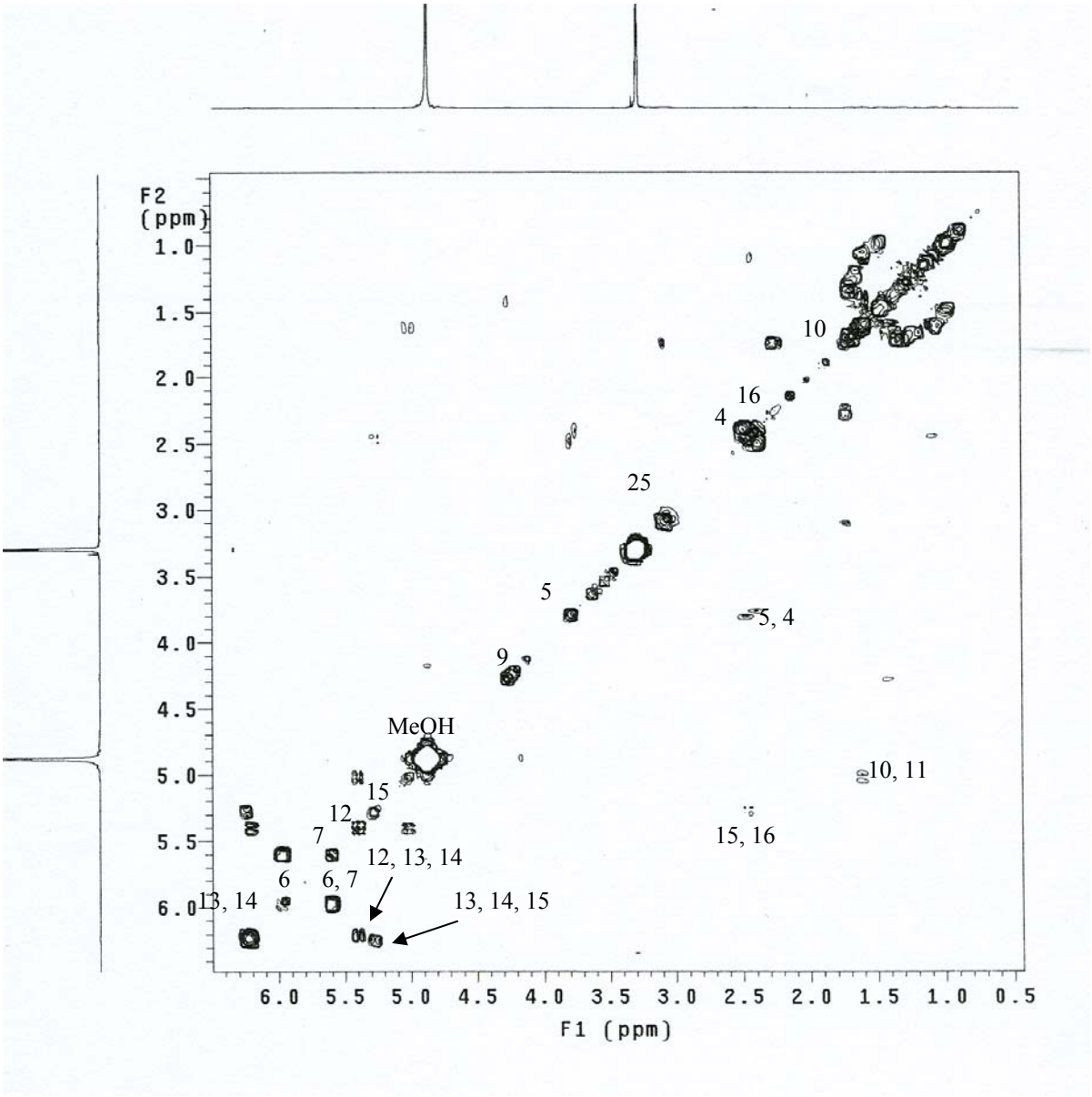

Figure 41. ^{1}H -^{1}H COSY of degradation product **4**.

Chemical Analysis of PLM-B Degradation Product **5**

Product **5** showed an increase in mass by 36 Da (*m/z* 550 $[M+H]^+$, *m/z* 548 $[M-H]^-$) consistent with addition of two H_2O molecules.

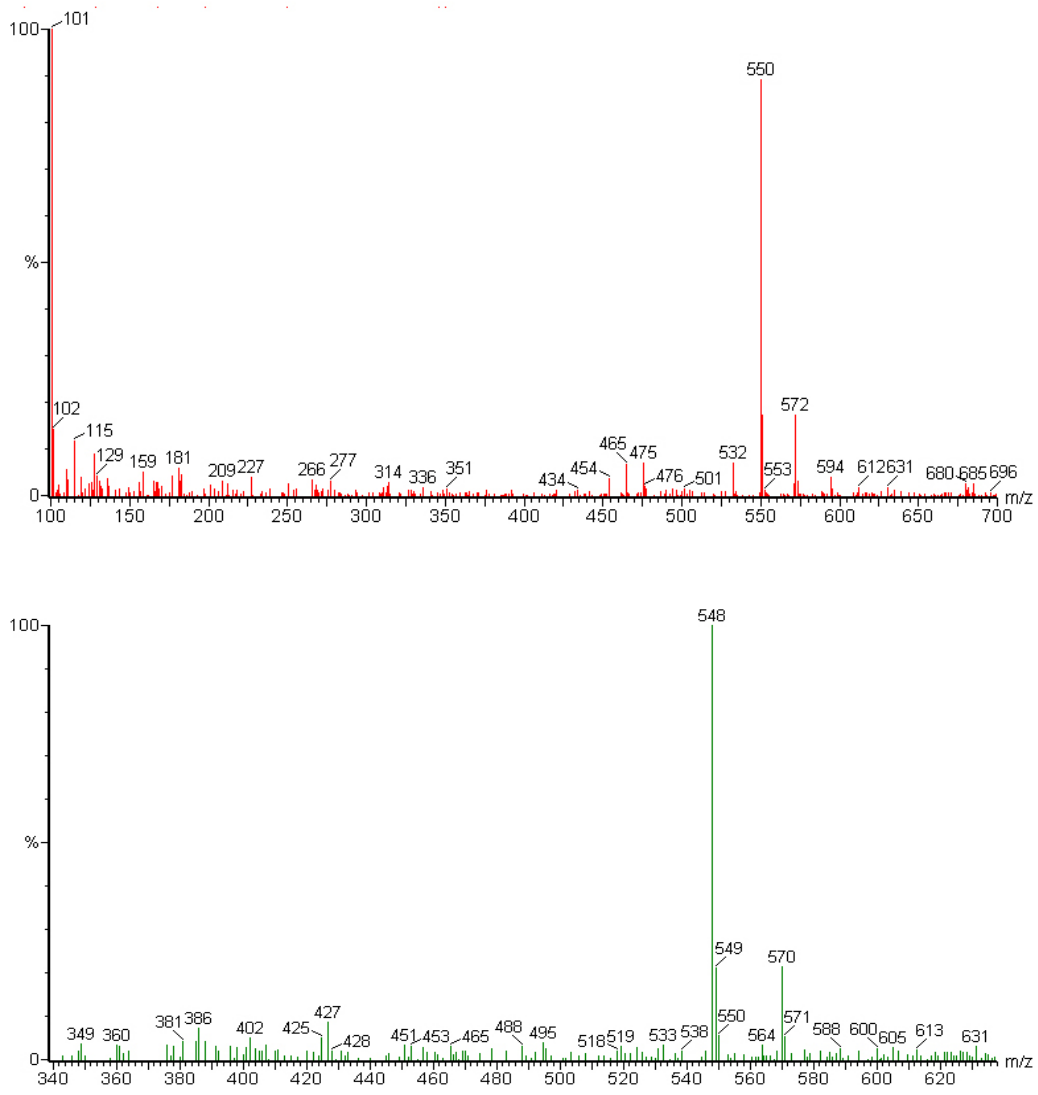

Figure 42. Mass spectroscopic analysis of product **5** in both positive and negative ESI mode.

A ^{1}H-NMR of product **5** could not be obtained due to insufficient material. Product **5** showed an increase in mass of 36 Da by LC/MS, and it is likely that it is formed as a result of hydration of the C-2/C-3 double bond (by Michael type addition) and lactone hydrolysis.

Proposed Pathway for PLM-B Degradation at Basic pH.

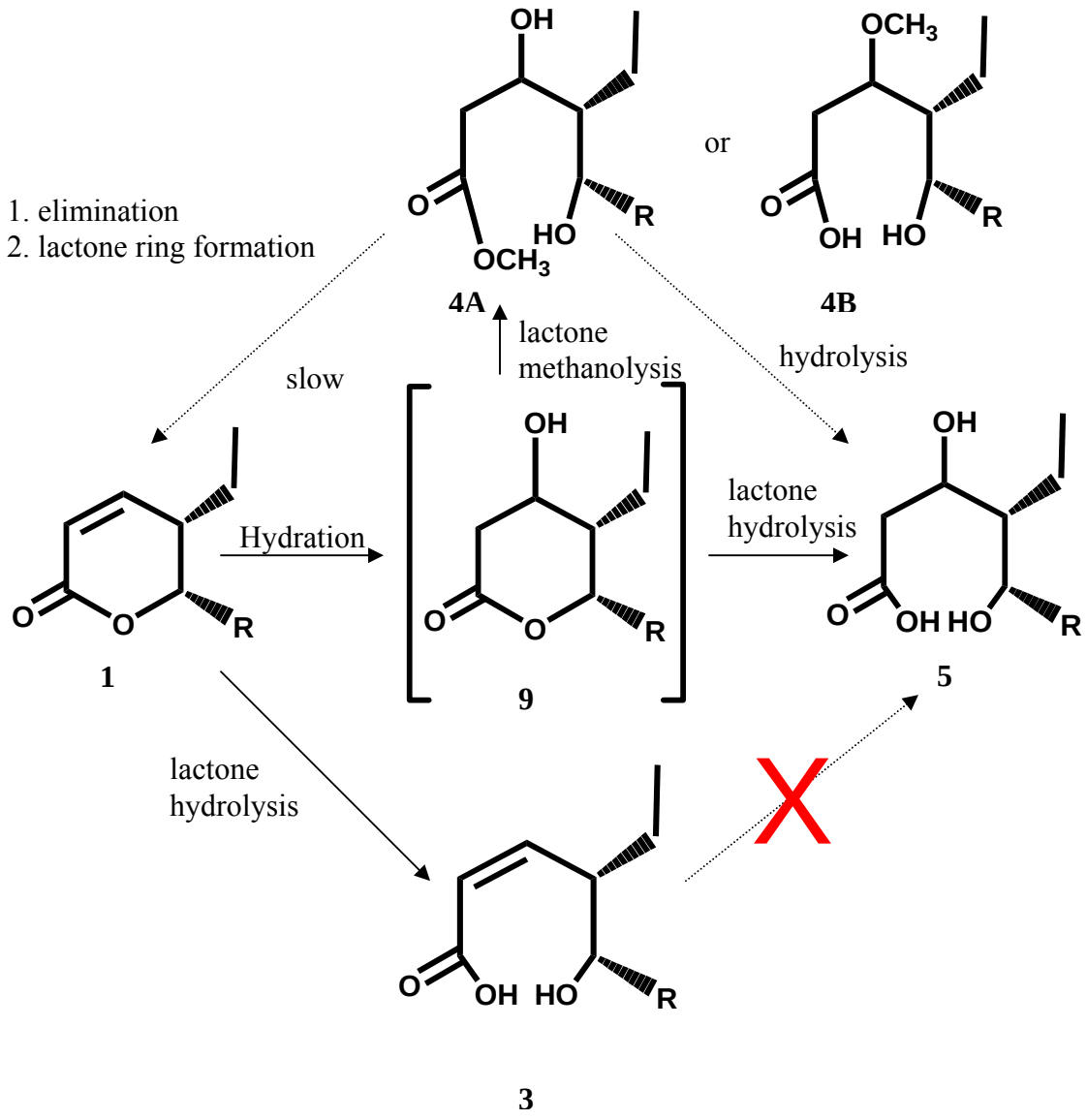

Scheme 2. A proposed degradation mechanism for PLM B in the basic aqueous medium.

Product **3** is formed directly by base-catalyzed hydrolysis of the lactone ring. It is a final product and neither water nor methanol was observed to add to C_2- C_3 based on the stability of product **3** under basic conditions (see Scheme 2). Product **4** and **5** involve addition across the C_2- C_3 double bond and it can be concluded (based on the stability of **3**) that this addition reaction must occur prior to the hydrolysis of the lactone. The proposed intermediate product **9**, was not observed when analyzing the mixture using LC/MS. Small peaks were observed in the HPLC traces of PLM-B under base degradation and it is possible that one of these peaks is peak **9**. The peaks were relatively small compared to **3**, **4** and **5** and did not increase during the time course of the degradation study. These observations suggest that the subsequent hydrolysis proceeds at least at a comparable rate to the addition reaction (see Scheme 2). The two step reaction for the formation of product **4** and **5** is slower than direct one step hydrolysis for the formation of **3**. Product **4** was found to be unstable and reverted back to PLM-B on storage in deuterated methanol (Figure 43). This observation indicates that product **4A** is likely and not **4B**. Lactone formation from **4A** is a transesterification reaction, rather than the esterification reaction required to convert **4B** to PLM-B. The conversion of **4A** to **5** is predicted to occur under basic conditions and likely occurred during our experiments, although no clear evidence of this conversion was observed.

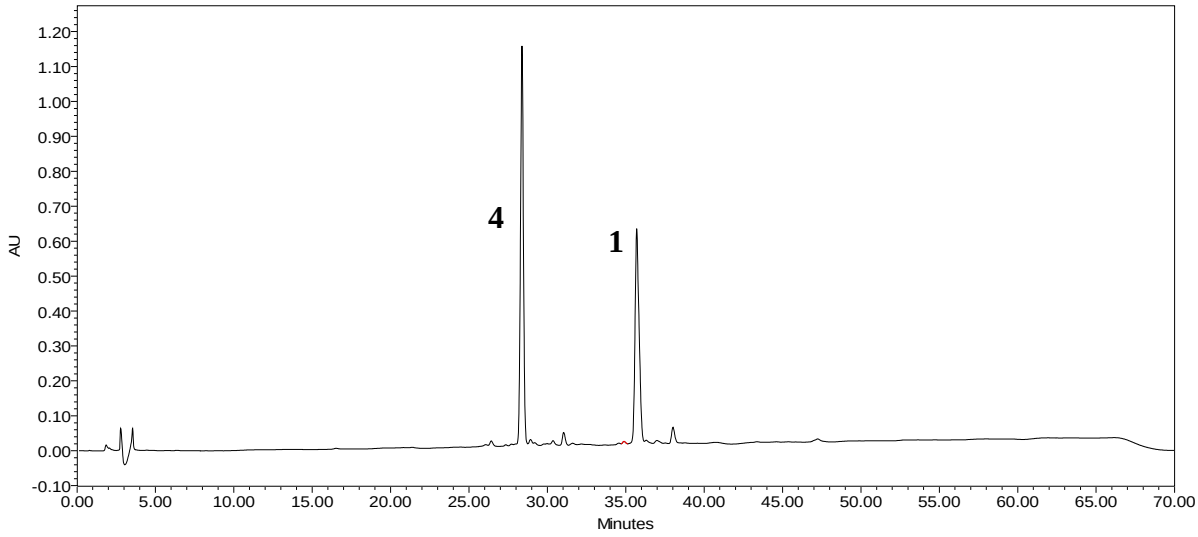

Figure 43. HPLC chromatogram of conversion of the degraded product **4** to PLM-B on storage.

Chemical Analysis of Acid Degradation Products

LC/MS analysis of PLM-B incubated at pH 2.0 indicated the formation of 3 degradation products. All three acidic degradation products showed a decrease in mass of 18 Da (*m/z* 496 $[M+H]^+$) but with different retention times [See Figure 23 and Table 21] consistent with formation of dehydration products. Further characterization of the acid degradants was carried out by NMR analysis.

Table 21. Comparison of the retention time and molecular mass of PLM-B and the degradation products **6**, **7** and **8**.

	PLM-B	**6**	**7**	**8**
Retention Time (min)	39	40.5	41.7	42.4
Molecular Mass	513	495	495	495
	514 $(m+H)^+$	496 $(m+H)^+$	496 $(m+H)^+$	496$(m+H)^+$

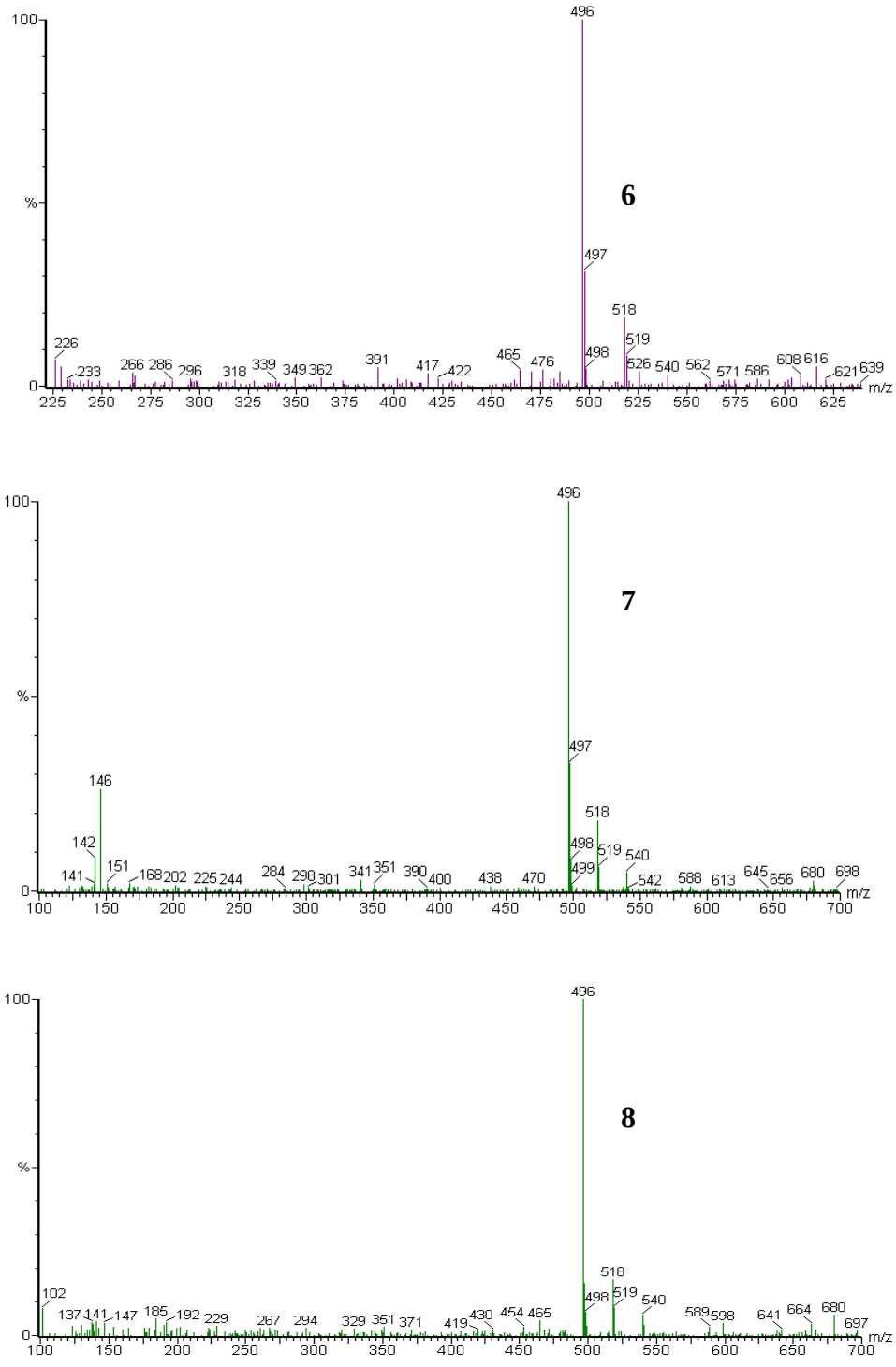

Figure 44. Mass spectroscopic analysis of acid degradation products **6**, **7**, **8** in positive ESI mode.

The ^{1}H-NMR and ^{1}H -^{1}H COSY spectra (Figure 45 and 46) of the decomposition product **8** showed an intact lactone ring (H-5 appears unchanged compared to PLM-B) as well as an intact C-2/C-3 double bond (see Table 20). The UV spectra of the acid degradants **8** (and other products) all show λ_{max} from 235-238 nm that was identical to PLM-B. This would preclude the dehydration of the C-11 hydroxyl group to form a double bond between C-10 and C-11 in all cases. If a C-10/C-11 double bond formed, a conjugated triene would be present, and would shift the λ_{max} of the compound to a longer wavelength. The ^{1}H-NMR spectrum of **8** indicated a slight upfield chemical shift of H-11 and a downfield shift for H-9 (Table 20). The chemical shift for the olefinic protons (H-12, H-13, H-14, H-15) can be assigned based on the COSY (Figure 46A-C) and no additional olefinic resonances are observed. Thus **8** cannot be a dehydration product which involves generation of a new double bond (i. e., loss of the OH group at C-8 or C-11). Formation of a phosphorinane derivative involves dehydration. HSQC analysis revealed a significant 14 ppm shift for C-11(Figure 47, Table 22) consistent with the formation of a C-9/C-11 phosphorinane derivative. This is a new compound and differs from C-8/C-9 cyclic phosphorinane [4] previously obtained by treatment of phospholine with DCC (Dicyclohexylcarbodiimide). Comparative ^{13}C- NMR chemical shifts of PLM-B and degraded product **8** are given below.

Table 22. Assignment of ^{13}C-NMR resonances for PLM-B and degraded product **8**. * overlapping signals for C_{17} - C_{21}. ND- Not Detected.

Assignment	δ (ppm) PLM-B	δ (ppm) **8**
C-2	120.08	120.08
C-3	151.32	151.68
C-4	39.54	39.65
C-5	81.34	81.68
C-6	126.71	127.22
C-7	136.20	136.43
C-8	ND	ND
C-9	77.60	79.30
C-10	39.60	37.50
C-11	63.69	77.0
C-12	133.47	130.97
C-13	123.68	132.86
C-14	121.88	126.67
C-15	139.41	141.84
C-16	36.70	41.20
C-17	25.97 *	26.13 *
C-18	26.00 *	26.14 *
C-19	25.99 *	26.18 *
C-20	26.05 *	26.20 *
C-21	33.40 *	33.07 *
C-22	21.81	21.85
C-23	10.42	10.35
C-24	33.33	35.43
C-25	36.14	35.93

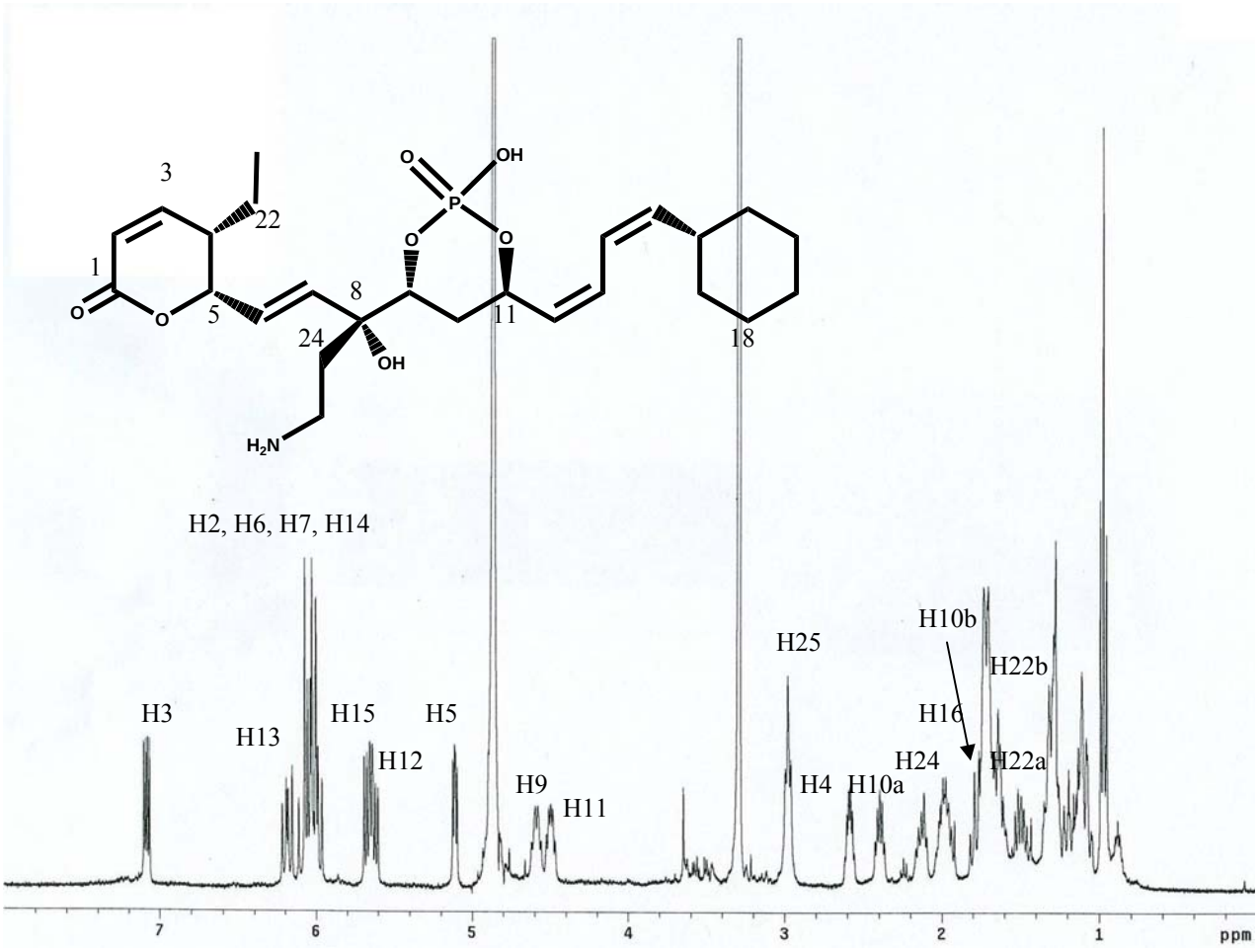

Figure 45. ^{1}H NMR of degradation product **8**.

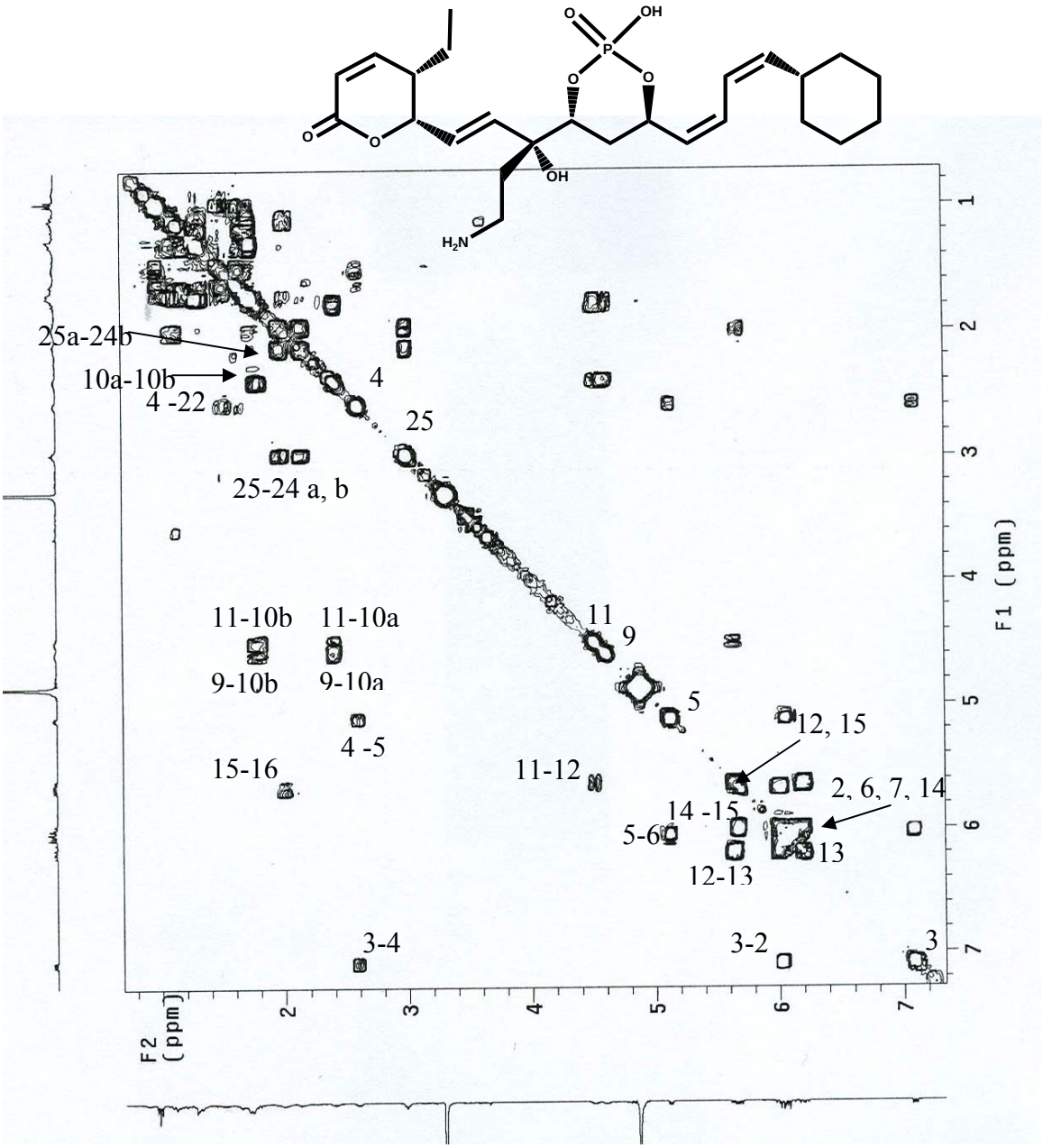

Figure 46A. ^{1}H -^{1}H COSY of degradation product **8**.

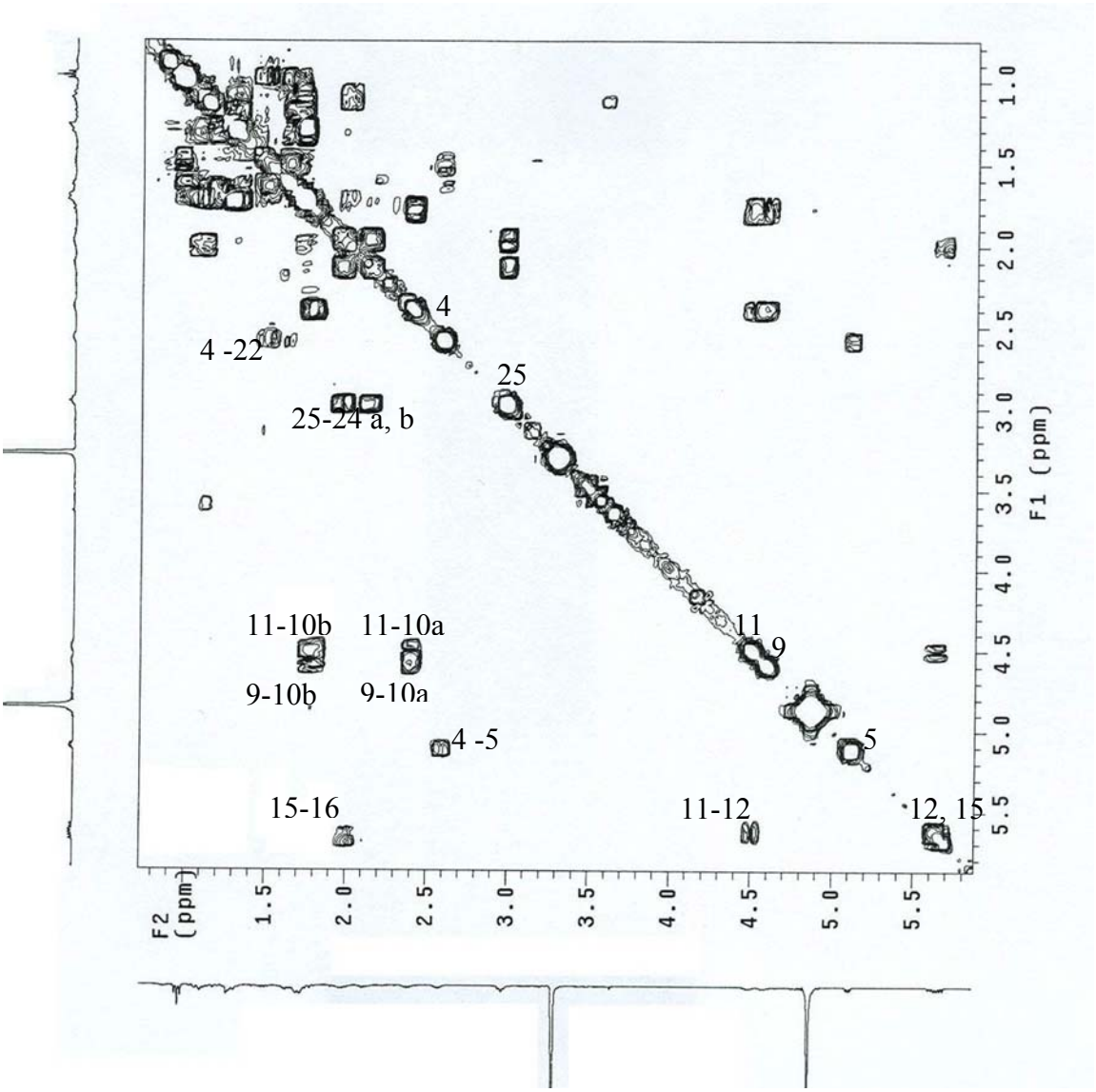

Figure 46B. ^{1}H -^{1}H COSY of degradation product **8** (upfield region).

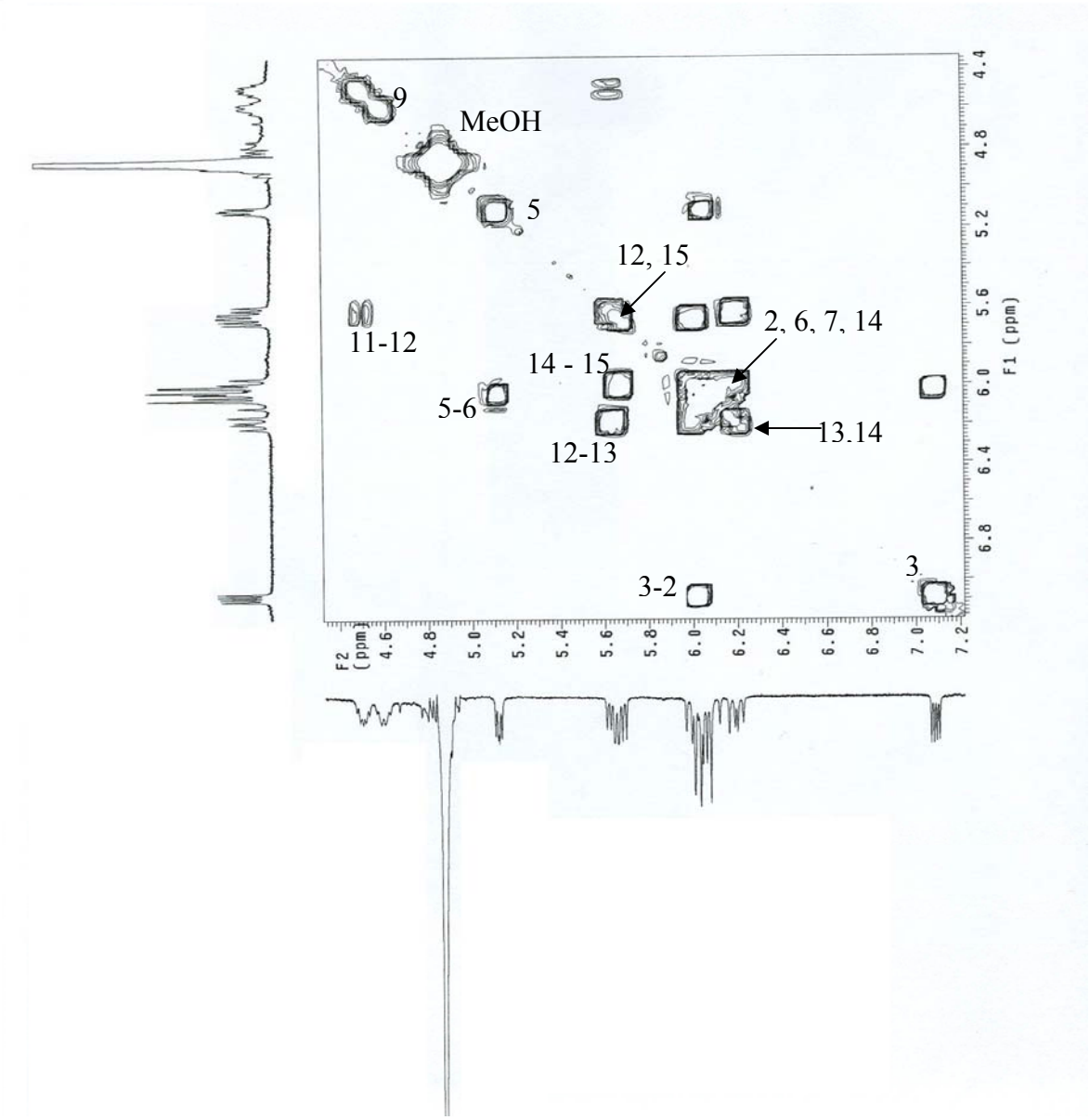

Figure 46C. ^{1}H -^{1}H COSY of degradation product **8** (downfield region).

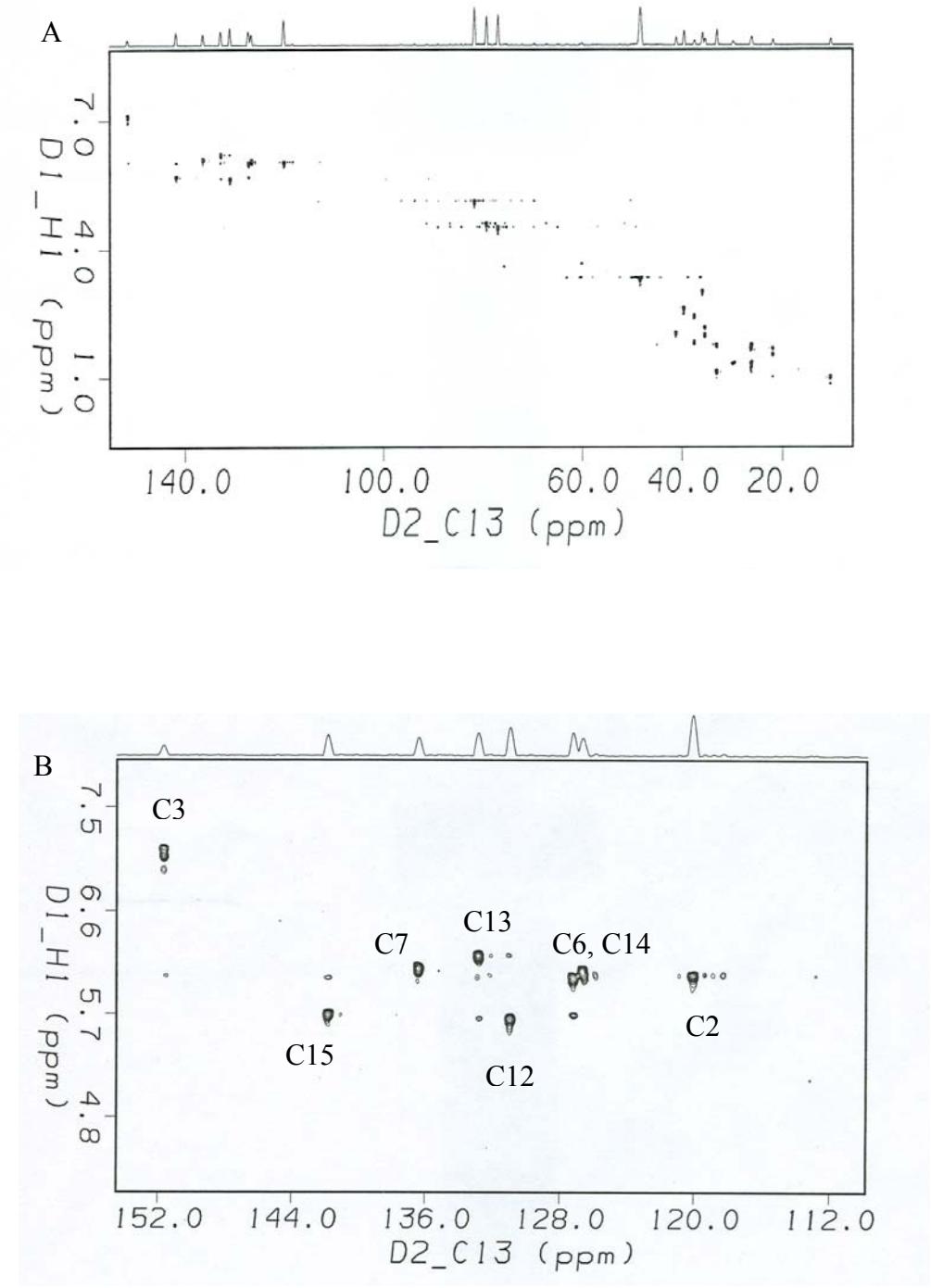

Figure 47. HSQC spectra (A) of product **8** and (B) downfield region (112-152 ppm).

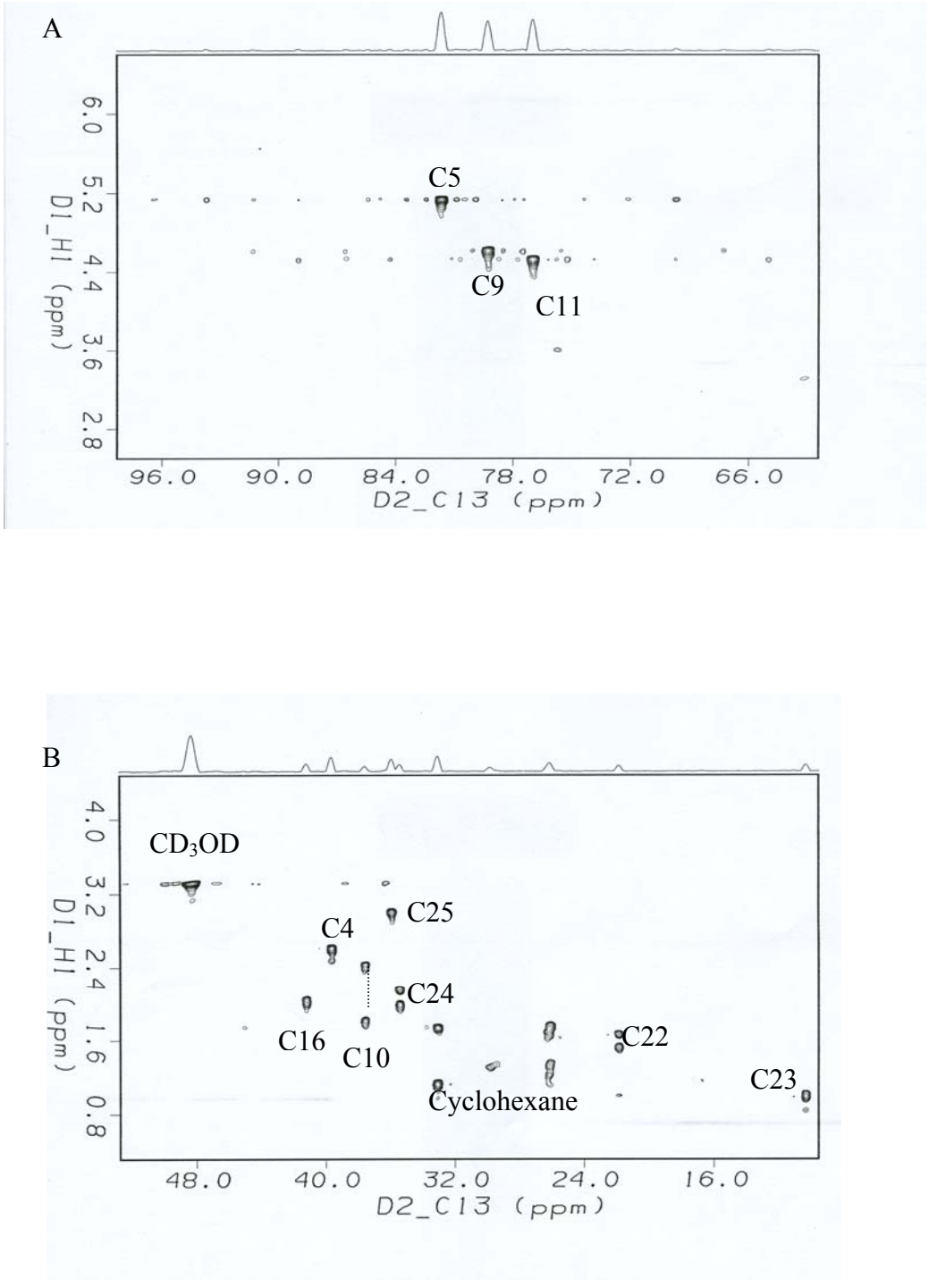

Figure 48. HSQC spectra (A) downfield (66-96 ppm) and (B) upfield (16-48 ppm) region of product **8**.

The ^{1}H NMR spectra of **6** and **7** appear to be mixtures, although single well-resolved HPLC peaks for **6** and **7** were collected. In the spectra of **6** and **7**, many new peaks appear in the double bond region between δ 5-7 ppm, but none integrate close to one, compared to the H-3 and H-2 resonances at 7.08 and 6.0 ppm respectively (Figure 49-50). The UV spectra of the acid degradants **6** and **7** all show λ_{max} of 235-238 nm, unchanged compared to PLM-B. It is likely that **6** and **7** contain various PLM-B products obtained by dehydration involving C-8 hydroxyl group. We can rule out a 1,4 dehydration involving the H-5 proton and C-8 hydroxyl group as H-5 resonance is clearly observed in the spectra of **6** and **7** and integrates to one as compared to H-3 resonance. It is unlikely that the C-10 hydroxyl group is lost as this would generate a conjugated triene which can be excluded based on the UV analysis of **6** and **7**. It is also possible that C-8/C-9 phosphorinane derivative may be among the acid degradants **6** and **7**. Degradant **6** may contain an intermediate which generates one of the products in **7** because in the kinetic analysis we saw that initially the production of **6** > **7** > **8**, but at the end of the degradation the yield of **7** > **6** > **8**. The presence of potential multistep processes and closely related products preclude a facile delineation of the acid.

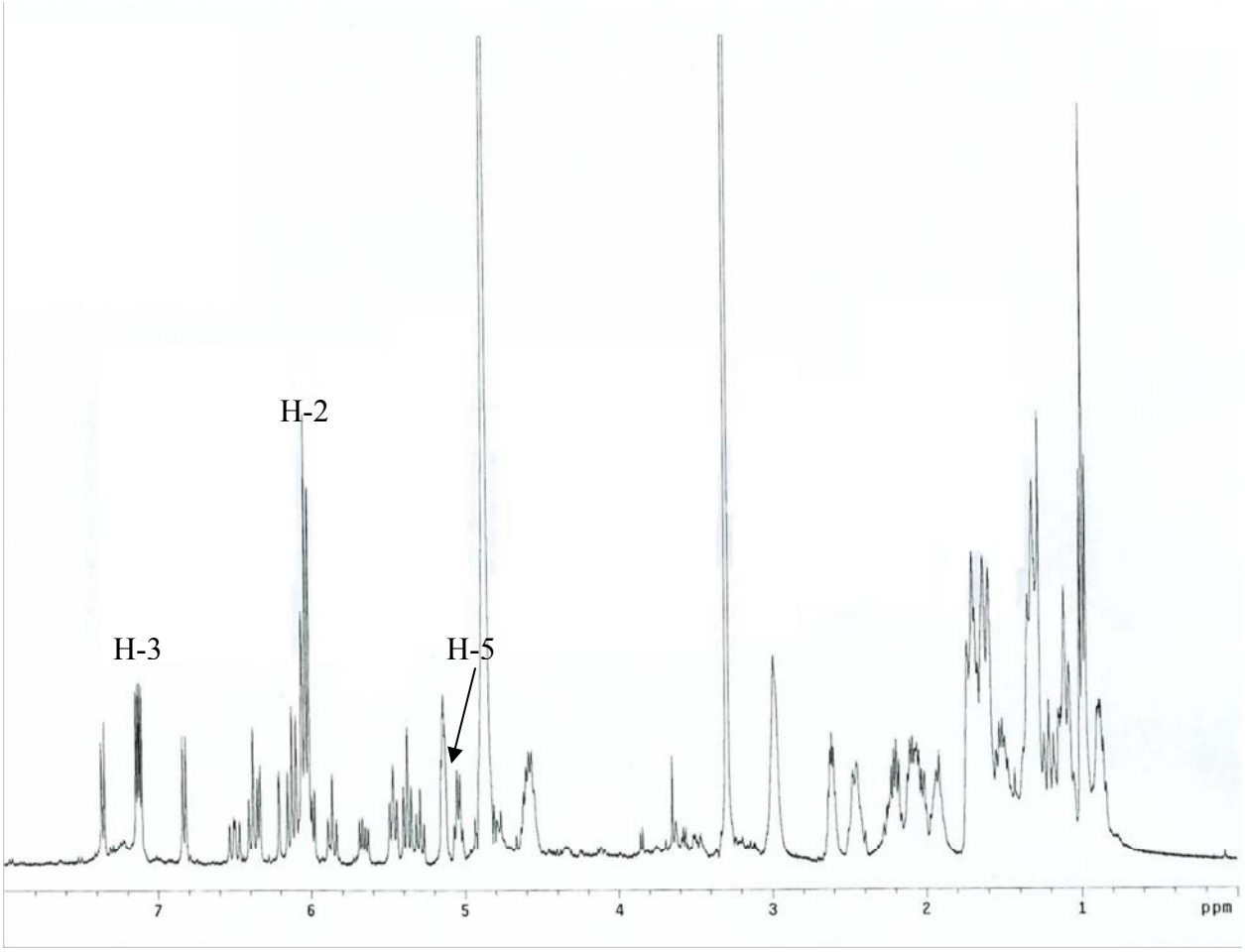

Figure 49. ^{1}H NMR of degradation product **6**.

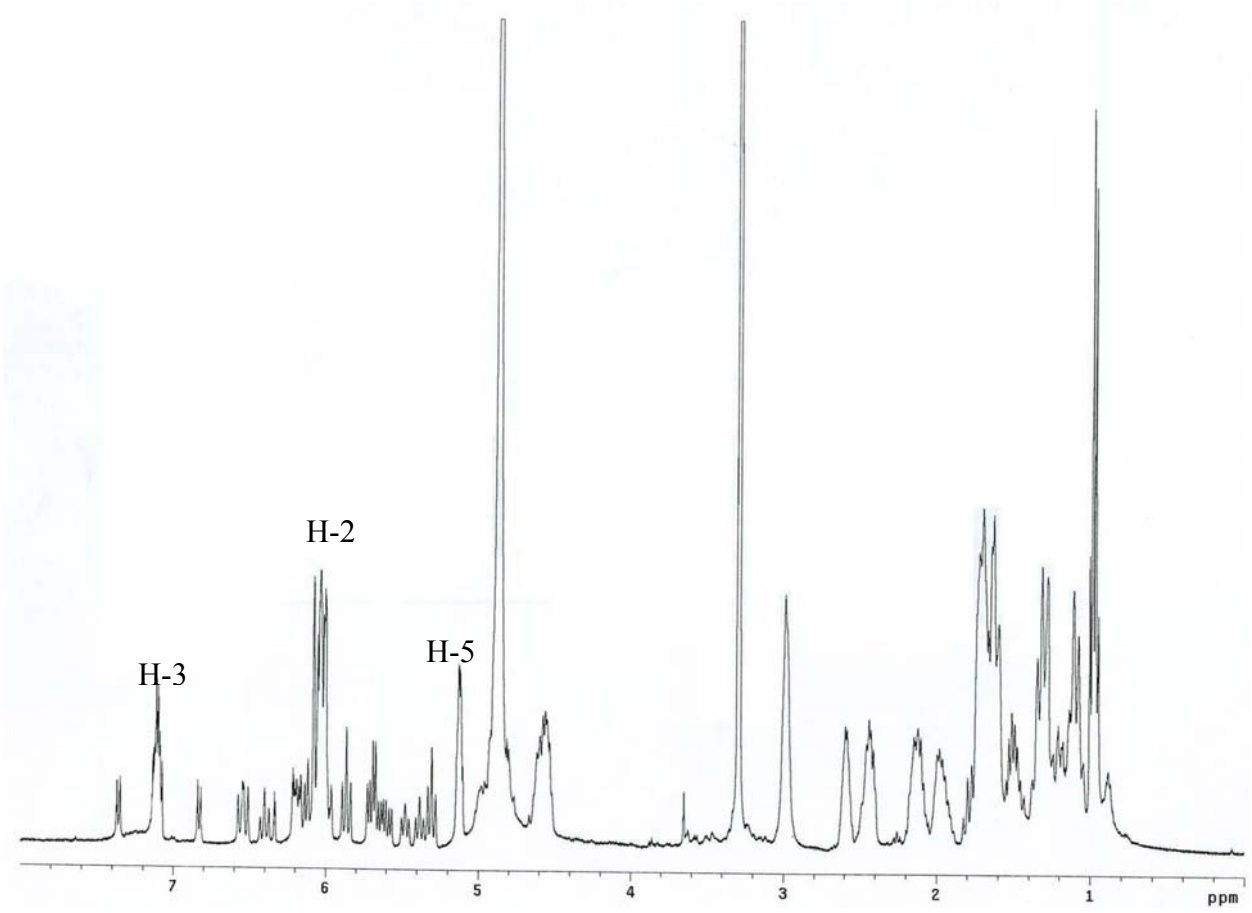

Figure 50. ^{1}H NMR of degradation product **7**.

The proposed degradation mechanism for PLM-B in the acidic aqueous medium is shown in scheme 3.

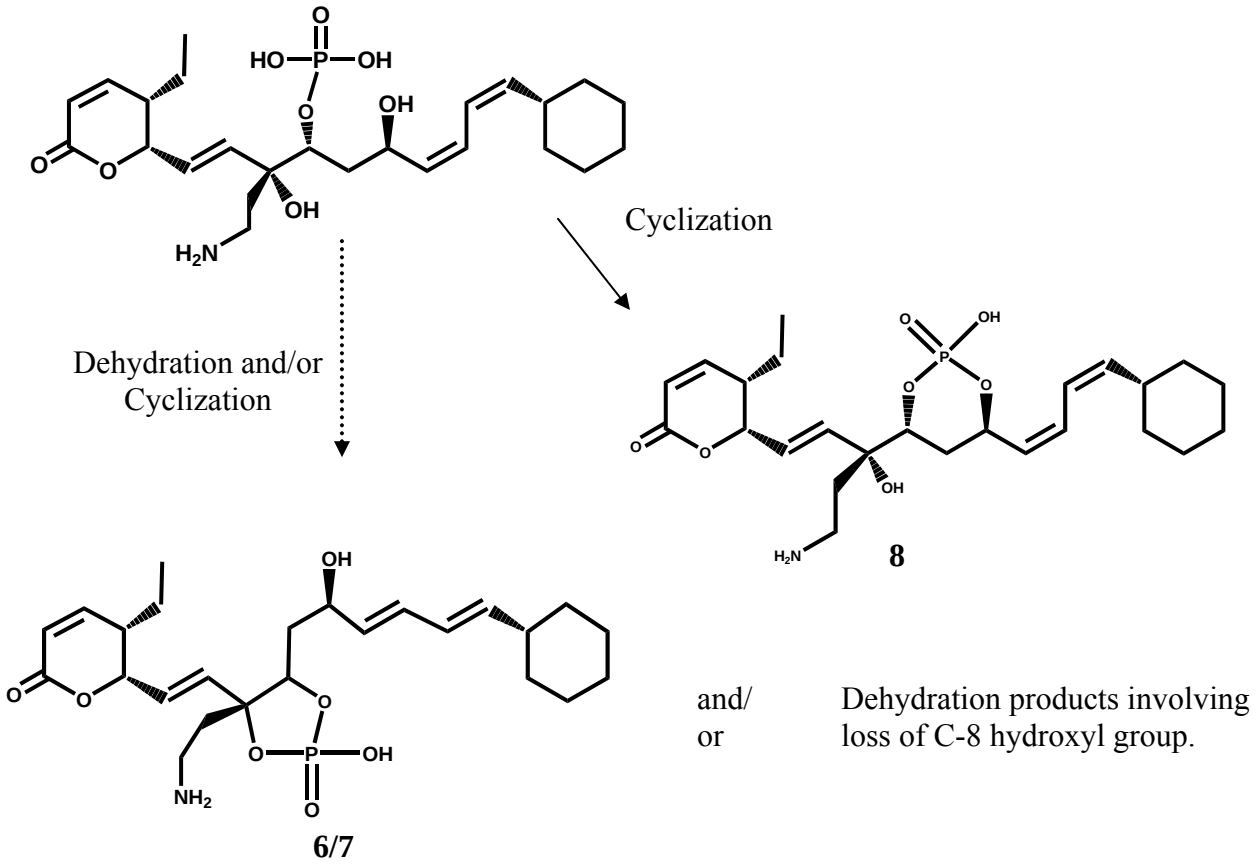

Scheme 3. A degradation mechanism for PLM B in the acidic aqueous medium.

Antifungal Activity of PLM-B and PLM-B Degradants

An antifungal assay demonstrated the potent activity of PLM B against the fungus *Rhodotorula glutinitis,* as indicated by a zone of inhibition. No significant antifungal activity was observed in degradation products of PLM B (Figure 52); a significantly reduced zone was seen for 0.08 mg of the combined acid degradants, and no clear zone was seen for 0.05mg of this mixture (5µL of 0.08 mg/mL and 0.05mg/mL of PLM-B degraded in 50µL of buffer at pH 2.0 and pH10.0). Similar observations of poor antifungal activity were made with the base degradants.

The rate of loss of antifungal activity associated with degrading PLM B in both acid (pH 2.0) and base (pH 10.0) was determined (Figure 51). Samples were withdrawn at specific times and the relative antifungal activity determined by measuring a zone of inhibition. The size of this same was then plotted against time. As can be seen, in both acid and base the antifungal activity decreases with the degradation of PLM-B.

(A)

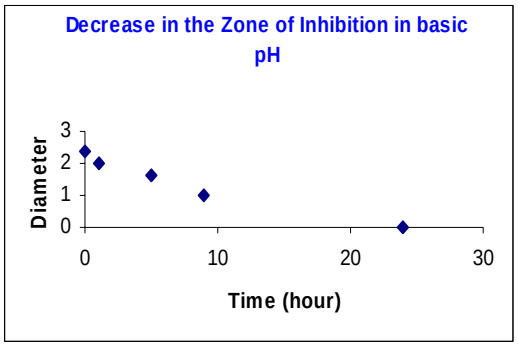

(B)

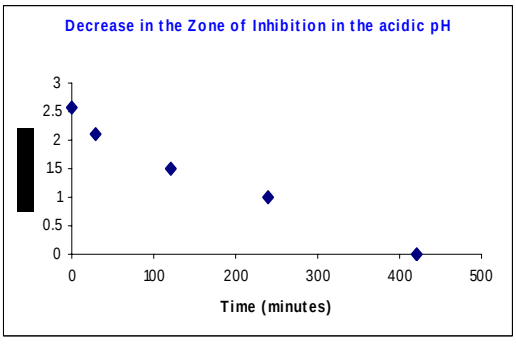

Figure 51. A time dependent decrease in PLM-B antifungal activity (as determined by a decrease in a zone of inhibition) stored at (A) basic and (B) acidic pH.

(A)

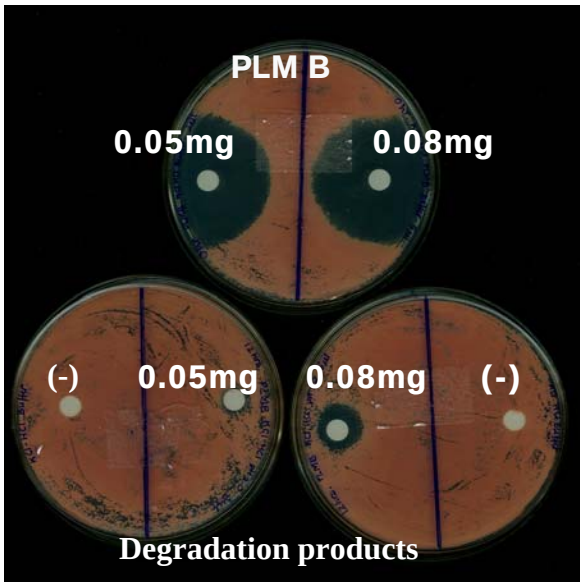

(B)

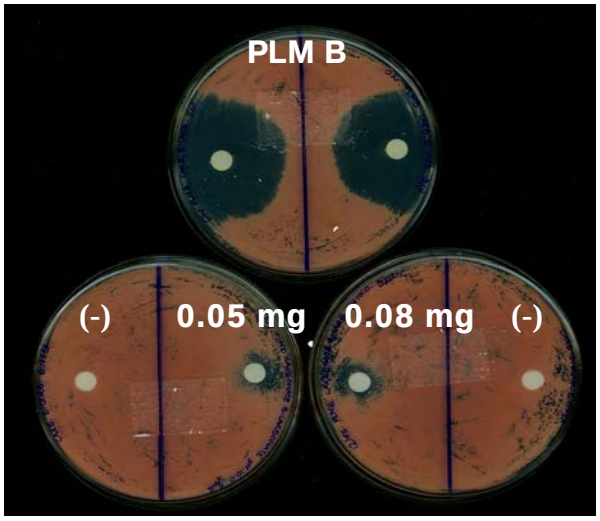

Figure 52. Assaying antifungal activity of PLM B and degradation products generated under acidic (A) and basic pH (B) at 2 different conditions.

(A) (B)

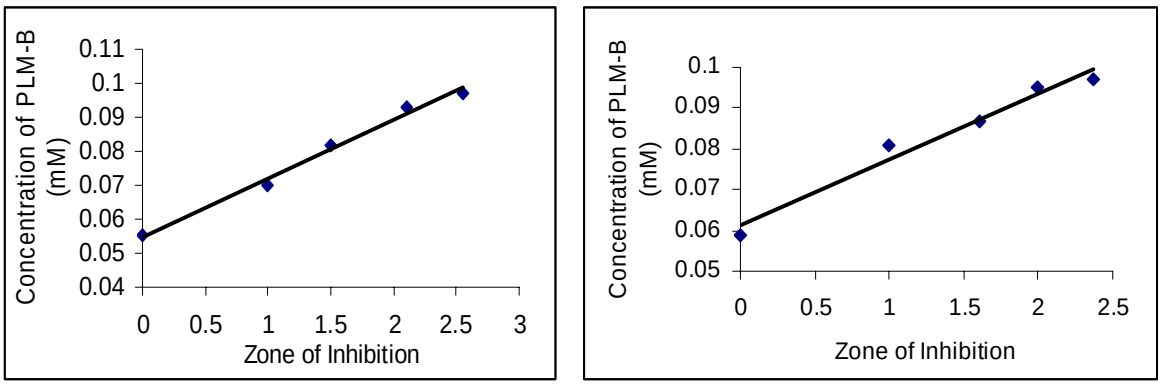

Figure 53. Decrease in the zone of inhibition with the decrease in concentration of PLM-B by degradation at (A) pH 2.0 (B) pH 10.0.

Decrease in the zone of inhibition with time was observed due to decrease in the concentration of PLM-B (0.05mg/mL) when incubated at pH 2.0 and 10.0 (Figure 53).

CONCLUSION

PLM-B decomposition was observed to exhibit a U-shaped pH-rate profile, described by the equation $k_{OBS} = k_H \times 10^{-pH} + k_{OH} \times 10^{pH-14}$ that demonstrated both acid ($k_H = 45 \pm 7\ M^{-1}\ h^{-1}$) and base ($k_{OH} = 448 \pm 73\ M^{-1}\ h^{-1}$) catalyzed decomposition. The rate of degradation was faster at high and low pH, whereas at pH 6.6, PLM-B exhibited maximum stability. PLM-B was found to degrade to three major products in basic aqueous conditions and more than three different products in acidic aqueous conditions. Mass spectroscopic analysis and NMR data of the basic pH degradation products indicate that hydrolysis of the lactone ring is the major decomposition product. The two other products formed involved an initial addition of water to C-2/C-3 double bond followed by hydrolysis of the lactone ring with either water or methanol. Among the acid degraded products, a C-9/C-11 cyclic phosphorinane derivative of PLM-B was identified.

Previous report suggested that the various substituents at C-18 of PLM-B moiety yielding PLM analogs A and C-F do not contribute to the antifungal activity [76]. In contrast, none of the PLM-B degradation products had significant antifungal activity, demonstrating that an intact lactone ring, the phosphate group and the C-8 hydroxyl group all contribute to the antifungal activity.

Phoslactomycin is quite stable but not as active as fostriecin. Details on the reported fostriecin instability have not been published and it remains to be seen if it is less stable than PLM-B. The apparent stability of PLM-B along with a mutant strain NP1 [2] which exclusively produces this product provides an exciting base for the continued development of this class of compounds for pharmaceutical applications.

REFERENCES

1. Lewy, D. S.; Gauss, C. M.; Soenen, D. R.; Boger, D. L. Fostriecin: chemistry and biology.*Curr Med Chem* **2002**, *9* (22)*,* 2005-2032.

2. Palaniappan, N.; Kim, B. S.; Sekiyama, Y.; Osada, H.; Reynolds, K.A. Enhancement and selective production of phoslactomycin B, a protein phosphatase IIa inhibitor, through identification and engineering of the corresponding biosynthetic gene cluster. *J. Biol. Chem*. **2003**, *278*, 35552-35557.

3. Fushimi, S.; Furihata, K.; Seto, H. Studies on new phosphate ester antifungal antibiotics phoslactomycins. II. Structure elucidation of phoslactomycins A to F. *J. Antibiot*. (Tokyo). **1989**, *42* (7), 1026-1036

4. Ozasa, T.; Tanaka, K.; Sasamata, M.; Kaniwa, H.; Shimizu, M.; Matsumoto, H.; Iwanami, M. Novel antitumor antibiotic phospholine. 2. Structure determination. *J. Antibiot.* **1989** , *42* (9), 1339-1343.

5. Kohama, T.; Enokita, R.; Okazaki, T.; Miyaoka, H.; Torikata, A.; Inukai, M.; Kaneko, I.; Kagasaki, T.; Sakaida, Y.; Satoh, A. Novel microbial metabolites of the phoslactomycins family induce production of colony- stimulating factors by bone marrow stroma cells .I. Taxonomy, fermentation and biological properties. *J. Antibiot*. (Tokyo). **1993**, *46* (10), 1503-1511.

6. Kohama, T.; Nakamura, T.; Kinoshita, T.; Kaneko, I.; Shiraishi, A. Novel microbial metabolites of the phoslactomycins family induce production of colony-stimulating factors by bone marrow stromal cells. II. Isolation, physico- chemical properties and structure determination. *J. Antibiot*.(Tokyo). **1993**, *46* (10), 1512 -1519.

7. Larsen, A. K.; Escargueil, A. E.; Skladanowski, A. Catalytic topoisomerase II inhibitors in cancer therapy. *Pharmacol. Ther.* **2003**, *99* (2), 167-181.

8. de Jong, S.; Zijlstra, J. G.; Mulder, N. H.; de Vries, E. G. Lack of cross-resistance to fostriecin in a human small-cell lung carcinoma cell line showing topoisomerase II-related drug resistance. *Can. Chemother. Pharmacol*. **1991**, *28* (6), 461-464.

9. Holm, C.; Stearns, T.; Botstein, D. DNA topoisomerase II must act at mitosis to prevent nondisjunction and chromosome breakage. *Mol. cell. Biol*. **1989**, *9*, 159-168.

10. Pommier, Y.; Kohn, K. W. In Topoisomerase II inhibition by antitumor intercalators and demethyl epipodophyllotoxins. Gazer,R.I., Ed.; CRC Press: Boca Raton, FL, **1989,** p. 175.

11. Liu, L. F. DNA topoisomerase poisons as antitumor drugs. *Annu. Rev. Biochem.* **1989**, *58,* 351-375**.**

12. Chen, G. L.; Yang, L.; Rowe, T. C.; Halligan, B. D.; Tewey, K. M.; Liu, L. F. Nonintercalative antitumor drugs interfere with the breakage-reunion reaction of mammalian DNA topoisomerase II. *J. Biol. Chem*. **1984**, *259*, 13560-13566

13. Boritzki, T. J.; Wolfard, T. S.; Besserer, J. A.; Jackson, R. C.; Fry, D. W. Inhibition of Type II topoisomerase by fostriecin. *Biochem. Pharmacol*. **1988**, *37*, 4063- 4068.

14. Roberge, M.; Tudan, C.; Hung, S. M.; Harder, K. W.; Jirik, F. R.; Anderson, H. Antitumor drug fostriecin inhibits the mitotic entry checkpoint and protein phosphatases 1 and 2A. *Cancer Res.* **1994**, *54* (23), 6115-6121.

15. McCluskey, A.; Sim, A.T. Serine-threonine protein phosphatase inhibitors: development of potential therapeutic strategies. *J. Med. Chem*. **2002**, *45* (6), 1151-1175.

16. Walsh, A. H.; Cheng, A.; Honkanen, R.E. Fostriecin, an antitumor antibiotic with inhibitory activity against serine/threonine protein phosphatases types 1 (PP1) and 2A (PP2A), is highly selective for PP2A. *FEBS Lett.* **1997,** *416* (3), 230-234.

17. Hastie, C.J.; Cohen, P.T.; Purification of protein phosphatase 4 catalytic subunit: inhibition by the antitumour drug fostriecin and other tumour suppressors and promoters. *FEBS. Lett*. **1998,** *431* (3), 357-361.

18. da Cruz e Silva, O. B.; da Cruz e Silva, E. F.; Cohen, P. T. Identification of a novel protein phosphatase catalytic subunit by cDNA cloning. *FEBS letters* **1988**, *242*(1), 106-110

19. Cohen, P.The structure and regulation of protein phosphatases. *Annu.Rev. Biochem.* **1989**, *58,* 453-508.

20. Brewis, N. D.; Street, A. J.; Prescott, A. R.; Cohen, P. T. PPX, a novel protein serine/threonine phosphatase localized to centrosomes. *EMBO J.* **1993**, *12*(3), 987-996.

21. Sheppeck, J.E.; Gauss, C. M.; Chamberlin, A.R. Inhibition of the Ser-Thr Phosphatases PP1 and PP2A by Naturally Occurring toxins. *Bioorg.Med.Chem*. **1997**, *5*, 1739-1750

22. Douglas, P.; Moorhead, G.B.; Ye, R.; Lees-Miller, S.P. Protein phosphatases regulate DNA-dependent protein kinase activity. *J. Biol. Chem*. **2001**, *276* (22), 18992-18998.

23. Hastie, C.J.; Cohen, P.T.; Purification of protein phosphatase 4 catalytic subunit: inhibition by the antitumour drug fostriecin and other tumour suppressors and promoters. *FEBS. Lett*. **1998,** *431* (3), 357-361.

24. Buck, S. B.; Hardouin, C.; Ichikawa, S.; Soenen, D. R.; Gauss, C. M.; Hwang, I.; Swingle, M. R.; Bonness, K. M.; Honkanen, R. E.; Boger, D. L. Fundamental role of the fostriecin unsaturated lactone and implications for selective protein phosphatase inhibition. *J. Am. Chem. Soc*. **2003**, *125* (51)*,* 15694-15695.

25. Roberge, M.; Tudan, C.; Hung, S. M.; Harder, K. W.; Jirik, F. R.; Anderson, H. Antitumor drug fostriecin inhibits the mitotic entry checkpoint and protein phosphatases 1 and 2A. *Cancer Res*. **1994**, 54(23), 6115-6121.

26. Usui, T.; Marriott, G.; Inagaki, M.; Swarup, G.; Osada, H. Protein phosphatase 2A inhibitors, phoslactomycins. Effects on the cytoskeleton in NIH/3T3 cells. *J. Biochem*. **1999**, *125*(5), 960-965.

27. Helps, N. R.; Brewis, N. D.; Lineruth, K.; Davis, T.; Kaiser, K.; Cohen, P. T. Protein phosphatase 4 is an essential enzyme required for organisation of microtubules at centrosomes in Drosophila embryos*. J. Cell Sci.* **1998**, 1331-1340.

28. Ho, D. T.; Roberge, M. The antitumor drug fostriecin induces vimentin hyperphosphorylation and intermediate filament reorganization. *Carcinogenesis* 1996, *17* (5), 967-972.

29. Hartwell, L.H.; Weinert, T.A. Checkpoints: controls that ensure the order of cell cycle events. *Science*. **1989**, *246*, 629-634.

30. Nurse, P. Universal control mechanism regulating onset of M phase. *Nature* **1990**, *344*, 503-508.

31. Lewin, B. Driving the cell cycle: M phase kinase, its partners, and subtrates. *Cell* **1990**, *61*,743-752.

32. Guo, X.W.; Thng, J. P. H.; Swank, R. A.; Anderson, H. J.; Tudan, C.; Bradbury, E. M.; Roberge, M. Chromosome condensation does not require p34cdc2 kinase activity and histone H1 hyperphosphorylation, but is associated with enhanced histone H2A and H3 phosphorylation. *EMBO J*. **1995**, *14*, 976-985.

33. Murray, A.W. Creative blocks:cell cycle checkpoints and feedback controls. *Nature* **1992**, *359*, 599-604.

34. Steinmann, K. E.; Belinsky, G. S.; Lee, D.; Schlegel, R. Chemically induced premature mitosis: differential response in the rodent and human cells and the relationship to cyclin B synthesis and p34cdc2/cyclinB complex formation. *Proc.Natl.Acad.Sci.USA*. **1991**, *88*, 6843-6847.

35. Cheng, A.; Balczon, R.; Zuo, Z.; Koons, J. S.; Walsh, A. H.; Honkanen, R. E. Fostriecin-mediated G2-M-phase growth arrest correlates with abnormal centrosome replication, the formation of aberrant mitotic spindles, and the inhibition of serine/threonine protein phosphatase activity. *Cancer Res*. **1998**, *58*(16), 3611-3619.

36. Felix M. A.; Cohen, P.; Karsenti, E. Cdc2 H1 kinase is negatively regulated by a type 2A phosphatase in the Xenopus early embryonic cell cycle: evidence from the effects of okadaic acid. *EMBO. J.* **1990**, *9*(3), 675-683.

37. Picard, A.; Labbe, J. C.; Barakat, H.; Cavadore, J. C.; Doree, M. Okadaic acid mimics a nuclear component required for cyclin B-cdc2 kinase microinjection to drive starfish oocytes into M phase. *J. Cell. Biol.* **1991**, 115(2), 337-344.

38. Yamashita, K.; Yasuda, H.; Pines, J.; Yasumoto, K.; Nishitani, H.; Ohtsubo, M.; Hunter, T.; Sugimura, T.; Nishimoto, T. Okadaic acid, a potent inhibitor of type 1 and type 2A protein phosphatases, activates cdc2/H1 kinase and transiently induces a premature mitosis-like state in BHK21 cells. *EMBO J.* **1990**, 9 (13), 4331-4338.

39. Tosuji, H.; Mabuchi, I.; Fusetani, N.; Nakazawa, T. Calyculin A induces contractile ring-like apparatus formation and condensation of chromosomes in unfertilized sea urchin eggs. *Proc. Natl. Acad. Sci .USA* 1992, 89 (22), 10613-10617.

40. Uemura, T.; Ohkura, H.; Adachi, Y.; Morino, K.; Shiozaki, K.; Yanagida, M. DNA topoisomerase II is required for condensation and separation of mitotic chromosomes in S. pombe. *Cell* **1987**, *50* (6), 917-925.

41. Solomon, M. J.; Glotzer, M.; Lee, T. H.; Philippe, M.; Kirschner, M. W. Cyclin activation of p34cdc2. *Cell* **1990**, 63(5), 1013-1024.

42. Lee, T. H.; Solomon, M. J.; Mumby, M. C.; Kirschner, M. W. INH, a negative regulator of MPF, is a form of protein phosphatase 2A. *Cell* **1991**, *64*(2), 415-423.

43. Clarke, P. R.; Karsenti, E. Regulation of p34cdc2 protein kinase: new insights into protein phosphorylation and the cell cycle. *J. Cell. Sci*. **1991**, *100,* 409-414.

44. Krek, W.; Nigg, E. A. Differential phosphorylation of vertebrate p34cdc2 kinase at the G1/S and G2/M transitions of the cell cycle: identification of major phosphorylation sites. *EMBO J.* **1991**, *10* (2), 305-316.

45. Norbury, C.; Blow, J.; Nurse, P. Regulatory phosphorylation of the p34cdc2 protein kinase in vertebrates. *EMBO J.* **1991**, *10* (11), 3321-3329

46. Bosc, D. G.; Luscher, B.; Litchfield, D. W. Expression and regulation of protein kinase CK2 during the cell cycle. *Mol. Cell. Biochem.* **1999**, 191, 213-222.

47. Ackerman, P.; Glover, C. V.; Osheroff, N. Phosphorylation of DNA topoisomerase II by casein kinase II: modulation of eukaryotic topoisomerase II activity in vitro. *Proc. Natl. Acad. Sci. USA* **1985**, *82*(10), 3164-3168.

48. Sahyoun, N.; Wolf, M.; Besterman, J.; Hsieh, T.; Sander, M.; LeVine, H.; Chang, K. J; Cuatrecasas, P. Protein kinase C phosphorylates topoisomerase II: topoisomerase activation and its possible role in phorbol ester-induced differentiation of HL-60 cells. *Proc.Natl. Acad. Sci. USA* 1986, 83(6), 1603-1607.

49. Rottmann, M.; Schroder, H. C.; Gramzow, M.; Renneisen, K.; Kurelec, B.; Dorn, A.; Friese, U.; Muller, W. E. Specific phosphorylation of proteins in pore complex-laminae from the sponge Geodia cydonium by the homologous aggregation factor and phorbol ester. Role of protein kinase C in the phosphorylation of DNA topoisomerase II. *EMBO J.* **1987**, 6 (13), 3939-3944.

50. Sunkara, G.; Navarre, C.B.; Kompella, U.B. Influence of pH and temperature on kinetics of Ceftiofur degradation in aqueous solutions. *J. Pharm. Pharmacol*. **1999**, *51*, 249- 255.

51. Honkanen, R. E.; Golden, T. Regulators of serine/threonine protein phosphatases at the dawn of a clinical era? *Curr. Med. Chem.* **2002**, 9 (22), 2055-2075.

52. Fry, D. W.; Besserer, J. A.; Boritzki, T. J. Transport of the antitumor antibiotic Cl-920 into L1210 leukemia cells by the reduced folate carrier system. Cancer research 1984, *44* (8), 3366-3370.

53. Le, L.H.; Erlichman, C; Pillon, L.; Thiessen, J. J.; Day, A.; Wainman, N.; Eisenhauer, E. A.; Moore, M.J. Phase I and Pharmacokinetic Study of Fostriecin given as an Intravenous Bolus Daily for Five Consecutive Days. *Investl. New. Drugs.* **2004**, *22*(2), 159-167

54. Boger D L; Ichikawa S; Zhong W. Total synthesis of fostriecin (CI-920). *J. Amer. Chem. Soc*. **2001**, *123*(18), 4161-4167.

55. Morrison, R.T.; Boyd, R.N. *Organic Chemistry*; Allyn and Bacon: Boston, 2002; pp 249-271.

56. Hopwood; Genetic Manipulation of Streptomyces - A Laboratory Manual. **1985**, 3-4.

57. Connors, K.A.; Amidon, G.L.; Stella, V.J. *Chemical stability of Pharmaceuticals: A handbook for pharmacists*; John Wiley & Sons: New York, 1986, 32-62

58. Carstensen, J.T.; Rhodes, C.T. *Drug stability Principles and Practices*; Marcel Dekker: New York, 2000, pp 57-112.

59. Claudius, John S.; Neau, S. H. The solution stability of vancomycin in the presence and absence of sodium carboxymethyl starch. *Int. J. Pharm.* **1998**, 168(1), 41-48.

60. Tinoco, I.; Sauer, K.; Wang, J.C.; Puglisi, J.D. *Physical Chemistry, Principles and applications in Biological Sciences*. Prentice Hall: New Jersey, 2002, 15-57.

61. Paesen, J.; Khan, K.; Roets, E.; Hoogmartens, J. Study of the stability of erythromycin in neutral and alkaline solutions by liquid chromatography on poly(styrene-divinylbenzene). *Intl. J. Pharma*. **1995**, 113(2), 215-222.

62. Paesen, J.; Claeys, P.; Cypers, W.; Roets, E.; Hoogmartens, J. Liquid chromatography of tylosin A and related substances on poly (styrene-divinylbenzene). *J. Chrom. A*. **1995**, 699, 93-97.

63. Mohammed E. Abdel- Hamid. FSQ spectrophotometric and HPLC analysis of some cephalosporins in the presence of their alkali-induced degradation products. *Farmaco.* **1998,** *53* (2), 132-138.

64. Paesen, J.; Cypers, W.; Busson, R.; Roets, E.; Hoogmartens, J. Isolation of decomposition products of tylosin using liquid chromatography. *J. Chrom. A.* **1995**, 699, 99-106.

65. Ozasa, T.; Suzuki, K.; Sasamata, M; Tanaka, K.; Kobori, M. ; Kadota, S.; Nagai, K.; Saito, T.; Watanabe, S.; Iwanami, M. Novel antitumor antibiotic phospholine .1. Production, isolation and characterization. *J. Antibiot.* (Tokyo). **1989**,*42*,1331-1338.

66. Bares, I. F.; Pehourcq, F.; Jarry, C. Development of a rapid RP-HPLC method for the determination of clonazepam in human plasma. *J. Pharm. Biomed. Anal*. **2004**, *36* (4), 865-869

67. Barker, J.; Ando, D.; Davis, R.; Frearson, M.J. *Mass spectrometry analytical chemistry by open learning*; John Wiley &Sons: New York, 1999; pp 19-48.

68. Perrin, D.D.; Boyd, D. Buffers for pH and Metal Ion Control; John Wiley &Sons: New York, 1974; pp 24-38.

69. Dawson, R.M.C.; Elliot, D.C.; Elliot, W.H.; Jones, K.M. *Data for Biochemical Research*; Oxford University Press: New York, 1986; pp 417-448.

70. Sluiter, C.; Kettenes-van den Bosch, J. J.; Hop, E.; Underberg, W.J.M.; Bult, A. Degradaton study of the investigational anticancer drug clanfenur. *Int .J. Pharm*. **1999** ,*185* (2), 227-235

71. Skinner, M.; Taylor, R.B.; Kanfer, I.The pH stability and acid degradation of the macrolide antibiotic, josamycin. *Eur. J.Pharm.Sci.* **1993**, 1, 61-72.

72. Styslo-Zalasik, M.; Li, Weiyong. Determination of topiramate and its degradation product in liquid oral solutions by high performance liquid chromatography with a chemiluminescent nitrogen detector. *J. Pharm. Biomed Anal.* **2005**, *37*(3), 529-534.

73. Fushimi, S.; Nishikawa, S.; Shimazu, A.; Seto, H. Studies on new phosphate ester antifungal antibiotics phoslactomycins. I. Taxonomy, fermentation, purification and biological activities. *J. Antibiot.* (Tokyo).**1989**, *42* (7), 1019-1025

74. Ariken, S.; Paetznick, V.; Rex, J.H. Comparative Evaluation of Disk Diffusion with Microdilution Assay in Susceptibility Testing of Caspofungin against Aspergillus and Fusarium Isolates. *J. Antimicrob.Chemother.***2002**, *465*, 3084-3087.

75. Levison, M.E.; Microbiological Agar Diffusion Assay for Metronidazole Concentrations in serum. *J. Antimicrob.Chemother.***1974**, *5*, 466-468.

76. Civitareale, C.; Fiori, M.; Ballerini, A.; Brambilla, G. Identification and quantification method of spiramycin and tylosin in feedingstuffs with HPLC-UV/DAD at 1 ppm level. *J.Pharm. Biomed. Anal.* **2004**, 36 (2), 317-325.

APPENDIX

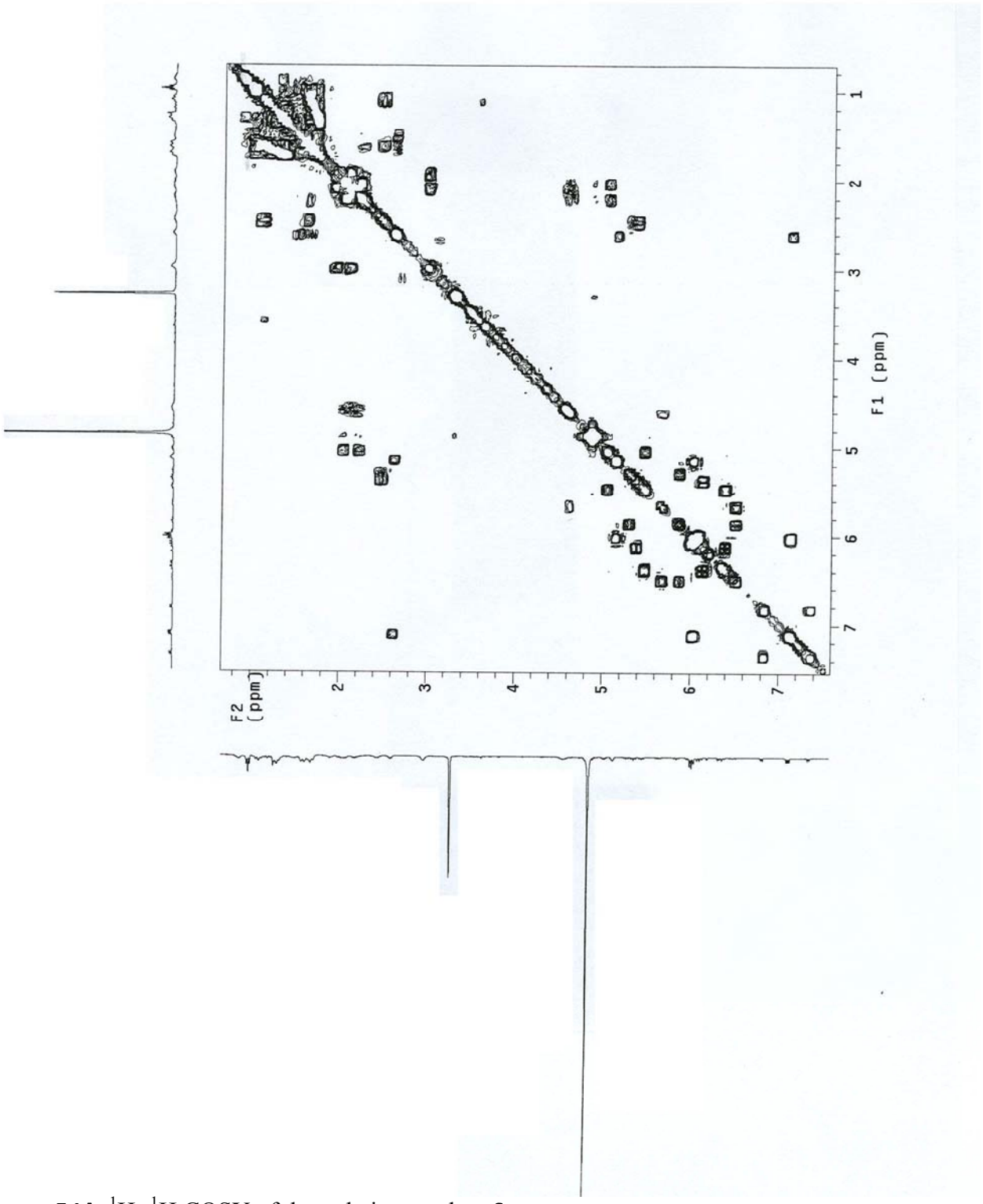

Figure 54A. ^{1}H -^{1}H COSY of degradation product **6**.

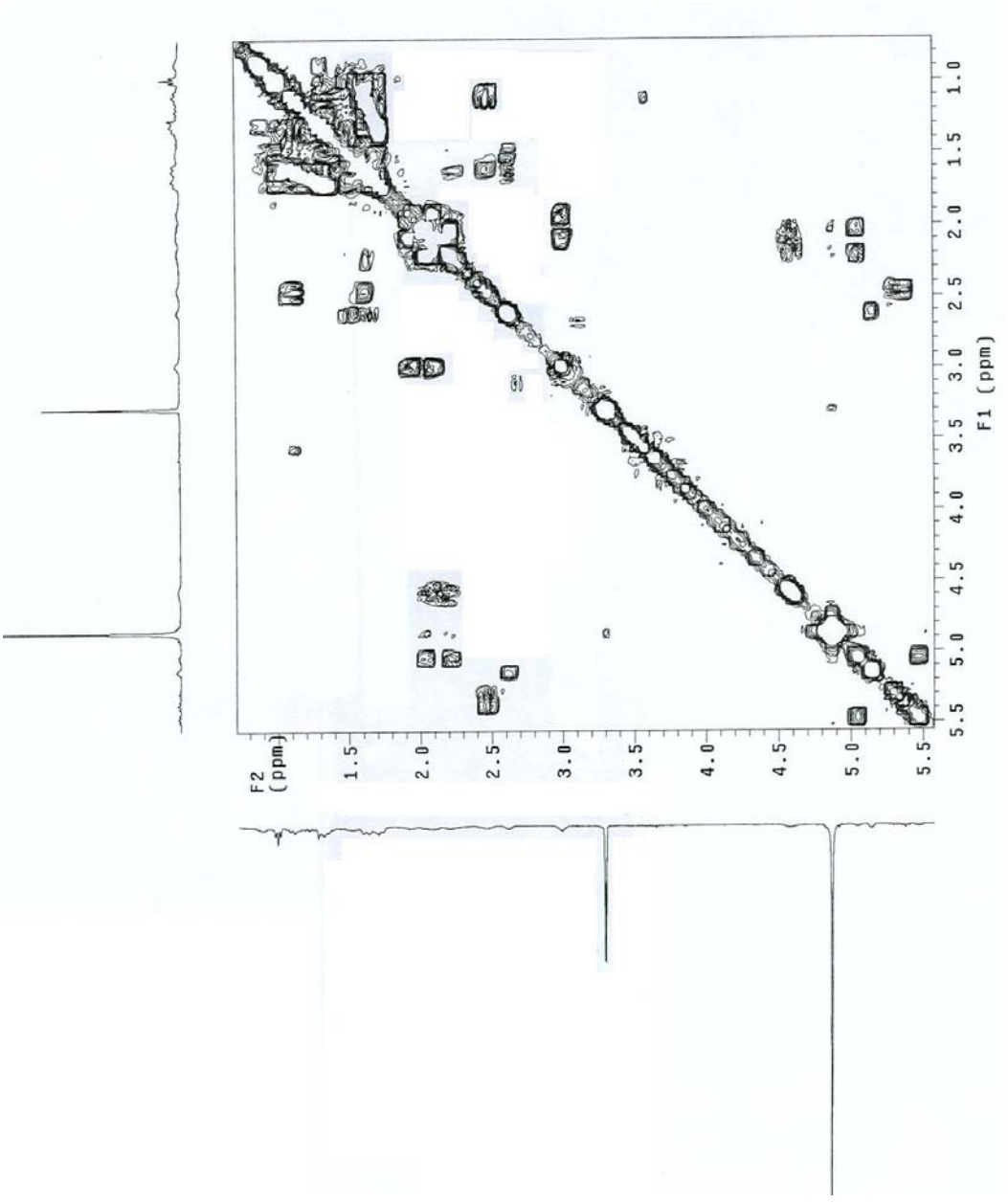

Figure 54B. ^{1}H -^{1}H COSY of degradation product **6** (upfield region)

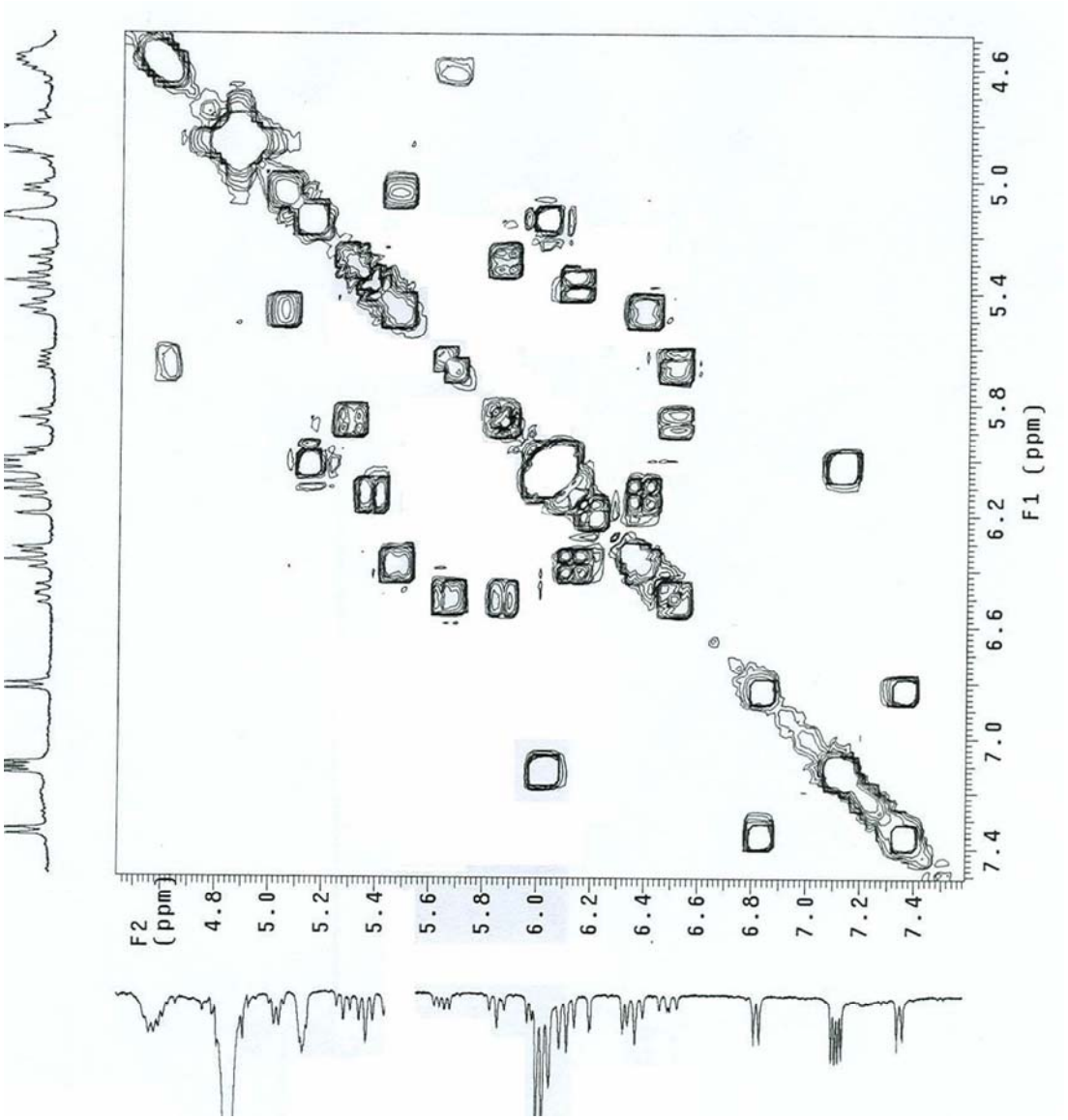

Figure 54C. ^{1}H -^{1}H COSY of degradation product **6** (downfield region)

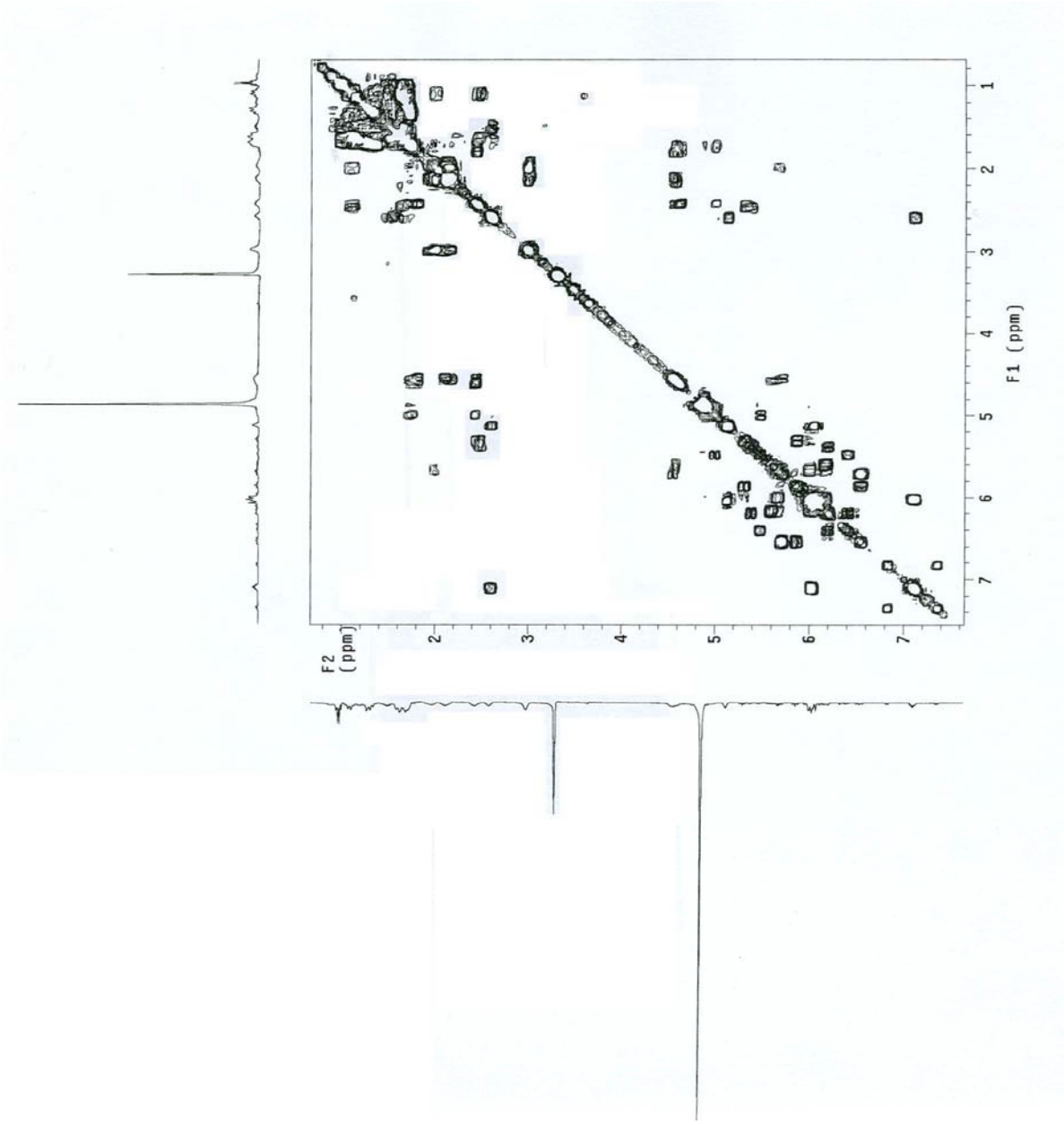

Figure 55A. ^{1}H -^{1}H COSY of degradation product **7**.

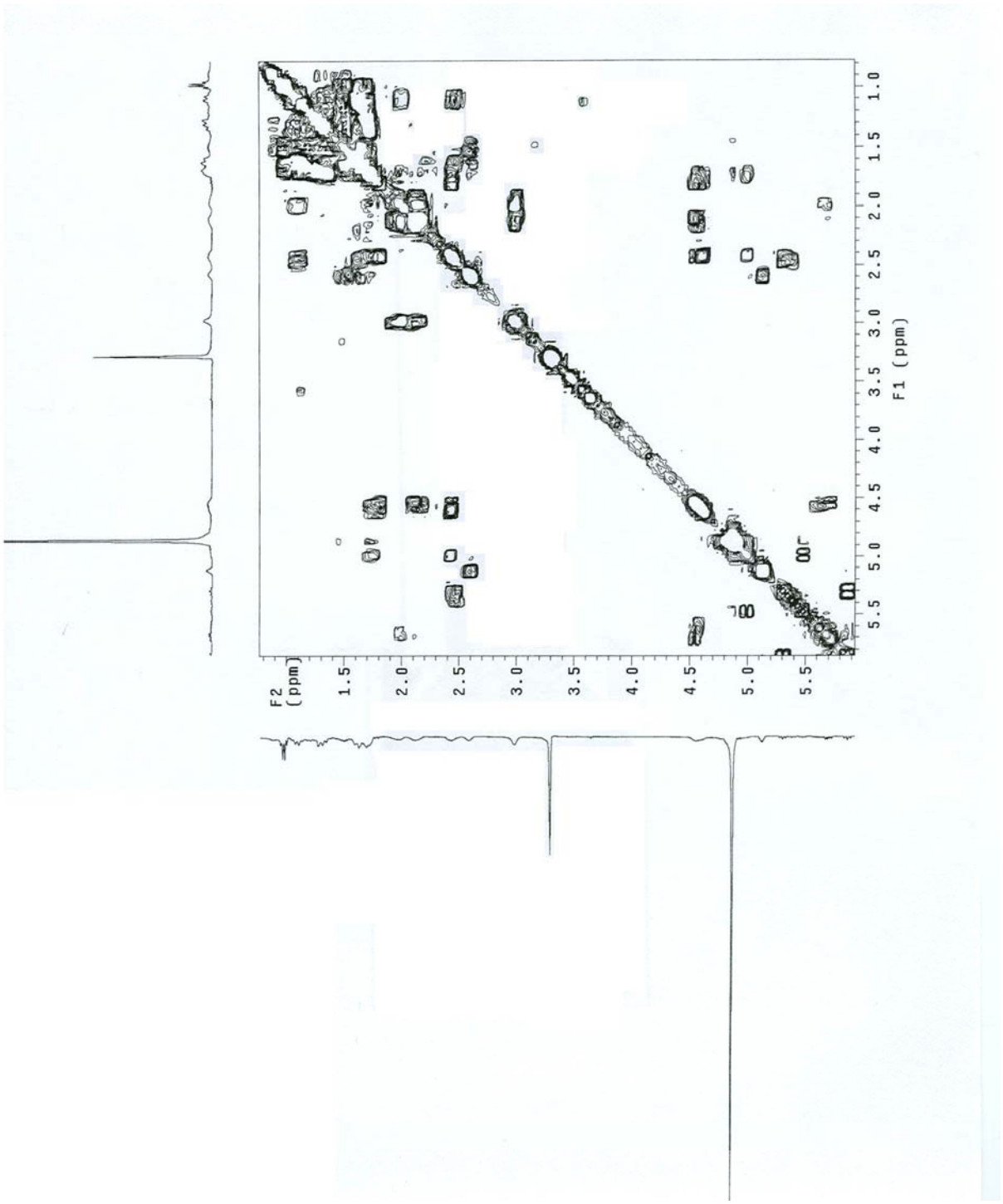

Figure 55B. ^{1}H -^{1}H COSY of degradation product **7** (upfield region).

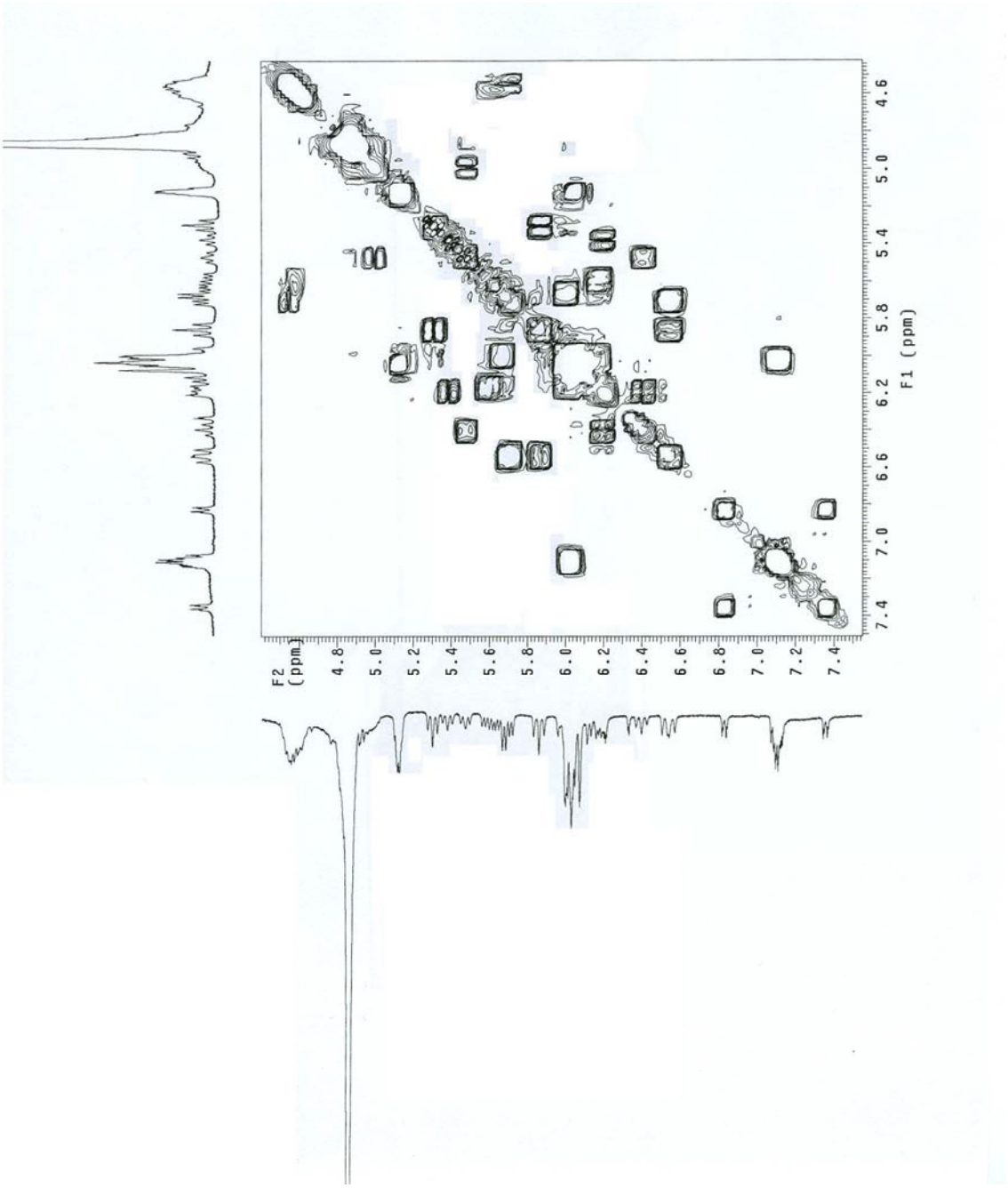

Figure 55C. ^{1}H -^{1}H COSY of degradation product **7** (downfield region).

Vita

Suparna Das Choudhuri was born in Calcutta, India on 8th June 1977. She received her Bachelor of Pharmacy degree in 2001 from Rajiv Gandhi University of Health Sciences, Karnataka, India. She joined Virginia Commonwealth University in 2003 and completed Master of Science in Medicinal Chemistry in 2005.